

INVESTIGATING THE EFFECT OF BIOCHAR ON THE  
FROST DURABILITY AND DURABILITY  
ASSESSMENT OF CONCRETE

by  
Adam B. Dunne

**© Copyright by Adam B. Dunne, 2025**

All Rights Reserved

A thesis submitted to the Faculty and the Board of Trustees of the Colorado School of Mines in partial fulfillment of the requirements for the degree of Doctor of Philosophy (Civil and Environmental Engineering).

Golden, Colorado

Date \_\_\_\_\_

Signed: \_\_\_\_\_

Adam B. Dunne

Signed: \_\_\_\_\_

Dr. Lori Tunstall  
Thesis Advisor

Golden, Colorado

Date \_\_\_\_\_

Signed: \_\_\_\_\_

Dr. D.V. Griffiths  
Professor and Department Head  
Civil and Environmental Engineering

## ABSTRACT

As the key binding constituent, cement plays a critical role in determining the engineering properties and durability of concrete. Since its production is responsible for 8% of the global CO<sub>2</sub> emissions, there is significant interest in technologies that reduce cement's carbon footprint. One emerging solution is the integration of biochar, a carbon negative, renewable material produced from the thermochemical conversion of biomass. Biochar's impact on the mechanical and fresh properties of concrete has been widely studied, while biochar's effect on concrete durability remains largely unknown. This thesis seeks to address this research gap by investigating the effect of biochar on the frost durability and durability assessment of biochar concrete.

In the first effort, biochar was used as a partial replacement of cement in mortars to investigate the validity of bulk electrical resistivity as an assessment of biochar mortar permeability. In conventional cementitious composites, bulk electrical resistivity measurements can be used as an approximation of permeability because electrical charge is only carried via electrolytic conductivity; dissolved charged ions in the pore solution migrate more easily (higher conductivity) in more permeable composites. However, cementitious composites that incorporate conductive materials can display both electrolytic conductivity and electric conductivity, both of which can affect bulk electrical resistivity measurements. Resistivity measurements cannot distinguish between these conductive pathways; thus, decreased resistivity may indicate increased electric conductivity through the solid phase or increased permeability, which is typically associated with decreased durability. This work found that while biochar can reduce matrix permeability, it also influences the electrical properties of mortars through changes to both electrical and electrolytic conductivity, making bulk electrical resistivity measurements a poor indicator of permeability changes.

In the second effort, biochar was used as a partial replacement of sand to evaluate compatibility between biochar and an air-entraining admixture and to explore biochar concrete's resistance to rapid freeze-thaw testing. Entrained air voids are typically integrated into concrete to provide resistance against frost damage, but reduced concrete permeability can also enhance this protection. To entrain the required 6 vol% air in concrete, concrete mixes with biochar required 970 - 2800% more air-entrainer compared to a control. Additionally, despite improved permeability at some replacement levels, non-air-entrained biochar concrete failed in less than 15 freeze-thaw cycles, compared to conventional concrete which failed in 97 freeze-thaw cycles. Air-entrained biochar concrete showed improvement, but still failed between 165 and 185 freeze-thaw cycles. This degraded freeze-thaw performance was attributed to biochar concrete's higher sorptivity, associated with pore refinement. When water freezes in small pores, higher tensile pressures are developed than when water freezes in large pores, leading to greater damage.

## TABLE OF CONTENTS

ABSTRACT .....	iii
LIST OF FIGURES.....	vii
LIST OF TABLES .....	ix
ACKNOWLEDGMENTS.....	x
CHAPTER 1 INTRODUCTION .....	1
1.1 Motivation.....	1
1.2 Background.....	1
1.3 Research Goal.....	3
1.4 Research Objectives and Tasks .....	3
1.5 Thesis Structure .....	5
CHAPTER 2 LITERATURE REVIEW .....	6
2.1 Introduction to Biochar.....	6
2.2 Electrical Resistivity .....	7
2.2.1 Background .....	7
2.2.2 Electrical Resistivity Testing Methods .....	9
2.3 Conductive Concrete .....	10
2.3.1 Factors Affecting Electrical Conductivity of Biochar.....	10
2.3.2 Electrical Percolation .....	11
2.4 Electrical Resistivity Assessment of Biochar Cementitious Composites .....	11
2.4.1 Biochar Percolation Threshold.....	12
2.5 Frost Durability.....	13
2.5.1 Mechanisms of Internal Frost Damage in Concrete.....	13
2.5.2 Testing and Evaluation of Frost Durability.....	14
2.5.3 Frost Durability Enhancement Measures .....	14
2.6 Air Entrainment in Concrete.....	15
2.6.1 Effects of Air Entrainment on Frost Resistance.....	15
2.6.2 Factors Affecting Air Entrainment.....	15
2.6.3 Testing and Evaluation of Air Entrainment in Concrete.....	16
2.6.4 Experimental Study on Frost Resistance of Air Entrained Concretes .....	16
2.7 Biochar Concrete and Frost Resistance .....	17
2.7.1 Biochar Surfactant Interference .....	17

CHAPTER 3	ELECTRICAL RESISTIVITY AS A DURABILITY ASSESSMENT TOOL OF BIOCHAR CEMENTITIOUS COMPOSITESTES .....	19
3.1	Introduction.....	19
3.1.1	Research Objective.....	21
3.2	Materials & Methods .....	21
3.2.1	Biochar .....	21
3.2.2	Mortar.....	23
3.2.3	Mix Design and Preparation.....	24
3.2.4	Experimental Methods .....	26
3.3	Results and Discussion .....	32
3.3.1	Biochar Conductivity .....	32
3.3.2	Volume of Permeable Void Space .....	34
3.3.3	Electrical Resistivity and Permeability .....	36
3.3.4	Percolation Threshold Prediction .....	41
3.4	Conclusion .....	42
CHAPTER 4	AN EVLAUATION OF BIOCHAR CONCRETE PERMEABILITY AND FROST DURABILITY WITHOUT AIR-ENTRAINMENT .....	45
4.1	Introduction.....	45
4.1.1	Research Objective.....	47
4.2	Materials and Methods .....	47
4.2.1	Biochar .....	47
4.2.2	Concrete .....	49
4.2.3	Mix Design and Preparation.....	49
4.2.4	Experimental Methods .....	51
4.3	Results and Discussion .....	54
4.3.1	Compressive Strength .....	54
4.3.2	Permeability .....	56
4.3.3	Hardened Air Void System .....	56
4.3.4	Freeze-Thaw Resistance.....	58
4.3.5	Water sorption .....	60
4.4	Conclusion .....	61
CHAPTER 5	AN EVLAUATION OF BIOCHAR CONCRETE FROST DURABILITY WITH AIR-ENTRAINMENT .....	63
5.1	Introduction.....	63

5.1.1	Research Objective.....	64
5.2	Materials and Methods .....	64
5.2.1	Biochar .....	64
5.2.2	Concrete .....	65
5.2.3	Air-Entraining Admixture.....	66
5.2.4	Mix Design and Preparation.....	66
5.2.5	Experimental Methods .....	67
5.3	Results and Discussion .....	71
5.3.1	AEA Efficacy.....	71
5.3.2	Air Void System.....	73
5.3.3	Freeze-Thaw Resistance.....	73
5.3.4	Water sorption.....	75
5.3.5	Compressive Strength .....	77
5.4	Conclusion .....	77
CHAPTER 6	CONCLUSIONS .....	79
6.1	Major Contributions.....	79
6.2	Major Conclusions.....	79
6.2.1	Objective 1: Separate the effects of changes in pore structure from changes in matrix conductivity.....	79
6.2.2	Objective 2: Evaluate the frost resistance of biochar concrete without air entrainment.....	80
6.2.3	Objective 3a: Assess the efficacy of a sulfonate-based air-entraining admixture with biochar.....	80
6.2.4	Objective 3b: Evaluate the first resistance of biochar concrete with air entrainment.....	80
6.3	Recommendations for Future Work .....	80
REFERENCES	.....	82
APPENDIX A	PERMISSIONS .....	96

## LIST OF FIGURES

Figure 2.1	Electrical Conductivity of Common Materials (Values in S/m) (adapted from [49]) .....	8
Figure 2.2	Differences between Porosity and Permeability (adapted from [53]).....	8
Figure 2.3	Schematic of (a) two-point uniaxial; and (b) four-point wenner (adapted from [52]).....	10
Figure 2.4	Percolation threshold of biochar cementitious composites .....	13
Figure 3.1	BC particle size distribution compared to OPC .....	22
Figure 3.2	Experimental tasks to evaluate BC mortar electrical resistivity and permeability; and BC electrical properties .....	26
Figure 3.3	(a) BC pellet; (b) and (c) setup to measure BC conductivity .....	28
Figure 3.4	RCON electrical resistivity testing set-up.....	30
Figure 3.5	(a) Water impermeability tester; (b) example depth of penetration measurement from exposed face of sample .....	31
Figure 3.6	BC Raman spectra.....	33
Figure 3.7	XRD patterns of BC.....	34
Figure 3.8	Volume of permeable void space.....	35
Figure 3.9	Relationship between bulk electrical resistivity and volume of permeable void space. The low $R^2$ suggests a weak correlation between bulk electrical resistivity measurements and the volume of permeable voids as determined by ASTM C642 [140]. .....	36
Figure 3.10	Relationship between depth of water penetration as a function of bulk electrical resistivity. Linear trend lines are included for each BC, showing a strong ( $R^2>0.94$ ) negative relationship .....	37
Figure 3.11	Difference in pore solution ionic speciation following BC exposure .....	39
Figure 3.12	Depth of water penetration versus formation factor .....	40
Figure 3.13	Electrical resistivity vs. depth of penetration of water of percolation mixes.....	42
Figure 4.1	Particle size distribution of mix constituents .....	48
Figure 4.2	Experimental tasks to evaluate BC concrete frost resistance and permeability .....	51
Figure 4.3	ASTM C1585 test set-up.....	54
Figure 4.4	Correlation between w/c ratio and 14-day compressive strength .....	55
Figure 4.5	Depth of water penetration as an evaluation of concrete permeability .....	56
Figure 4.6	Hardened air content ASTM C457. Error bars indicate standard deviation of the triplicate samples tested.....	57
Figure 4.7	Test results of RMDE for non-air entrained concretes .....	59
Figure 4.8	Mass change of concrete at associated freeze-thaw cycle .....	59

Figure 4.9	Water absorption vs. time .....	60
Figure 5.1	Particle Size Distribution of BC & OPC.....	64
Figure 5.2	Experimental tasks to evaluate biochar concrete frost resistance and biochar compatibility with AEA .....	68
Figure 5.3	ASTM C1585 test set-up.....	71
Figure 5.4	FI Test End Point; (a) OPC-only and (b) PW BC.....	72
Figure 5.5	Comparison of AEA dose; (a) Control, (b) PW, (c) MW .....	73
Figure 5.6	Test Results of RDME .....	74
Figure 5.7	Mass Change of Concrete exposed to Freeze-Thaw Cycles .....	75
Figure 5.8	PW BC Concrete Mass Loss at 170 FT cycles .....	75
Figure 5.9	14-day compressive strength of air-entrained concrete. Error bars indicate the standard deviation of the nine samples tested.....	77

## LIST OF TABLES

Table 1-1	Relationship between research objective and associated tasks .....	4
Table 2-1	Summary of thermochemical processes for biochar preparation (adapted from [37]) .....	6
Table 3-1	Biochar feedstock & pyrolysis parameters .....	22
Table 3-2	BC characteristics.....	23
Table 3-3	Mortar mixture proportions (g).....	24
Table 3-4	Superplasticizer dosage (wt% of BC) & wet mix flow (mm).....	24
Table 3-5	Mortar mix design proportions to achieve BC percolation.....	25
Table 3-6	BC electrical conductivity and resistivity measurements .....	32
Table 3-7	$I_D/I_G$ ratio derived from Raman spectra.....	33
Table 3-8	Electrical resistivity of mortar samples at 28 d.....	37
Table 3-9	Expressed pore solution conductivity ( $\sigma$ , in mS/m) and resistivity ( $\rho_0$ , in $k\Omega \cdot cm$ ).....	38
Table 3-10	Electrical resistivity of percolation mortars .....	41
Table 4-1	BC Characteristics.....	49
Table 4-2	Aggregate characteristics .....	49
Table 4-3	Mix proportions ( $kg/m^3$ ) .....	50
Table 4-4	Superplasticizer dosage (mL/100kg) & slump (mm).....	50
Table 4-5	Air content & spacing factor .....	57
Table 4-6	Rates of sorptivity .....	61
Table 5-1	BC characteristics.....	65
Table 5-2	Aggregate characteristics .....	66
Table 5-3	AEA characteristics.....	66
Table 5-4	Mix proportions ( $kg/m^3$ ) .....	67
Table 5-5	Slump (mm) .....	67
Table 5-6	Predicted vs. actual AEA dosages (mL/100kg CM) .....	72
Table 5-7	AVS parameters .....	73
Table 5-8	Concrete Rates of Sorptivity .....	76

## ACKNOWLEDGMENTS

Completing this PhD has been a journey filled with challenges, discoveries, and growth. It would not have been possible without the support, guidance, and encouragement of many individuals, to whom I am deeply grateful.

First and foremost, I would like to express my sincere gratitude to my advisor, Dr. Lori Tunstall, for her invaluable mentorship, patience, and unwavering support throughout this research. Her insightful guidance and constant encouragement have been instrumental in shaping this academic adventure.

I am also deeply thankful to my committee members, Dr. Geoff Brennecka, Dr. Ahmadreza Hedayat, and Professor Cara Phillips for their constructive feedback, thought-provoking discussions, and for pushing me to refine my ideas and approaches.

Special thanks go to my colleagues and friends in the Tunstall Materials Research Group for their camaraderie, intellectual discussions, and for making this journey more enjoyable.

To my family, especially my wife and three daughters, your unwavering love and encouragement have been my greatest source of strength. Your belief in me, even during the toughest moments, kept me going. A heartfelt thank you to my wife Ana for her patience, understanding, and unwavering support through the late nights and long research hours.

Finally, I would like to acknowledge the funding and institutional support from United States Air Force, which made this research possible.

## CHAPTER 1 INTRODUCTION

### 1.1 Motivation

In 2015, 196 parties at the United Nations Climate Change Conference in Paris, France, adopted *The Paris Agreement*, an international treaty to combat climate change and to accelerate and intensify action needed for a sustainable low carbon future [1]. The production of cement, a constituent in concrete, is one of the worst offenders, responsible for ~8% of the global anthropogenic CO<sub>2</sub> emissions. While cement usage in developed nations has peaked, the industry anticipates considerable growth in many developing regions as demand for infrastructure expands [2]. Many technologies are being investigated to offset carbon emissions during production; one solution gaining popularity is the incorporation of biochar. *Biochar* is a carbon-rich material obtained from the thermochemical conversion of biomass in an oxygen-deprived environment [3]. Instead of the biomass decomposing and releasing CO<sub>2</sub> back into the atmosphere, the carbon is bound up into the structure of the biochar. Even considering the energy required to transform the biomass, the resulting biochar is highly carbon negative, making it an appealing strategy for the production of carbon-neutral construction materials [4].

### 1.2 Background

As a structural material, concrete plays a fundamental role in the construction industry and is used in many infrastructure applications to build strong, durable, and resilient structures. Properly designed, proportioned, transported, placed, finished, and cured concrete can provide decades of service while requiring little to no maintenance [5]. Concrete durability is controlled by its resistance to the penetration of aggressive media and is inextricably linked to its permeability [6]. The durability provisions codified in industry standards like the American Concrete Institute's 318, *Building Code Requirements for Structural Concrete* [7] currently rely on prescriptive limitations like the water-to-cementitious materials ratio (w/c) and an associated specified compressive strength level for acceptance purposes. Typically, for conventional concrete, as w/c decreases, permeability decreases, resulting in more durable concrete. However, driven by calls for more sustainable concrete, current mix design technology incorporates various supplementary materials and admixtures, and a wide variation in permeability is often observed at the same w/c. Thus, the concrete industry has started shifting towards performance-based specifications [8].

*Electrical resistivity* is a material property that can be used to assess the pore structure of concrete. In conventional un-reinforced concrete, the conduction of electrical current is mainly electrolytic, meaning that the current transfers via dissolved charged ions (Ca<sup>+</sup>, K<sup>+</sup>, Na<sup>+</sup>, SO<sub>4</sub><sup>2-</sup>, and OH<sup>-</sup> [9, 10]) released during the dissolution of cement powder and present in the saturated cement pores [11]. Consequently, the

electrical resistivity of concrete is highly dependent on microstructural characteristics, like capillary pore size distribution, volume, size, and connectivity. A higher resistivity indicates a finer pore network with less connectivity, features that correlate with low water permeability [6]. Assessing concrete's permeability via resistivity measurements is appealing because it allows for non-destructive, in-situ monitoring of existing concrete structures [12]. It also supports the transition from prescriptive standards to performance-based standards since it supports in-situ performance evaluation to confirm that the mix design is delivering the intended properties.

Unfortunately, these methods require additional considerations when applied to electrically conductive cementitious composites. This unique concrete class exhibits both electrolytic and electric conductivity, but bulk resistivity measurements cannot distinguish these conductive pathways. Thus, decreased resistivity could be interpreted as either increased permeability (increased electrolytic conduction) or increased electrical conductivity (via a network of conductive inclusions). Several studies [13-20] have evaluated the electrical resistivity of biochar cementitious composites. Other than Yang and Wang [19], each of these studies observed increased conductivity of their cementitious composites as biochar content increased. These studies concluded that biochar's high carbon content must act as a conductive inclusion in the matrix. However, only one study reported a direct measurement of biochar conductivity [17], and none separate the effects of biochar on electrolytic versus electric conductivity; thus, it is equally likely that the biochar increases conductivity via changes to the pore network, which could indicate increased permeability and decreased durability with the addition of biochar.

Due to its excellent water resistance, concrete is an ideal building material in situations where other structural materials like wood and steel would rapidly deteriorate [21]. However, in certain conditions or environments, concrete is susceptible to chemical and physical causes of deterioration [22]. In cold climates, damage to concrete can be caused by frost action (freezing and thawing cycles), which can deteriorate hardened concrete in the presence of moisture [21]. Freeze-thaw (FT) damage can manifest in two different ways in concrete: surface and internal. The methods to enhance the frost resistance of concrete include the purposeful entrainment of air bubbles and decreasing permeability through a lower w/c ratio or the addition of supplementary cementitious materials [23, 24]. Internal frost damage results from hydraulic pressure [25, 26] and crystallization pressure [27] due to the movement of water and the growth of ice crystals in the pores of the cement paste. Entrained air voids prevent internal frost damage by providing escape boundaries to shorten the length displaced water must flow, which decreases the development of hydraulic pressure in the paste [25]. They also host ice crystals that attract water from the capillary pores, inducing shrinkage (cryo-suction) that offsets the crystallization pressure. *Air entrainment* is the process by which numerous tiny air bubbles are intentionally integrated and dispersed throughout the concrete paste matrix [28]. This effect is achieved by using an air-entraining admixture, a surfactant-

based solution that is added to the fresh concrete mixture to promote air bubble formation and stabilization. Biochar has been studied extensively for its effects on fresh and hardened concrete properties [29, 30]. However, only three studies [31-33] have investigated biochar's effect on frost durability; none of which followed the standard rapid-freeze thaw test procedures prescribed in ASTM C666 [34], nor included any air entrainment.

Overall, this research will have wide-ranging impacts on the correlation of electrical resistivity measurements to durability qualifications, like standardized in AASHTO T358 [35]. This research is also the first study to present data on the frost durability of air-entrained biochar concrete and the compatibility of biochar with air-entraining admixtures.

### **1.3 Research Goal**

The goal of this research is to investigate the effect of biochar on the frost durability and durability assessment of concrete. To address the knowledge gaps identified in the existing literature, this investigation plans to address the following research questions:

- Does biochar act as a conductive filler material?
- Can the electrical resistivity measurement of biochar cementitious composites serve as an indicator of its permeability?
- How does varying the percentage of biochar as a sand replacement affect the concrete's permeability and frost resistance?
- Does adding biochar as a concrete amendment affect the efficacy of air-entraining admixtures?
- How does air-entrained biochar concrete perform in rapid freeze-thaw testing?

### **1.4 Research Objectives and Tasks**

To address the research goal and questions defined in section 1.3, the following research objectives have been developed:

- Objective 1: Many studies have reported that biochar acts as a conductive filler material due to decreased electrical resistivity in cementitious composites. To understand if electrical resistivity measurements are a good indicator of permeability in these composites, it's first necessary to understand how biochar can affect electrical properties. This objective focuses on separating the electrolytic conduction through the liquid phase (connected to permeability) and electrical transport through the solid matrix (not connected to permeability) to evaluate the efficacy of resistivity measurements as a durability assessment tool for predicting permeability in biochar cementitious composites.

- Objective 2: While other researchers have concluded that biochar has no discernable effect on the frost durability of non-air entrained biochar concrete, it is unclear if this is due to less paste or to other intrinsic properties of the biochar. This objective investigates how biochar influences freeze-thaw resistance in non-air entrained concrete through microstructural modification and moisture transport mechanisms.
- Objective 3: No research has explored air-entrained biochar concrete. Since air-entrainment is a requirement for concretes in environments experiencing freeze-thaw, this missing foundation is addressed through this objective by a) assessing the efficacy of a sulfonate-based air-entraining admixture with biochar and b) evaluating the frost resistance of biochar concrete with air entrainment.

To accomplish the research goal and objectives, the following associated research tasks have been developed. Table 1-1 provides the relationship between the objectives and associated tasks.

Table 1-1 Relationship between research objective and associated tasks

Objective	Associated Tasks
1: Separate the effects of changes in pore structure from changes in matrix conductivity.	<ul style="list-style-type: none"> <li>- Measure the electrical conductivity of each biochar.</li> <li>- Estimate the percolation threshold of biochar using geometrical model.</li> <li>- Perform bulk electrical resistivity measurements.</li> <li>- Extract pore solution and measure electrical conductivity.</li> <li>- Assess permeability by depth of water penetration testing.</li> </ul>
2: Evaluate the frost resistance of biochar concrete without air entrainment.	<ul style="list-style-type: none"> <li>- Conduct rapid freeze-thaw testing.</li> <li>- Assess permeability by depth of water penetration testing.</li> <li>- Perform compression strength testing.</li> <li>- Characterize hardened air void system.</li> <li>- Evaluate concrete sorptivity.</li> </ul>
3a: Assess the efficacy of a sulfonate-based air-entraining admixture with biochar.	<ul style="list-style-type: none"> <li>- Perform foam index testing on biochar-cement slurries.</li> <li>- Evaluate air content of fresh concrete using pressure meter.</li> </ul>
3b: Evaluate the frost resistance of biochar concrete with air entrainment.	<ul style="list-style-type: none"> <li>- Conduct rapid freeze-thaw testing.</li> <li>- Perform compression strength testing.</li> <li>- Characterize hardened air void system.</li> <li>- Evaluate concrete sorptivity.</li> </ul>

## 1.5 Thesis Structure

This thesis is structured in a manuscript-based format, with each main chapter based on an article that has been submitted or in the process of being submitted to a peer-reviewed journal. These main chapters follow the formatting of the original manuscripts and contain the sections such as abstracts, introductions, materials and methods, results, discussions and conclusions. In total, this thesis is comprised of six chapters, with the main chapters located in Chapter 3 through Chapter 5. Collectively, these independent studies address the overarching theme of investigating the effect of biochar on the frost durability and durability assessment of concrete. Although some content could overlap—specifically in the introductory and methodology sections—each chapter focuses on addressing the research objectives discussed in section 1.4.

Chapter 2 provides a comprehensive review of the literature relevant to the two central themes of this thesis: electrical resistivity as a non-destructive assessment of concrete durability and the frost durability of cementitious materials. The key research gaps driving the research questions and research goal are contextualized.

Chapter 3 is derived from a submitted manuscript, which investigated the bulk electrical resistivity of biochar cement mortars at increasing levels of cement replacement with biochar. This work evaluated the efficacy of biochar as a conductive filler material by directly measuring biochar conductivity and estimating the percolation volume fraction of biochar. To separate the effects of changes in pore structure from changes in matrix conductivity, depth of water penetration was tested to understand permeability and cement pore solution extracted to isolate the microstructural effects from chemical effects on electrical resistivity.

Chapter 4 evaluates the frost resistance of biochar concrete mixtures formulated without air entrainment to establish a baseline of freeze-thaw performance compared to conventional concrete. Biochar was used as a partial replacement of sand in order to evaluate the influence of biochar on frost durability without affecting the binding phase, which largely controls the permeability of the concrete. Freeze-thaw durability was assessed through ASTM C666 [34] rapid-freeze thaw testing, hardened air void analysis, compression testing, permeability measurement, and sorptivity analysis.

Chapter 5 investigates the frost resistance of air-entrained biochar concretes and evaluates biochar compatibility with air-entraining admixtures. Freeze-thaw durability was assessed through ASTM C666 [34] rapid-freeze thaw testing, hardened air void analysis, compression testing, and foam index testing.

Chapter 6 discusses the main conclusions and scientific contributions developed by this work and recommendations for future work. The references for the entire thesis are compiled at the end.

## CHAPTER 2 LITERATURE REVIEW

This chapter provides a comprehensive review of the literature relevant to the two central themes of this thesis: electrical resistivity as a non-destructive assessment of concrete durability and the frost durability of cementitious materials. The chapter begins with an introduction of biochar. Next, the principles and applications of bulk electrical resistivity in concrete, including the mechanisms governing electrolytic and electrical conductivity are discussed. Finally, Chapter 2 concludes with a summary of the relevant literature related to the frost resistance of concrete, to include mechanisms, testing and evaluation, and enhancement measures. A detailed overview of air entrainment is then discussed, including how it prevents frost-related damage in concrete. Due to limited experimental work related on biochar concrete and frost resistance, biochar's interactions in wastewater treatment systems was reviewed. Biochar has been shown to interfere with surfactants in these applications and thus can serve as a conceptual basis for predicting adverse interactions between biochar and air-entraining admixtures in concrete.

### 2.1 Introduction to Biochar

Biochar is a highly porous, carbon-rich substance obtained through the thermal decomposition of biomass in an oxygen-limited environment [3]. The thermochemical processes that can be used to produce biochar are slow or fast pyrolysis, gasification, torrefaction, carbonization, flash carbonization, and hydrothermal carbonization, as summarized in Table 2-1. These processes are distinguished depending on the process parameters (temperature range, residence time, heating rate, etc.) [36].

Table 2-1 Summary of thermochemical processes for biochar preparation (adapted from [37])

Thermochemical process	Temperature range (°C)	Residence time	Heating rate
Slow pyrolysis	100—1000	Minutes to hours	Slow (< 10 °C min <sup>-1</sup> )
Fast pyrolysis	300—1000	< 2 s	Very fast (~1000 °C s <sup>-1</sup> )
Torrefaction	200—300	Minutes to hours	Slow (< 10 °C min <sup>-1</sup> )
Gasification	700—1500	Seconds to minutes	Moderate-very fast
Hydrothermal carbonization	175—300	30 min to 16 h	Slow
Flash carbonization	300—600	~30 min	Slow

Biomass is composed of organic or inorganic material, derived from living or recently living organisms [38]. Often times, biomass such as wood and agricultural residuals are referred to as lignocellulosic materials, which include the natural organic polymers cellulose, hemicellulose, and lignin

[39]. Other non-lignocellulosic materials like animal manure, industrial waste, and municipal solid waste can also be used as a biomass feedstock [40]; these also contain a mixture of organic and inorganic compounds, but are primarily composed of proteins, lipids, saccharides, and inorganics [41]. The species of biomass, growing condition, and geography of the region all factor into the proportions of the elements in a biomass, however its elemental composition is mainly a combination of carbon, oxygen, sulfur, and nitrogen [42]. Therefore, variation in the biomass polymeric composition directly influences the physicochemical properties of the biochar.

The heat treatment temperature (HTT), which is the highest temperature that a biomass is exposed to during thermochemical processing, is one of the most important parameters governing the physicochemical properties of the resultant biochar [43]. During thermochemical conversion, biomass undergoes a series of complicated and only partially understood chemical reaction mechanisms: decarboxylation, dehydration, de-carbonylation, de-methoxylation, intermolecular derangement, condensation, aromatization, etc. [44]. The HTT significantly governs which of these reactions dominates. As the temperature increases, degradation and depolymerization of the polymeric composition of the biomass occurs, resulting in a product with modified structural arrangements and surface functionalities, as well as, increased surface area, porosity, and extensive aromatic features.

Thermochemical processing of biomass also intrinsically drives out hydrogen [45] and oxygen [46], resulting in an increased percentage of carbon in the resultant biochar compared to the feedstock. Increased heating temperature and residence time further increase the biochar's carbon content [47]. Elemental analysis (O/C-H/C ratios), proximate analysis (ash and fixed carbon), and mineral matter characterization are all factors that must be considered when evaluating a biomass [39].

## **2.2 Electrical Resistivity**

### **2.2.1 Background**

The movement of charged particles is known as electric current, and the process by which it flows through a material is called electrical conduction. A material's electrical resistivity,  $\rho$  ( $\Omega\cdot\text{m}$ ) is its ability to oppose the flow of electrical current. Resistivity is determined by passing a current through a specimen of a known cross-sectional area and then measuring the resultant voltage drop over a specified distance. The reciprocal of electrical resistivity is electrical conductivity,  $\sigma$  (S/m), which measures how readily a material allows electric current to transport. The range of these two material properties is significant, as illustrated in Figure 2.1. Metals like silver and copper are very conductive, with values of  $10^7$  S/m, whereas an insulator like quartz is on the opposite side of the spectrum, with values around  $10^{-18}$  S/m.

Traditional, un-reinforced concrete is typically considered a poor semiconductor or an insulator, with conductivity measuring  $10^{-5}$  to  $10^{-8}$  S/m [48].

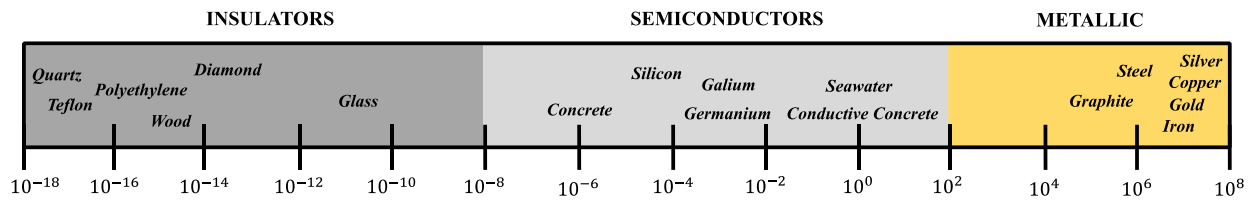


Figure 2.1 Electrical Conductivity of Common Materials (Values in S/m) (adapted from [49])

In conventional un-reinforced concrete, the conduction of electrical current is mainly electrolytic, meaning that the current is transferred via dissolved charged ions released during the dissolution of cement powder (mainly  $K^+$ ,  $Na^+$ ,  $OH^-$ , and to a lesser extent  $Ca^{2+}$  and  $SO_4^{2-}$  [9, 10]) and present in the saturated cement pores [11]. Consequently, the electrical resistivity of concrete is highly dependent on its microstructural characteristics, like capillary pore size distribution, volume, size, and permeability. As seen in case b in Figure 2.2, a more porous concrete microstructure with a greater degree of interconnectedness leads to higher permeability and a greater transport rate, yielding lower resistivity [50]. Therefore, mixture characteristics that influence the microstructure, such as water-cement ratio, presence of pozzolanic or polymeric admixtures, slag cement, air-entrainment, aggregate type, aggregate volume fraction, degree of consolidation, curing method, and cure age, all impact concrete resistivity [51]. To a lesser degree, concrete resistivity may also be dependent on environmental factors like moisture conditions and ambient temperature [52].

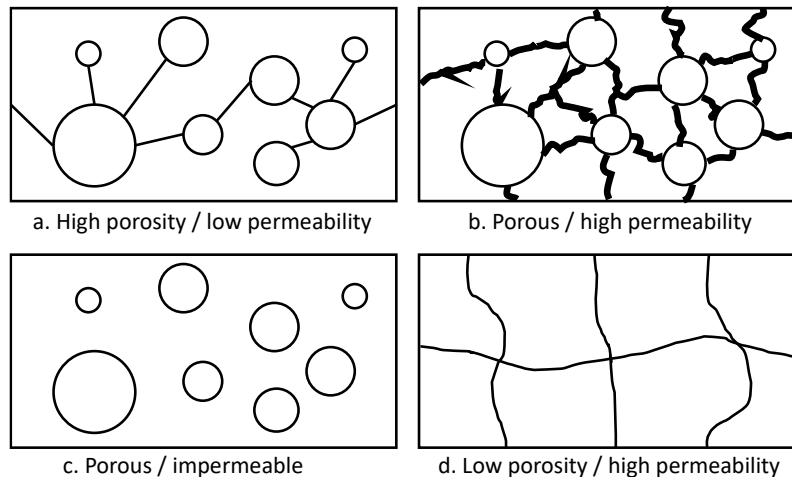


Figure 2.2 Differences between Porosity and Permeability (adapted from [53])

## **2.2.2 Electrical Resistivity Testing Methods**

In conventional unreinforced cementitious composites, electrical resistivity measurements can be used as an approximation of permeability, i.e. a durability assessment tool, because electrical charge is only carried via electrolytic conductivity; dissolved charged ions in the pore solution migrate more easily (higher conductivity) in more permeable composites. Cosoli et al. [54] provide a systematic review of the techniques for measuring the electrical resistivity of mortar and concrete elements and offer recommendations for approaching resistivity measurements. The two primary methods are briefly summarized below. As long as the appropriate geometry factor is accounted for, either method can be used and will yield comparable values [52].

### **2.2.2.1 Two-Probe Method**

The two-probe or "uniaxial" method is a non-destructive test mainly used in laboratory-based testing situations to measure bulk electrical resistivity. This method places a cylindrical concrete specimen between two parallel metal plate electrodes and moist sponge contacts. Once a current is applied, the resistance is computed from the drop in the voltage potential between the two electrodes [52]. A schematic of this testing method is seen in Figure 2.3(a) below. ASTM C1876-19 [55] is the only recognized test method for the bulk electrical resistivity of concrete.

### **2.2.2.2 Four-Point Method**

The four-point method, or more commonly known as the Wenner probe method, is also a non-destructive technique. A four-point setup measures surface resistivity by placing four linearly and equally spaced electrodes. This setup is preferred for in-situ testing since the probes can be placed on the surface of the concrete. Current is applied to the two outer electrodes, and the electrical potential (V) created across the two inner electrodes is measured [56]. A schematic of this testing method is seen in Figure 2.3(b) below. The American Association of State Highway and Transportation Officials (AASHTO) designation T358 [35], formerly designated as provisional standard TP 95, is the only recognized standard for surface resistivity testing.

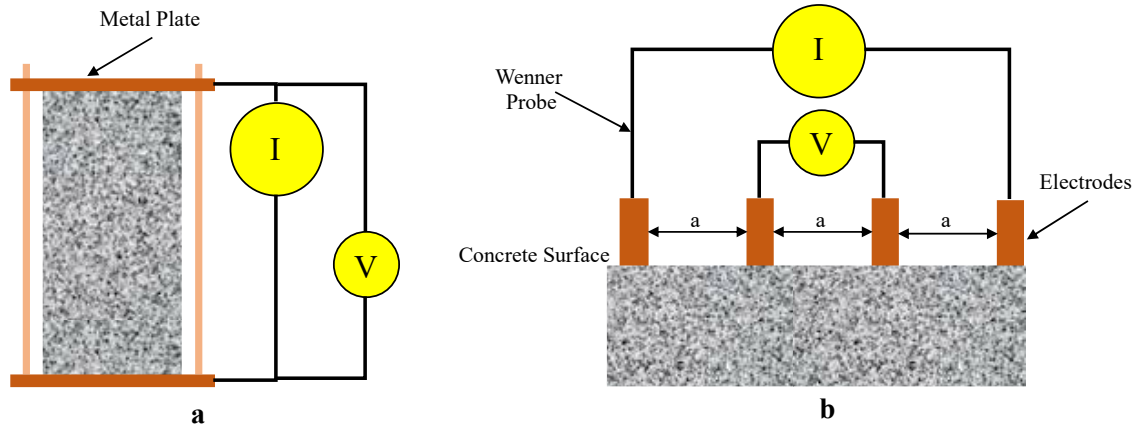


Figure 2.3 Schematic of (a) two-point uniaxial; and (b) four-point wenner (adapted from [52])

## 2.3 Conductive Concrete

Conductive concretes are cement-based composite materials synthesized by integrating conductive fillers into the concrete mix. Conductive concretes exhibit reduced electrical resistivity as the fillers develop a continuous, electrically conductive network within the cement matrix, shifting the conduction from electrolytic to electric. This mechanistic shift transfers electric current via conductive pathways in the bulk matrix rather than the pore network. Various materials have been studied and proven to provide conductive enhancement to cementitious mixes. The most popular have been microfibrinous materials like steel fiber and carbon fiber, due to their low cost, enhancement of mechanical properties, and high aspect ratio, which allows formation of conductive pathways at lower volumes [57]. However, nanomaterials like graphene are receiving increased attention for use in concrete since they not only enhance conductivity but also improve both mechanical properties and durability [58]. Recent research has produced conductive concretes with conductive measurements as low as  $10^0$  S/m through the use of steel fibers, carbon fiber, and graphite powder [59, 60, 61]. Due to biochar's high carbon content, it too can function as a conductive filler.

### 2.3.1 Factors Affecting Electrical Conductivity of Biochar

In an extensive review, Malijaee et al. [62] highlighted many of the key physical and chemical properties of biochar influencing the performance of cementitious materials and provided a roadmap for the proper selection of biochar as an SCM. However, this review did not investigate the factors that affect the electrical conductivity of biochar. Therefore, the present work provides insight into some of the biomass factors, thermochemical processing parameters, and biochar properties that influence biochar electrical conductivity and the conductivity of cementitious biochar composites.

Different carbon materials are formed according to the electronic orbital arrangement and crystallization modes of carbon elements, such as carbon black, carbon fiber, and graphene. Due to this regular arrangement of carbon atoms, carbon materials typically exhibit excellent electrical conductivity [63]. Many researchers have observed increasing biochar conductivity with increasing thermochemical processing temperature, achieving measurable electrical conductivity at an HTT of around 600 °C, a significant increase in the magnitude of conductivity between 600 °C to 800 °C, and a plateau in conductivity beyond 1000 °C [45, 47, 64-71].

While HTT appears to be the best indicator for biochar conductivity, carbon content [69, 72, 73], ash content [74, 75], volatile matter [72, 76], biomass source [73], and pyrolysis heating rate and residence time [69, 77] may contribute to changes in conductivity making it difficult to predict a biochar's conductive potential without direct assessment. The measurement set-ups found in studies performed by Gabhi et al. [72] and Giorcelli et al. [78] can provide researchers with a guide to perform DC conductivity measurements of their biochars.

### **2.3.2 Electrical Percolation**

In a comprehensive review of over twenty single and hybrid functional fillers, Wang and Aslani [57] concluded that the design of functional filler content should be mainly based on the percolation threshold theory. This statistical theory states that percolation, or connectivity, of the conductive filler throughout the cementitious matrix is required to achieve high electrical conductivity in cementitious composites. This means that the volume fraction of the filler should be equal to or greater than the value required to form a continuous path of filler touching one another. The range of filler content at which electrical conductivity increases is the percolation threshold, and using conductive fillers beyond this optimum content is costly without benefit [79].

## **2.4 Electrical Resistivity Assessment of Biochar Cementitious Composites**

So far, only seven experimental studies [13-20] have investigated the electrical resistivity of BC cementitious composites. Other than Yang and Wang [19] each of these studies observed decreased resistivity of their cementitious composites as BC content increased. These studies conclude that due to the high carbon content of BC, it must act as a conductive inclusion in the bulk matrix. Yet, only one study directly measures the conductivity of their BC [17] and three of these studies do not even report carbon content [13, 17, 18]. Cementitious composites that incorporate conductive materials can display both electrolytic conductivity and electric conductivity. However, resistivity measurements cannot distinguish between these conductive pathways; thus, decreased resistivity could be interpreted as either increased permeability (increased electrolytic conduction) or increased electrical conductivity (via a

network of conductive inclusions). Obtaining the conductivity of the biochar itself, as discussed in section 2.3.1, is important for discerning these effects, since we certainly would not expect a non-conductive filler to improve the electrical conductivity of the bulk matrix. In this case, any decreases in concrete resistivity would be attributed to increased pore connectivity or porewater ionic strength, which is again not the targeted outcome for a conductive concrete.

#### 2.4.1 Biochar Percolation Threshold

As discussed in section 2.3.2, the design of electrically conductive filler content should be mainly based on the percolation threshold theory [57]. The change in magnitude of conductivity is typically plotted against volume percentage of conductive filler. Only the Jeong et al. study [17] considered in this review reported the percolative behavior of their waste coffee powder biochar cementitious composites. However, instead of reporting volume percentage, they reported the percolation threshold of their biochar cementitious composites as a function of biochar wt%, noting that the threshold was between 0.02 and 0.05 wt.%. These data are reproduced as a function of biochar volume percentage in Figure 2.4, along with the data from Khan et al. [13]. While Khan et al. do not report a percolation threshold, by assuming a biochar density of  $2 \text{ g/cm}^3$  and converting reported biochar weight percentages into volume percentages, normalized by paste volume (assuming a double in volume from anhydrous to hydrous cement) we are able to approximate a comparison between the two studies. The other studies which evaluated electrical resistivity are not included in this figure, since there was not a large increase in conductivity compared to their reference mortars.

The conductivity of the specimens in the Jeong et al. [17] study increases nearly eight orders of magnitude despite a fractionally low, total volume fraction of about 0.1% biochar. Also, the concrete specimens of the Khan et al. [13] study see a noticeable increase of conductivity at a volume fraction of around 0.7% biochar inclusion.

**Research Gap:** Existing studies conclude that biochar acts as a conductive filler material due to decreased resistivity in mortars; however, none of these studies have separated the effects from electrolytic conductivity and electric conductivity on electrical resistivity measurements. Thus, it is equally likely that the biochar increases conductivity via changes to pore microstructure and/or chemistry, which could result in increased permeability and decreased durability. A more thorough investigation that separates electrolytic and electric contributions to conductivity is needed to evaluate the efficacy of resistivity measurements as a durability assessment tool for predicting permeability in biochar cementitious composites.

An ancillary benefit of this thesis, is that it's the first to evaluate existing geometric models for percolation threshold as a predictive tool to produce conductive biochar cementitious composites.

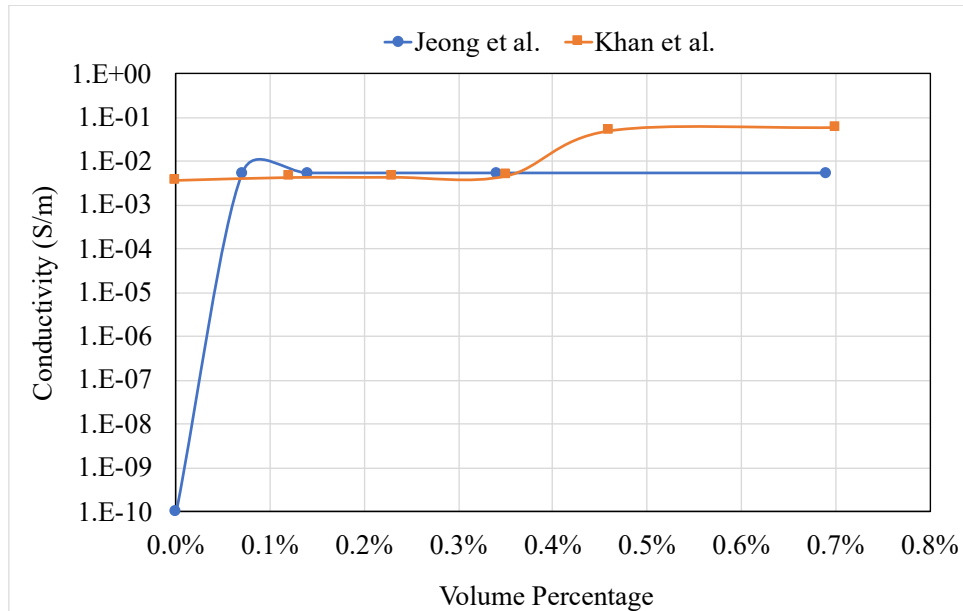


Figure 2.4 Percolation threshold of biochar cementitious composites

## 2.5 Frost Durability

The frost durability of concrete is its ability to prevent deterioration caused by repeated freezing and thawing (FT) cycles. Frost damage occurs when concrete is exposed to both water and freezing temperatures. The two different types of deterioration due to frost damage are recognized as surface damage and internal damage [80]. Internal frost damage, the focus of the present work, is caused by the progressive expansion of the cement paste matrix from repeated freezing and thawing cycles [21]. The mechanisms by which internal frost damage occurs in the cement paste are discussed in further detail in the next section.

### 2.5.1 Mechanisms of Internal Frost Damage in Concrete

The internal deterioration of concrete under FT cycles evolves through three stages: water penetration, water freezing, and internal structural failure [24]. Although water is essential for the hydration of cement, it is also an agent of deterioration. Water initially exists in the hydrated cement paste in several forms: 1) capillary water; 2) adsorbed water; 3) interlayer gel water; and 4) chemically combined water [81]. It is also classified depending on the degree of ease in which it can be removed. “Non-evaporable” water is considered what remains in a sample of hardened cement paste after oven-drying to 105 °C, a rough approximation of the quantity of chemically combined water. But, depending on the paste’s permeability, some amount of gel water can be included. Whereas, the remaining water (capillary + adsorbed) removed by oven-drying is referred to as “evaporable” water. The amount of evaporable water

remaining in concrete in-service depends on the ambient environmental conditions and will usually leave the concrete pores in some saturation state [82]. It is this evaporable water that is freezable and makes concrete vulnerable to water-related destructive phenomena [21]. The water in gel pores cannot freeze because they are too small to allow the nucleation of ice crystals [83]. Subsequent exposure to moisture can also cause resaturation of the pores depending on the permeability of the concrete [21]. External water also enters concrete through cracks, which can develop as minor and superficial plastic shrinkage cracks formed in fresh concrete or wide and deep cracks formed in hardened concrete due to direct overloads or due to stresses produced by humidity or thermal gradients [22].

In the second stage, when the ambient temperature drops slightly below the melting point of water ( $0^{\circ}\text{C}$ ), a portion of the freezable water will freeze. The lower the temperature, the greater the amount that will freeze [26]. Finally, internal structural failure results from the movement of water and the growth of ice crystals in the pores of the cement paste. As ice crystals form from the water in saturated capillary pores, a volumetric dilation of  $\sim 9\%$  occurs, displacing the surrounding unfrozen water [84]. The force generated by the displacement of unfrozen water through the porous cement paste matrix generates a hydraulic pressure governed by Darcy's law. Internal damage results when this frictional resistance is large enough to exceed the tensile strength of the concrete [25, 26]. The growth of ice crystals in the pores also exerts crystallization pressure, generating outward stresses into the pore wall as the ice crystal attempts to grow [85, 86].

### **2.5.2 Testing and Evaluation of Frost Durability**

Internal frost damage to concrete is routinely evaluated per ASTM C666 [34]. In this test method, concrete samples are cured for 14 days and then subjected to rapidly repeated cycles of freezing and thawing. This is accomplished by alternately lowering the temperature in a chamber from  $4$  to  $-18^{\circ}\text{C}$  and raising it from  $-18$  to  $4^{\circ}\text{C}$  in not less than 2 hours nor more than 5 hours. The test is complete when either 300 FT cycles have been completed or when the relative dynamic modulus of elasticity (RDME) of the sample reaches 60% of the initial modulus. RDME is used to evaluate the frost resistance because when concrete is exposed to FT cycles, it gradually loses its elastic performance (stiffness), leading to the loss of dynamic modulus of elasticity and the reduction in strength [87].

### **2.5.3 Frost Durability Enhancement Measures**

Three mechanisms contribute to enhanced internal FT durability: (a) improved internal pore system; (b) reduced water absorption; and (c) controlled crack resistance. These mechanisms are mainly achieved by incorporating air-entraining admixtures (AEAs), supplementary cementitious materials (SCMs), or

fibers [24]. However, it is well established that the best way to prevent internal cracking is to ensure that the hardened concrete has an adequate system of entrained air voids, incorporated via AEAs [80].

## **2.6 Air Entrainment in Concrete**

Air entrainment is the process by which numerous, small air bubbles are intentionally integrated and dispersed throughout the concrete paste matrix. This effect is achieved by using an air-entraining admixture, a surfactant-based solution that is added to the fresh concrete mixture to promote air bubble formation and stabilization [28]. Surfactants (surface active agents) are amphiphilic molecules consisting of a hydrophilic head and hydrophobic tail, usually a long hydrocarbon chain [88]. The surfactant type is based on the chemical nature of the hydrophilic head, which can be differentiated into: anionic (-), cationic (+), amphoteric (+/- depending on pH), or anionic (no charge) [88]. The majority of modern AEAs in concrete are anionic because of their low cost and proven compatibility with cementitious systems [89]. Surfactants are efficient air entrainers because they adsorb at the air-liquid interface of bubbles and reduce the surface tension by disrupting the cohesive forces between adjacent liquid molecules [90].

### **2.6.1 Effects of Air Entrainment on Frost Resistance**

As discussed in section 2.5.1, internal frost damage results from either hydraulic pressure or crystallization pressure due to the movement of water and growth of ice crystals in the capillary pores of the cement paste. Based on the work of Powers [26, 91], the effectiveness of an entrained air system depends on the void spacing. This spacing factor ( $\bar{L}$ ) is based on the assumptions that the size of spheres and their spacing is uniform. The maximum value of the spacing factor is usually taken as 0.20 mm to ensure safe FT durability [92].

### **2.6.2 Factors Affecting Air Entrainment**

As Whiting and Stark [93] documented, all aspects of the concrete construction process affect the ability to achieve adequate control of air content. They grouped these variables into five major categories: 1) concrete materials, 2) concrete mix design, 3) production procedures, 4) construction practices, and 5) environmental conditions. One particularly problematic interaction is incompatibility with superplasticizers, which are designed to improve the workability of the concrete by making the mixture more fluid [94]. However, since sufficient viscosity of the matrix to counteract bubble buoyancy is a critical requirement of bubble formation and stabilization [95], an increase in superplasticizer dosage has been observed to result in air loss and an increase in spacing factor [94, 96-98]. This may also be problematic when biochar is introduced into air-entrained mixes, because its porous microstructure

promotes water retention during the mixing stage, leading to a loss of workability which necessitates incorporation of superplasticizer [99]. To prevent additional water in the mix during the mixing stage, numerous researchers have recommended that concrete mixes with biochar have higher superplasticizer dosage to achieve a similar slump as control mixes [100-104].

### **2.6.3 Testing and Evaluation of Air Entrainment in Concrete**

The testing and evaluation of air entrainment in concrete has been traditionally based on the total air volume in fresh concrete. Despite recent advancements, current specifications still rely on the measurement of total volume of air as outlined in standards like American Concrete Institute's Building Code Requirements for Structural Concrete, ACI 318-19(22) [7], which are based on the work done by Klieger [105, 106]. The standard is established based on assumptions for paste contents and one type of AEA. It is recommended that air content of concrete be in the range of 3 to 7% depending on the size and type of aggregates and the severity of the exposure conditions. The three methods proposed by ASTM for assessment of total air content (entrained + entrapped air) in fresh concrete, are the pressure method (C231 [107]), the volumetric method (C173 [108]), and the gravimetric method (C138 [109]). All the methods measure only air content, but not other parameters. Moreover, these test methods cannot differentiate between desirable entrained air and undesirable entrapped air [23]. Recent research on concrete mixtures prepared with modern AEAs suggests that the minimum air content could be as low as 3.5% and still yield durable concrete [98]. The air content and the specific surface, void frequency, and spacing factor of the air-void system in hardened concrete can be directly measured per the procedures of ASTM C457 [92]. The test method describes three different procedures for microscopical determinations of the air void system, which are commonly executed by a computerized apparatus, with image analysis.

### **2.6.4 Experimental Study on Frost Resistance of Air Entrained Concretes**

The development of an adequate, entrained air void system is essential for protection against frost damage. This is well-illustrated by the work of Malhotra [97], who investigated the frost resistance of non-air-entrained, air-entrained, and air-entrained+superplasticized concrete using ASTM C666 [34]. The water-to-cement ratio of the mixes ranged from 0.35 to 0.70. He found that regardless of w/c ratio, the non-air-entrained concrete samples (plain) had very low DF (<31), however, when air-entrained, all samples displayed high DF (>90). In the case of the air-entrained superplasticized (AEA & SP) concrete at a 0.70 w/c ratio, the bubble spacing factor was higher than the recommended 0.20 mm, but still retained a high DF (97) as well. His results show that w/c ratio is not a strong predictor for DF of air-entrained samples.

## 2.7 Biochar Concrete and Frost Resistance

There is limited study on the durability performance of cementitious composites incorporating biochar as most researchers have focused on mechanical performance [29], [30]. The long-term performance of concrete exposed to harsh environments is largely unknown [110]. Only three [31, 32, 33] publications have investigated the effect of biochar on the FT properties of concrete, none of which incorporated air entrainment. The two studies, [31] and [32], are not discussed in further detail because their conclusions are based only on compressive strength after FT exposure rather than a standardized assessment of RDME like in ASTM C666, which limits their applicability to this analysis. On the other hand, Chen et al. [33] integrated surfaced-treated pine-nut-shell biochar as a cement replacement in concrete at dosages up to 9% by weight. They reported that the incorporation of pre-soaked biochar dosages lower than 5% had better freeze-thaw resistance compared to the control. Although this study reported RDME like ASTM C666, the samples were not submerged in water for the freezing phase and were only subjected to 12-hour long FT cycles, whereas ASTM C666 procedure A requires freeze and thaw of samples in water and freeze thaw cycles are much more rapid (<6 hrs).

***Research Gap:** While other researchers have concluded that biochar has no discernable effect on the frost durability of concrete, it is unclear if the improvement is due to less paste or to other intrinsic properties of the biochar. Additionally, no one has evaluated air-entrained biochar concrete. Since air-entrainment is a requirement for concretes in environments experiencing freeze-thaw, this missing foundation is a critical gap that warrants further investigation. For biochar to be adopted as a construction material, a satisfactory frost durability must be ensured.*

### 2.7.1 Biochar Surfactant Interference

There is no existing literature on biochar interaction with AEAs used in concrete. However, it is well known that the carbon in fly ash interferes with AEA efficacy [111, 112, 113]. Additionally, biochar has been researched as an adsorbent in wastewater treatment for environmental contaminants [114], which can coexist with surfactants that are widely used in household cleaning detergents, personal care products, textiles, paints, pesticide formulations, and pharmaceuticals [115]. Several studies have found that the presence of cationic, anionic, and nonionic surfactants can interfere with the adsorption ability of biochar [116, 117]. For example, when biochar, an anionic and antibiotic molecule were combined in an aqueous solution, the non-polar groups on biochar and anionic surfactants had strong hydrophobic attraction, significantly decreasing biochar adsorption capacity for the antibiotic molecules [118]. Given that biochar has shown to interact strongly with the hydrophobic groups on surfactants, it is likely that carbonaceous biochar will also interact strongly with AEAs similarly to fly ash, thus necessitating higher dosages to attain adequate air-entrainment.

**Research Gap:** *The efficacy of air-entraining admixtures with biochar has not yet been explored, and there is a need to assess if higher dosages will be required to attain adequate air-entrainment in biochar concrete to provide adequate frost protection.*

## CHAPTER 3 ELECTRICAL RESISTIVITY AS A DURABILITY ASSESSMENT TOOL OF BIOCHAR CEMENTITIOUS COMPOSITES

### Abstract

This chapter investigates the bulk electrical resistivity of biochar cement mortars at increasing levels of cement replacement with biochar. Several studies conclude that biochar acts as a conductive inclusion in cementitious composites based on the evidence of decreased bulk resistivity with increasing biochar loads; however, decreased resistivity can result from both increased electrolytic conduction via ions in the pore solution and increased electrical conductivity via the percolation of conductive inclusions. This work evaluates the efficacy of biochar as a conductive filler by directly measuring biochar conductivity in addition to measuring the permeability and resistivity of biochar-cement mortars. Four distinct biochars were evaluated at cement replacement levels of 5, 10, and 15 wt% to assess the potential for conductivity at typical volume incorporations of biochar. At these loadings, only one type of biochar resulted in a composite with decreased resistivity compared to the control. Although bulk resistivity measurements would suggest that this biochar can act as a conductive filler, further analysis indicates that the decreased resistivity is actually due to changes in electrolytic conductivity, resulting from changes in the cement pore solution. To ensure that sufficient biochar was included to create a percolating network capable of electric conduction, a geometric model was used to predict that a 27% volume fraction (or 27-43 wt%) of biochar would be necessary to form a conductive network. At the predicted percolation threshold of 27 vol%, two of the biochars acted as conductive inclusions, reducing the electrical resistivity of the cementitious composite through electric conduction.

### 3.1 Introduction

Historically, concrete durability provisions codified in industry standards like the American Concrete Institute's 318, *Building Code Requirements for Structural Concrete* [7] relied on prescriptive limitations like the water-to-cement ratio (w/c) and compressive strength. Generally speaking, as w/c decreases, permeability decreases. This typically results in a stronger, more durable concrete, since the penetration of aggressive media is inhibited. However, driven by calls for more sustainable concrete, modern mix designs often integrate various supplementary materials and admixtures; and a wide variation in permeability is now often observed at the same w/c [8].

Electrical resistivity is one of the ways concrete permeability can be measured. In conventional unreinforced concrete, the conduction of electrical current is mainly electrolytic, meaning that the current is transferred via dissolved charged ions ( $\text{Ca}^+$ ,  $\text{K}^+$ ,  $\text{Na}^+$ ,  $\text{SO}_4^{2-}$ , and  $\text{OH}^-$  [9], [10]) released during the dissolution of cement powder and persisting in the cement pore solution [11]. Consequently, the electrical

resistivity of concrete is highly dependent on microstructural characteristics, like capillary pore size distribution, volume, and connectivity. A higher resistivity typically indicates a finer pore network with less connectivity, features that correlate with low water permeability [6]. Assessing concrete's permeability via resistivity measurements is appealing because it allows for non-destructive, in-situ monitoring of existing concrete structures.

However, these methods require additional considerations when applied to conductive concretes. Driven by the demand for multifunctional construction materials, in recent years considerable attention has been given to the development of electrically conductive cementitious composites. The uses of this special class of concrete are wide-ranging, from de-icing applications [79], [119], electromagnetic interference, shielding effectiveness [120], and structural health monitoring [121]. These conductive composites exhibit both electrolytic and electric conductivity, but bulk resistivity measurements are not able to distinguish these conductive pathways. Thus, decreased resistivity could be interpreted as either increased permeability (increased electrolytic conduction) or increased electrical conductivity (via a network of conductive inclusions). To achieve significant decreases in resistivity within a cementitious composite, electrically conductive components must be integrated into the cementitious matrix [57]. At the percolative threshold, an electrically conductive network is formed as the components reach a volume fraction necessary to make contact, leading to a reduction in resistivity of several orders of magnitude. This mechanistic shift transfers electric current via conductive pathways in the bulk matrix rather than the pore network.

Since the electrical conductivity of cementitious composites is affected by electron transport through both the pore network and bulk matrix, demonstrating the efficacy of a conductive filler requires demonstration that the electrical conductivity of the bulk matrix is increased. Else, an increase in electrical conductivity could be caused by increased pore connectivity, which is associated with increased permeability and decreased durability of the cementitious composite. Obtaining the conductivity of the conductive filler itself is important for discerning these effects, since a non-conductive filler cannot improve the electrical conductivity of the bulk matrix. In this case, any increases in concrete conductivity would be attributed to increased pore connectivity or increased ionic strength of the porewater.

Various materials are able to increase the conductivity of cementitious mixes. The most popular are microfibrous materials like steel fiber and carbon fiber, which form conductive pathways at low incorporation volumes thanks to the high aspect ratio of the fibers [57]. Waste products, like copper slag [122] have also been identified as suitable conductive fillers while providing the additional benefit of decreasing the concrete's carbon footprint. However, nanomaterials like graphene are receiving increased attention for use in concrete since they not only enhance conductivity but also improve mechanical properties and durability [58]. Carbon-based materials typically exhibit excellent electrical conductivity

due to the regular arrangement of carbon atoms [63]. Biochar (BC), a carbon-rich material obtained from the thermochemical conversion of biomass in an oxygen-deprived environment [3], offers multifold potential benefit for conductive concretes, such as increased conductivity, decreased permeability [110], and decreased carbon footprint [4]. BCs typically begin to achieve measurable electrical conductivity at thermochemical conversion temperatures of around 600 °C, a significant increase in the magnitude of conductivity between 600 °C and 800 °C, and a plateau in conductivity beyond 1000 °C [45, 47, 64-71]. Several publications [13-20] have studied the electrical resistivity of BC cementitious composites. Other than Yang and Wang [19] each of these studies observed increased conductivity of their cementitious composites as BC content increased. These studies conclude that the BC must act as a conductive inclusion in the matrix. However, only one study directly measures the conductivity of the BC [17] and none separate the effects of BC on electrolytic versus electric conductivity; thus, it is equally likely that the BC increases conductivity via changes to pore microstructure and/or chemistry, which could result in increased permeability and decreased durability.

### **3.1.1 Research Objective**

The objective of this study is to investigate the bulk electrical resistivity of biochar cement mortars as a function of cement replacement with BC. This work aims to separate electrolytic and electric conductivity by characterizing changes in water permeability and permeable pore space, and by directly measuring the conductivity of the BCs. Additionally, this work applies percolation threshold theory to predict the volume of BC required to form an electrically conductive network. This study focuses on cement replacement levels ranging from 5-43 wt%, which spans both commonly reported cement replacement limits (after which strength decreases are commonly observed) and the predicted percolation threshold volume.

## **3.2 Materials & Methods**

### **3.2.1 Biochar**

#### **3.2.1.1 Feedstock and preparation**

Four different feedstocks were used to produce the biochar in this study: Mixed wood species (MW), Pistachio Shells (PS), Walnut Shells (WS), and Olive Pit (OP). The pyrolyzed product, biochar (BC), was provided by three different manufacturers. The pyrolysis processing parameters: heat treatment temperature (HTT), heating rate, and residence time used to produce each BC are summarized in Table 3-1.

Table 3-1 Biochar feedstock & pyrolysis parameters

Biochar	Feedstock	HTT (°C)	Heating Rate	Residence Time
MW	Mixed Wood Species	700	Slow	10 m
PS	Pistachio Shells	1100	Fast	4 s
WS	Walnut Shells	800	Slow	<5m
OP	Olive Pit	800	Slow	<5m

### 3.2.1.2 Biochar characterization

To integrate the BCs into the cementitious composites, they were first milled in a Retsch RS 300 vibratory disc mill for three minutes. After milling, a Microtrac S3500 laser particle size analyzer was used to measure the effective particle size, d50, of BC in isopropanol. The refractive index of each BC sample was set at 2.42. The particle size distribution of each biochar, as compared to a Type I/II ordinary Portland cement (OPC), is shown in Figure 3.1.

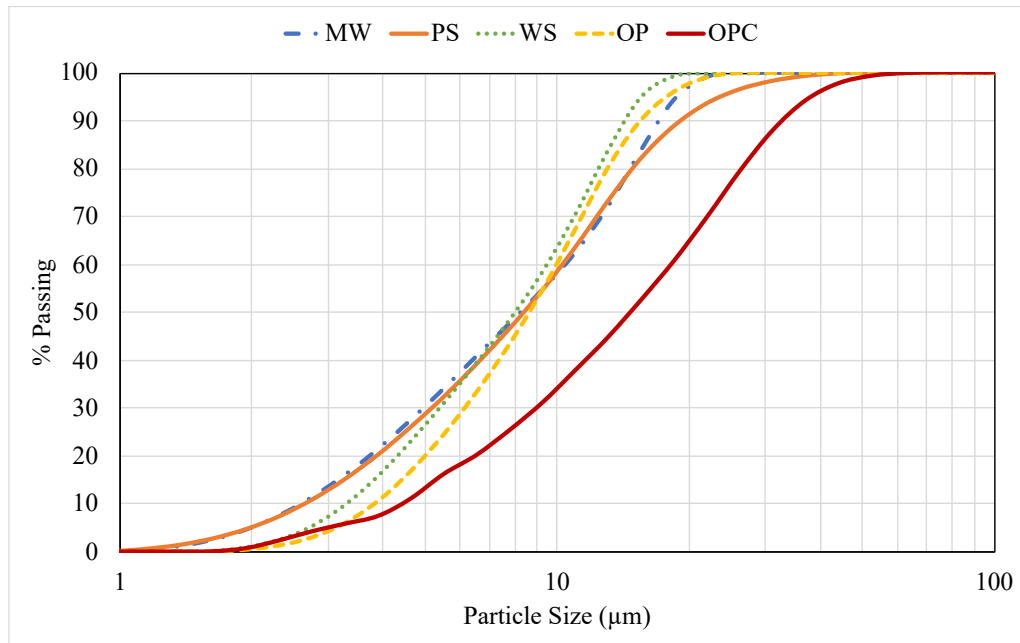


Figure 3.1 BC particle size distribution compared to OPC

The skeletal density of the milled BC was measured using a Micromeritics AccuPyc II with helium as the displacement medium without additional sample preparation steps. The density measurement was

conducted by averaging five cycles of pressurized inlet gas into a known volume and sample mass. The bulk density of the milled BC was determined by filling a pycnometer cylinder of known volume with BC without applying any compaction and measuring the mass five times consecutively. After each set of measurements, the cylinder was emptied, cleaned, and refilled. This process was repeated two more times, resulting in 3 total measurements. The bulk density ( $\rho_B$ ) reported in Table 3-2 the average of three density measurements, calculated as the mass of BC divided by the volume of the container.

Each BC used in this study was stored in closed buckets from the time of milling until use. Since these containers permit some exposure to the ambient atmosphere, the ambient moisture content of the BC was measured and accounted for in the mortar mix designs as a component of the total water content. Using a PerkinElmer TGA 8000, 5-20 mg of the biochar was heated under a nitrogen flow to 105 °C at 10 °C/min and isothermally held until the weight stabilized, typically under 60 minutes. The mass loss that occurred during this thermal program was taken as the in-situ moisture content of the biochar.

Per ASTM D7582 [123], proximate analysis was conducted using a LECO TGA and ceramic crucibles. The volatile matter, fixed carbon content, and ash content were reported as the wt% of the dry char (dry basis) to compare all chars without the influence of variable ambient moisture. Ultimate analysis was run on each biochar to determine the carbon, hydrogen, nitrogen, and sulfur mass percentages. . Oxygen content was reported as the difference between the carbon, hydrogen, nitrogen, sulfur, and ash content. The physical and chemical characteristics of the biochar used in this study are reported in Table 3-2.

Table 3-2 BC characteristics

BC	d50 ( $\mu\text{m}$ )	Skeletal Density ( $\text{g}/\text{cm}^3$ )	Bulk Density ( $\text{g}/\text{cm}^3$ )	Moisture Content %	Ash Content %	Volatile Matter %	Fixed C%	C%	H%	N%	S%	O%
MW	8.24	2.68	0.768	4.95	76.6	19.9	3.52	12.1	0.8	0.10	0.40	10.0
PS	13.7	1.94	0.465	6.26	3.40	17.3	84.9	73.0	2.2	1.40	0.10	19.9
WS	8.01	1.75	0.490	11.3	4.21	5.00	90.8	78.3	2.4	0.55	0.11	14.4
OP	8.73	1.88	0.451	11.7	4.57	7.74	88.2	74.8	2.3	0.40	0.09	17.8

### 3.2.2 Mortar

The mortars in this study utilized a Type I/II cement conforming to ASTM C150 [124] and a silica/quartz ASTM C778 [125] graded sand with a specific gravity of 2.65 and maximum size of 0.595 mm (No. 30 sieve).

### 3.2.3 Mix Design and Preparation

#### 3.2.3.1 Mix Design

A total of 13 mortar mixes including a control mix (plain mortar with no biochar, ‘REF’) were initially prepared for this study. The cement was replaced with each BC at 5, 10, and 15 wt% (BC5, BC10, and BC15, respectively). These BC loadings were chosen to evaluate the conductive potential of BC at commonly incorporated levels [16], [19], [103], [126]. All mortars were prepared with the same water-to-cement ratio (w/c) of 0.45 to ensure that variations in water content did not impact the permeability characteristics of the mortars. The biochar was not considered part of the cementitious content in this calculation. The sand-to-cement plus BC ratio was 2.75 by volume. The mix proportions are provided in Table 3-3.

Table 3-3 Mortar mixture proportions (g)

Sample	OPC	BC	Sand	Water
REF	1000	0	2,230	450
BC5	950	50	2,230	427.5
BC10	900	100	2,230	405
BC15	850	150	2,230	382.5

Cement, sand, and BC were dry-mixed for 2 minutes. Then water mixed with superplasticizer was slowly added and mixing was continued for another 4 minutes until a homogeneous mix was achieved. Before casting, the workability of the blended mortars was characterized using ASTM C1437 [127] to measure the flow of the mortar. The average values of the spreading diameter (mm) are reported in Table 3-4. To maintain a similar flow to the control, a polycarboxylate-based high range water reducing and superplasticizing admixture (SP) (Sika®ViscoCrete®-2100) was used at 3-8% of the BC weight.

Table 3-4 Superplasticizer dosage (wt% of BC) & wet mix flow (mm)

Sample	REF	MW5	MW10	MW15	PS5	PS10	PS15	WS5	WS10	WS15	OP5	OP10	OP15
SP	0	4.5	3.6	4.8	7.3	6.8	6.6	5.1	5.0	7.0	6.2	6.1	7.9
Flow	99	95	107	94	110	112	93	96	98	89	96	99	105

### 3.2.3.2 Percolation Threshold Mix Design

The electrical performance of conductive cementitious composites is dependent on the formation of a continuously conductive network within the matrix, which occurs when the filler is included at volumes at or above its percolation threshold [57]. Therefore, we theorized that given the BC's relatively low bulk density and high porosity, a higher volume fraction than previously studied might be required to achieve an interconnected conductive network. In the present study, the volume fraction required for percolation in cement mortars was estimated from a geometrical model of percolation developed by Garboczi et al. [128]. This model assumes that filler particles can be approximated as ellipsoids of revolution and predicts the volume fraction of particles at percolation values ( $p_c$ ) based on a given aspect ratio ( $a/b$ ), where  $a$  is the length of the symmetry axis and  $b$  is the length of each axis perpendicular to the symmetry axis.

As all the BCs had very similar particle size distribution (Figure 3.1), the OP BC was selected for analysis, since it is the most conductive. A TESCAN S8000G scanning electron microscope was used to measure the aspect ratio of the milled OP BC particles and determined to be 1.74. Using the geometrical data from Garboczi et al. [128], we predicted that the volume fraction of BC required to create a conductive network corresponds to a volume fraction of 27.1% at percolation. Given the water demand challenges posed by such high BC incorporation [100], [101], [103], [104], [129], [130], [131], the mix design was amended from using a constant w/c ratio of 0.45 to a water-to-binder (w/b) ratio of 0.45, where both the cement and BC were considered binders. As the most conductive BC, a percolation mix was also made for the OP BC at a w/b of 0.38. Further details on this approach are discussed in section 3.3.4. The 5 additional mortar mixes were then prepared using the mix proportions provided in Table 3-5. To compare the mixes in Table 3-3 and Table 3-5, we focused only permeability as a function of bulk electrical resistivity.

Table 3-5 Mortar mix design proportions to achieve BC percolation

BC	wt% replacement	w/b	w/c	SP:BC	Flow
MW	43.0%	0.45	0.79	0.40%	94
PS	26.6%	0.45	0.61	0.0%	116
WS	28.0%	0.45	0.63	2.0%	102
OP-1	25.9%	0.45	0.61	0.0%	112
OP-2	24.8%	0.38	0.50	0.5%	94

### 3.2.3.3 Casting & Curing

Each mortar mix was cast in 50-mm cubic brass molds to evaluate variation in electrical resistivity as a function of biochar type and replacement amount. The mix was also cast in disposable cylinder molds (102 mm (d) by 203 mm (h)) to test for variation in permeability and void volume. Fresh mortar was placed in two layers, manually compacting with a dowel rod in between layers. The cast specimens were placed on a vibration table for 10 minutes to attain sufficient compaction. The cubic molds were covered in plastic wrap (Saran®). All cast specimens were initially cured under ambient conditions (at about 23°C and 25% relative humidity) until demolding 24 hours after casting. Subsequently, hardened mortar samples were placed in a saturated calcium hydroxide (limewater) bath for 28 days of wet curing at room temperature.

### 3.2.4 Experimental Methods

The objective of this study was to investigate the bulk electrical resistivity of biochar cement mortars as a function of cement replacement with BC. This goal was accomplished by separating the effects of electrolytic and electric conductivity by characterizing changes in water permeability and permeable pore space, and evaluating the conductive potential of the BCs. Additionally, the conductivity of the pore solution was considered to evaluate effects to electrolytic conductivity. Figure 3.2 provides an outline of the experimental plan to investigate these research tasks.

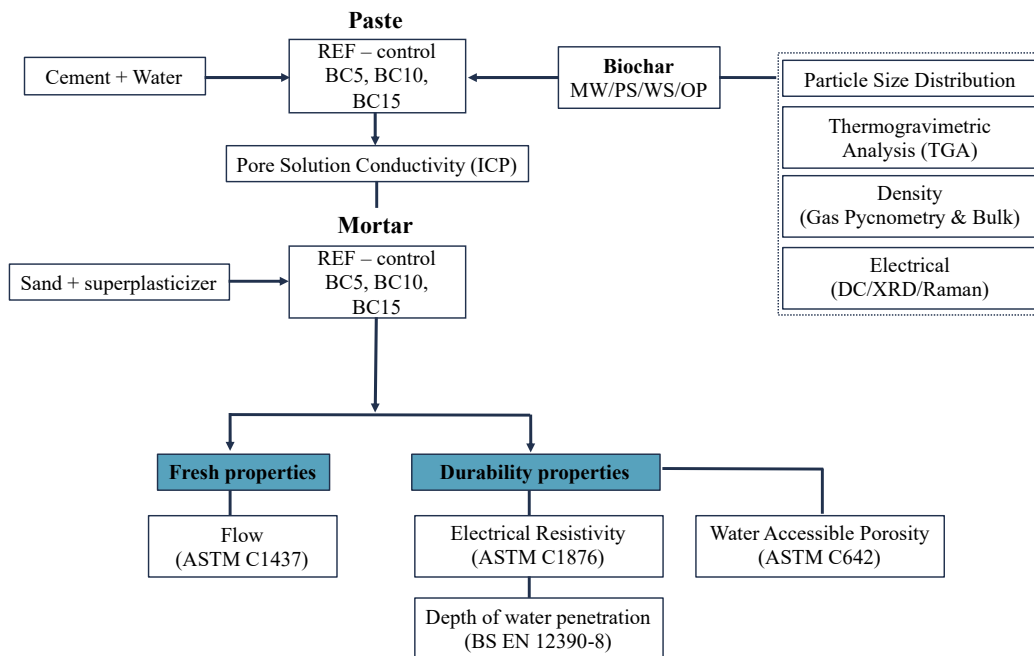


Figure 3.2 Experimental tasks to evaluate BC mortar electrical resistivity and permeability; and BC electrical properties

### 3.2.4.1 Biochar Analysis

#### 3.2.4.1.1 Electrical Conductivity

To measure the electrical conductivity of the BC powders, the material was first pelletized (Figure 3.3a) using a Carver bench top manual hydraulic press with 1500 bar of forming pressure. It is necessary to first pelletize the BC because the electrical conductivity is dependent on the effective contact between carbon particles [72]. Electrical conductivity was measured using the setup shown in Figure 3.3b, derived from Giorelli et al. [132]; two solid copper cylinders, 25.4 mm in diameter and 7.62 cm in length, were encapsulated in a hollow Plexiglass cylinder with a nominal inner diameter of 26 mm. With a slightly larger inner diameter the copper rods are able to fit inside the Plexiglas cavity and slide. This arrangement forms an internal chamber between the two copper cylinders, where the BC pellet was inserted. Electrically insulated sheets, composed of 3-mm-thick plexiglass and 3-mm-thick rubber sheets were placed between the copper cylinders and the load surfaces of a smaller hydraulic press, which was used to keep constant pressure between the two cylinders (Figure 3.3c). The resistance of the BC fillers was measured using a Siglent SDM3065X multimeter. The conductivity of the BC was then calculated from the resistance using Equation 3.1:

$$\sigma = \frac{1}{\left(\frac{R \times A}{L}\right)} \quad (3.1)$$

where  $\sigma$  is the BC conductivity (S/m),  $R$  is the BC resistance ( $\Omega$ ),  $A$  is the surface area ( $\text{m}^2$ ) of each copper electrode, and  $L$  is the distance (m) between the two copper electrodes measured as the thickness of the BC pellet.

#### 3.2.4.1.2 Degree of graphitization and crystallization

The degree of graphitization and crystallinity of the BCs were examined via X-ray diffraction (XRD) patterns obtained from monochromatic  $\text{CuK}\alpha$  radiation (Malvern Panalytical Empyrean) at 45 kV and 40 mA between  $5^\circ$  and  $60^\circ$  ( $2\theta$ ) at a scanning rate of  $0.0286^\circ/\text{s}$  ( $2\theta$ ). The diffraction patterns were analyzed using HighScore Plus software from PANalytical. Raman spectroscopy was used to further characterize the structural features of the BC. Raman measurements were performed from 200 to  $4000 \text{ cm}^{-1}$  at room temperature using a WITec (alpha300 R) Raman microscope equipped with a 514-nm laser excitation source.

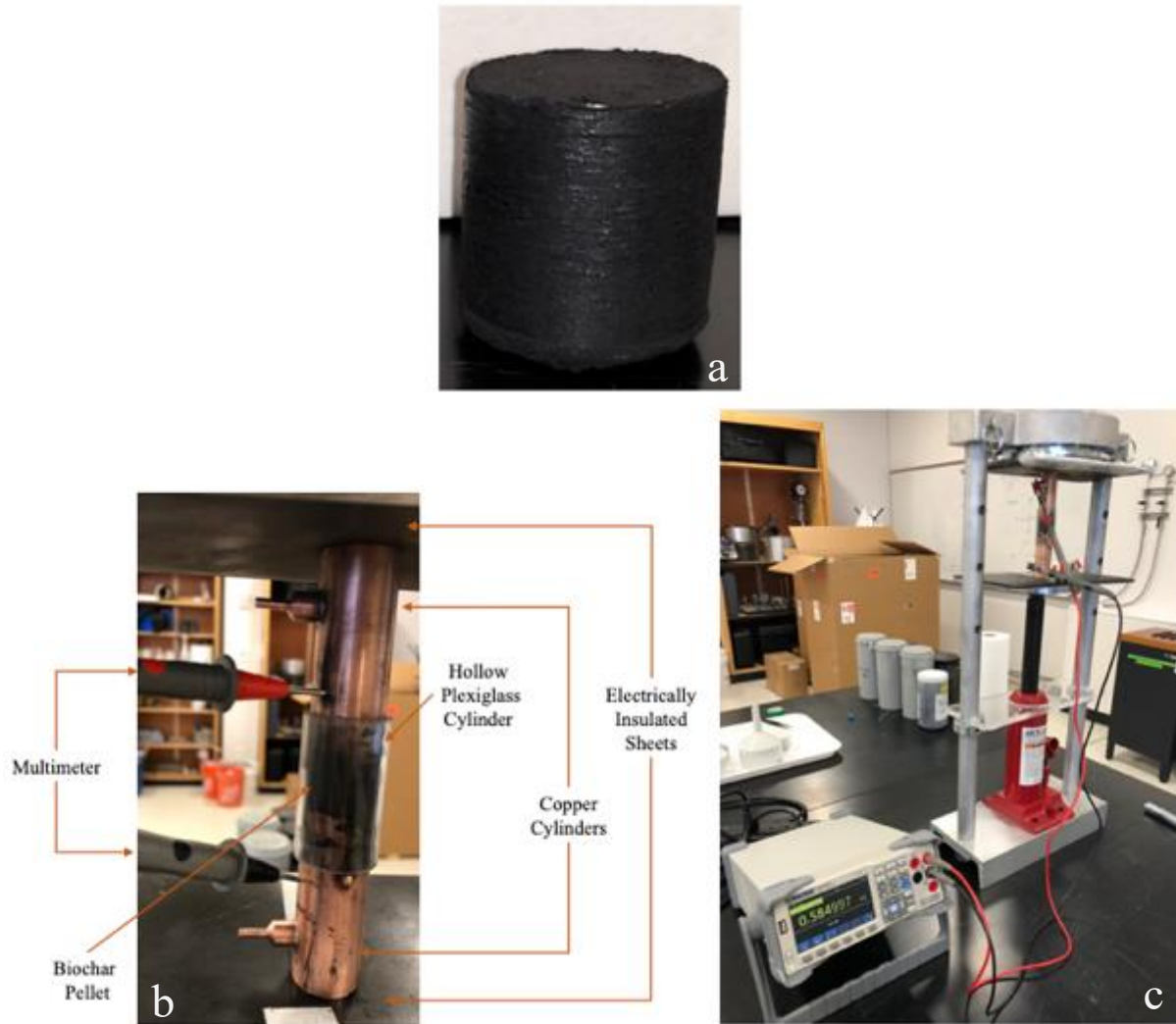


Figure 3.3 (a) BC pellet; (b) and (c) setup to measure BC conductivity

### 3.2.4.1.3 Cement Pore Solution Conductivity

To evaluate how changes in cement pore solution chemistry influence the resistivity of BC mortars, pore solution conductivity was directly measured. Pore solution extraction from long-term cured concrete requires a special apparatus [133] and can be very difficult [134]. Therefore, pore solutions were extracted from cement paste slurries and evaluated for electrical conductivity. Pore solution preparation was adapted based on the work of Gao et al. [135]. To follow the same mortar mix designs from this study (Table 3-3 and Table 3-5), cement paste slurries were prepared with each BC as a partial replacement of cement at each replacement level and with a water-to-binder ratio of 5.0 by weight, where BC was considered a binder material. The BC and OPC were mixed with deionized water in a 50 mL sealed vial for 3 minutes with a vortex mixer, then cured at 25 °C for 24 hours. This curing duration was selected

because beyond 24 hours, the only ions present in a paste in concentrations above a few millimole per liter are  $K^+$ ,  $Na^+$ , and  $OH^-$  [136]. A mixing scoop was used to break up the hardened paste and a vortex mixer was used to agitate the solution for 2 minutes. To separate the liquid pore solution from the solid residue, vacuum filtration was performed using 0.45- $\mu m$  filter paper and Buchner funnel connected to a vacuum pump. The pH of the filtrate was measured first using a Hanna Instruments 2209 pH meter. Then, the electrical conductivity of the filtrate was measured using a Vernier GoDirect® Platinum-Cell Conductivity meter, which was calibrated using the provided high-concentration conductivity standard solution with a known conductivity of 12,880  $\mu S/cm$ .

The expressed pore solution was then prepared for analysis by inductively coupled plasma optical emission spectrometry (ICP-OES) by first filtering 2 mL of filtrate through a 0.45- $\mu m$  filter. Then, the solution was diluted with 10 mL of distilled water to ensure that the analytes fell within the optimal detection ranges of the instrument. Finally, the dilute solution was acidified with six drops of nitric acid to prevent precipitation, stabilize the sample, improve ionization efficiency, and minimizes interferences, ensuring accurate ICP-OES analysis. The prepared sample concentrations were then analyzed for total concentrations of metals and major inorganic cations using an Optima 8300 ICP-OES from PerkinElmer using the Waters Method. In all ICP-OES analytical runs, a Sc internal-calibration standard was continuously introduced into the plasma along with each sample, and samples were analyzed in triplicate. The initial ionic concentration of the expressed cement pore solution without biochar was subtracted from the final concentrations measured for each BC and replacement level and the difference was recorded. Positive ionic concentrations indicate that the BC sample released that ion in excess of what was present in the simulated cement pore solution, whereas negative concentrations indicate the biochar removed those ions from the cement pore solution.

### **3.2.4.2 Mortar Analysis**

#### **3.2.4.2.1 Electrical Resistivity**

Resistivities of the concrete samples were measured after 28 days of limewater curing in saturated surface dry (SSD) condition to maintain comparable complete saturation states of the capillary and gel pores [6]. The resistance of the samples was measured as per the two-pole (uniaxial) method using a commercially available instrument (Giatec RCON™) meeting the requirements of ASTM C1876 [55]. The apparatus was modified as depicted in Figure 3.4 to accommodate small mortar cube samples. A narrow band (100 Hz to 10 kHz) sweep frequency mode was used for measurements to reduce the electrode-mortar contact interface effect [52, 54]. Sponges saturated with limewater were used as the conductive medium between the specimens and the stainless-steel plate electrodes to provide good

electrical contact and minimize resistance [137]. To reduce temperature variability, the cylinders were tested at 23.0 °C +/-2.0 °C [138]. Before testing, the exact cross-sectional area ( $A$  in mm<sup>2</sup>) and length ( $L$  in mm) of the cylinders were measured to correct for geometry, using Equation 3.2:

$$k = \frac{A}{L} \quad (3.2)$$

where,  $k$  = shape factor (mm).

The resistivity,  $\rho$  ( $\Omega$ -mm), of the samples were then calculated using Equation 3.3:

$$\rho = k \times R \quad (3.3)$$

where,  $R$  = measured resistance ( $\Omega$ ).

The average resistivity of four samples are reported as the final result. Given the non-destructive nature of the electrical resistivity test, the samples made for resistivity testing were then used for compressive strength evaluation.

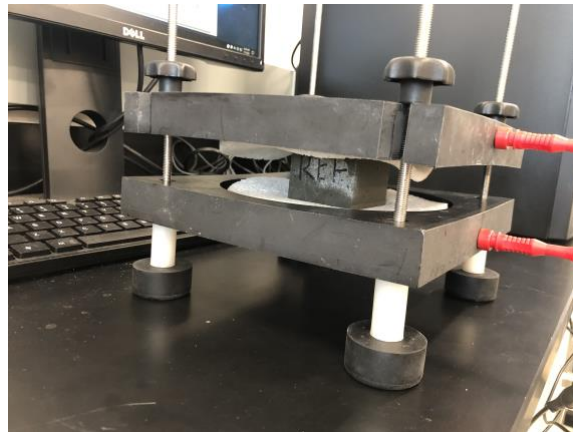


Figure 3.4 RCON electrical resistivity testing set-up

### 3.2.4.2.2 Permeability

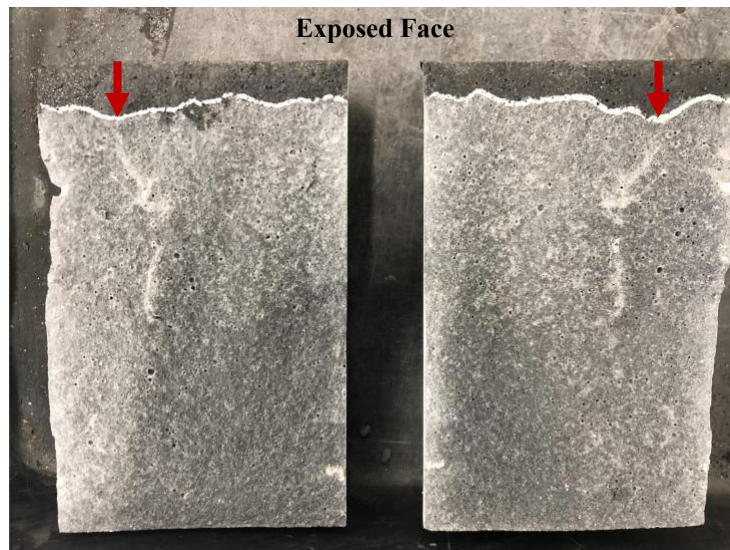
#### 3.2.4.2.2.1 Depth of Water Penetration

British Standard EN 22390-8 [139] was implemented to determine the depth of penetration of pressurized water in hardened mortars; this can serve as an evaluation of mortar permeability. A three-test point TESTING Bluhm & Feuerherdt GmbH water impermeability tester with water measurement was used to test each BC mortar at each cement replacement level (Figure 3.5a). The water pressure was maintained at  $5 \pm 0.50$  for a duration of 72 hours. The cylinders were split into two halves and the depth

of penetration was measured from the exposed face (Figure 3.5b), using a digital caliper. The reported value was determined by averaging the measurements obtained from the two halves of the split mortar cylinders, with each test conducted on a total of two samples for each BC at each replacement level, totaling 24 samples.



(a)



(b)

Figure 3.5 (a) Water impermeability tester; (b) example depth of penetration measurement from exposed face of sample

#### 3.2.4.2.2.2 Water Accessible Porosity

ASTM C642 [140] was also used as a test method to determine the volume percentage of permeable pore space in a hardened specimen given its continued relevance in recent BC studies [130], [141], [142].

The four-step procedure of ASTM C642 is briefly summarized as follows: 1) determine the oven-dry mass,  $A$ , of the sample after 24 hours at 110 °C; 2) record the saturated mass,  $B$ , after immersion for 48 hours in tap water; 3) boil the sample for 5 hours and again record the saturated mass,  $C$ ; and 4) determine the immersed apparent mass,  $D$ , by suspending the specimen in water in a basket attached to a wire, connected to an ae Adam Nimbus® precision balance sixteen hours following the boil. This procedure was conducted on three specimens that were wet-cut from a cylinder cast as described in section 3.2.4.2 and the void volume percentage was calculated using Equation 3.4. The reported value is an average of the volume percentage from the three specimens.

$$\text{Voids, \%} = \left( \frac{C-A}{C-D} \right) * 100 \quad (3.4)$$

### 3.3 Results and Discussion

#### 3.3.1 Biochar Conductivity

The bulk DC conductivity of the BCs was measured and reported in Table 3-6. When considering the spectrum of electrical conductivity [49], the BCs in this study can be categorized as semiconductors; however, others have reported that BC can attain metallic-level conductivity ( $\sigma = 300,000$  mS/m) depending on feedstock and processing [78]. While the BCs investigated in this study do not attain metallic-level conductivity, each has a higher conductivity than the reference mortar (31 mS/m), therefore each BC has the potential to improve the conductivity of a mortar if it forms a continuous network.

Table 3-6 BC electrical conductivity and resistivity measurements

BC	Bulk DC Conductivity, $\sigma$ (mS/m)	Resistivity, $\rho$ (k $\Omega$ ·cm)
MW	100	1.00
PS	80	1.25
WS	460	0.217
OP	3,500	0.029

To complement our direct measurements, both Raman spectroscopy and X-ray diffraction (XRD) were also used to characterize the BC. These methodologies are often more accessible to researchers and allowed us to compare our work with other works on BC cementitious composites.

Raman analysis is a well-suited, nondestructive tool for the characterization of crystalline, nanocrystalline, and amorphous carbons [143]. The spectra of BCs are known to exhibit two main overlapping bands around 1,350-1,370  $\text{cm}^{-1}$  and 1,580-1,600  $\text{cm}^{-1}$ , commonly referred to as the D and G

bands [144]. As shown in Figure 3.6, the signals for these two main bands were observed from the spectrum of the BCs in this study at around 1341  $\text{cm}^{-1}$  and 1604  $\text{cm}^{-1}$ . Similar BC Raman spectrum D and G bands have been observed by several other researchers [78], [145], [146]. One of the most common ways to assess the degree of carbonization of BCs is through the ratio of the intensities (height) of the two peaks ( $I_D/I_G$ ), which is reflected in Table 3.7. While the ratios followed the pattern of decreasing with increasing HTT [147], since the ratio of all the BCs are all close to 1.0, this suggests that the carbon has not progressed much in its transformation to nanocrystalline graphite [148]; rather, it mainly consists of amorphous carbon structures.

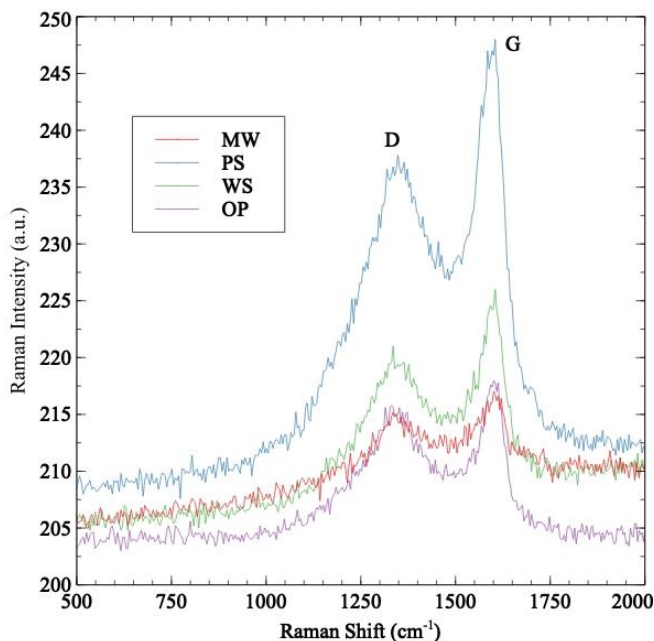


Figure 3.6 BC Raman spectra

Table 3-7  $I_D/I_G$  ratio derived from Raman spectra

BC	MW	PS	WS	OP
$I_D/I_G$	0.99	0.96	0.98	0.99

Although Raman spectrometry is a powerful tool for the structural characterization of carbons, when evaluating highly disordered carbon materials, the D band intensity can be strongly influenced by the finite domain size and the orientation of crystallites because a Raman microprobe signal results from a limited volume of particle surface. Therefore, it can be beneficial to validate Raman spectroscopy results with XRD. In this method, more particles are analyzed and the  $d_{002}$  interlayer spacing determined from XRD measurements come from a volume of randomly oriented particles, averaging any preferred

orientation of crystallites [149]. The XRD results are presented in Figure 3.7. The MW BC has predominantly small, sharp peaks characteristic of a crystalline material that are expected for BCs with higher ash contents [150, 151]. Conversely, the XRD patterns of PS, WS, and OP showed a broad hump in the  $2\theta$  range from  $16^\circ$  to  $32^\circ$  suggesting the BCs contain an increased amount of disordered material in the form of amorphous carbon [151]. None of the BCs displayed true graphite formation, which is characterized by the emergence of more defined peaks at  $2\theta \sim 26^\circ$  and  $2\theta \sim 43^\circ$ . While amorphous silica can also show a broad hump in this range ( $\sim 22^\circ$ ) [152], given that the maximum peak intensity occurs closer to  $\sim 24^\circ$  and that PS, WS, and OP are predominantly carbon, we conclude that the broad hump seen in Figure 3.7 represents amorphous carbon.

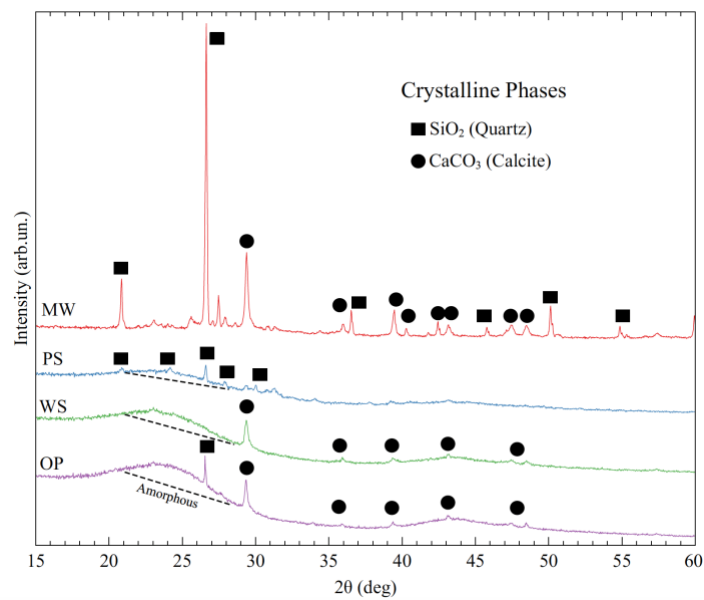


Figure 3.7 XRD patterns of BC

The results from the evaluation of the BC electrical conductivity via these three different methods underscores the importance of performing bulk material property measurements like DC conductivity. Raman Spectroscopy and XRD both suggest negligible BC electrical conductivity due to a low degree of graphitization and the presence of highly disordered carbon phases. However, the microstructural information provided by these methods do not directly translate to the bulk electrical transport properties of the BC, which integrate structural features, particle-to-particle contact, and macroscopic packing conditions.

### 3.3.2 Volume of Permeable Void Space

Figure 3.8 presents the results of the water-accessible porosity. From Figure 3.8, it can be seen that as BC replacement level increases void space decreases for all BCs, suggesting a denser microstructure.

However, several of the composites (WS5, OP5, and OP10) have higher void percentages than the reference mortar, which is inconsistent with the depth of penetration data.

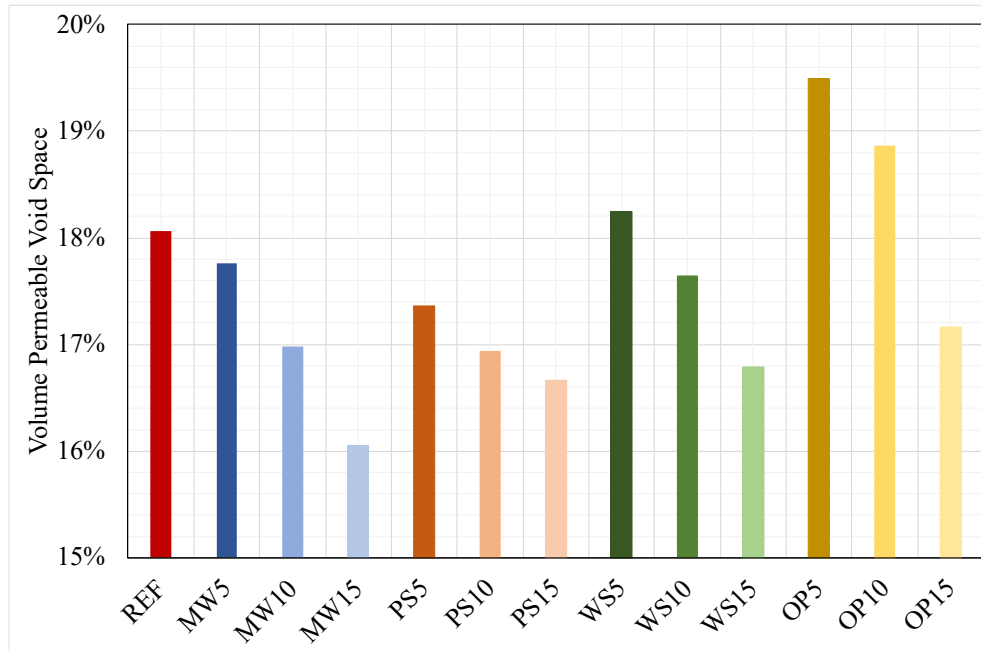


Figure 3.8 Volume of permeable void space

In a recent study, Almarshoud et al. [153] found that there is no correlation between bulk electrical resistivity measurements and the volume of permeable voids as determined by ASTM C642 [140]. This conclusion is also corroborated by the data determined in this study and displayed in Figure 3.9. Bu et al. [154] further highlight that while ASTM C642 [140] may provide a consistent measure of voids, users need to be conscious that it does not measure total porosity and should be used sparingly when applied to concrete durability applications. This methodology is also detracted by the fact that it requires drying the specimen to 105 °C, which can induce microstructural cracking and add an apparent increase in the permeable porosity of the concrete [155]. Although this method is often applied as a surrogate for permeability measurements, this is not the intended application of the standard and we caution other researchers against this approach. Our work, and the work of others [153, 154, 155], indicate that ASTM C642 [140] method is not a reliable indicator of permeability.

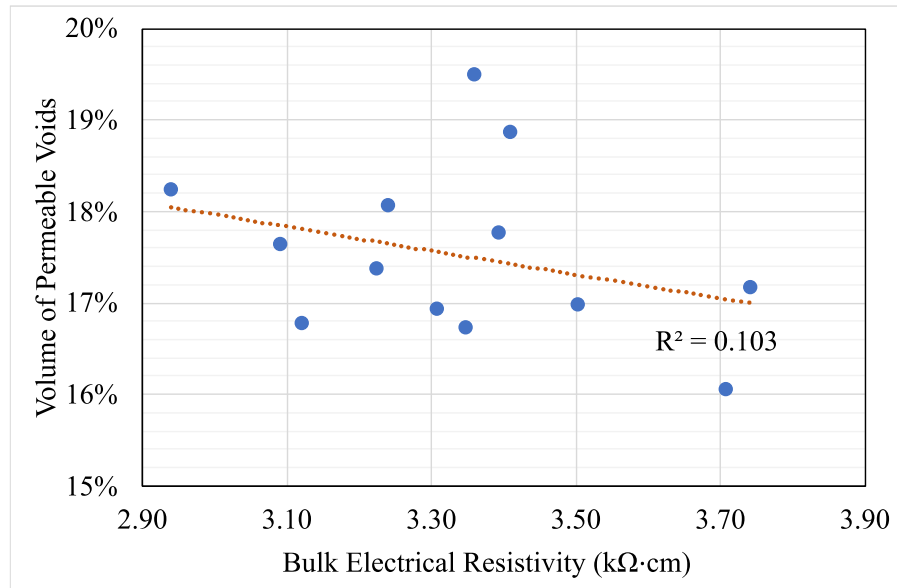


Figure 3.9 Relationship between bulk electrical resistivity and volume of permeable void space. The low  $R^2$  suggests a weak correlation between bulk electrical resistivity measurements and the volume of permeable voids as determined by ASTM C642 [140].

### 3.3.3 Electrical Resistivity and Permeability

The electrical resistivity of the mortar samples was measured via the bulk-resistivity method. As indicated in Table 3-8, only the WS BC mortar shows a decrease in mortar resistivity compared to a control and each BC mortar showed a relative increase in resistivity with increased BC content. This trend is consistent with a study using a rice husk BC pyrolyzed at 550 °C [19], but contradicts seven other studies which report increased electrical conductivity with increasing BC content [13-20]. Most of these studies conclude that because BC has a high carbon content and the resistivity of their samples decreases, the BC acts as a conductive inclusion in the bulk matrix; only one study supports the claim with direct conductivity measurements [17]. While most works on BC in cementitious composites conclude that observed reductions in resistivity are due to the inclusion of conductive BC in the bulk matrix, a combination of microstructural changes and BC conductivity can affect the measured resistivity [156].

Table 3-8 Electrical resistivity of mortar samples at 28 d

Specimen	Mortar resistivity (kΩ·cm)		
	5	10	15
MW	3.4	3.5	3.7
PS	3.2	3.3	3.4
WS	3.0	3.1	3.1
OP	3.4	3.4	3.7
REF	3.2		

To evaluate the relationship between permeability and resistivity, we measured the water penetration depth of each mortar and plotted the results as a function of electrical resistivity. As shown in Figure 3.10, the relationship between depth of penetration and bulk resistivity is as expected, in that resistivity increases with decreasing permeability for all four BCs. Yet, there is one notable exception—the WS BC-cement mortar is both less permeable and less resistive than the control. A cursory analysis might lead one to conclude that the WS BC is acting as a conductive conclusion; however, it is imperative to also consider the influence of the pore solution conductivity.

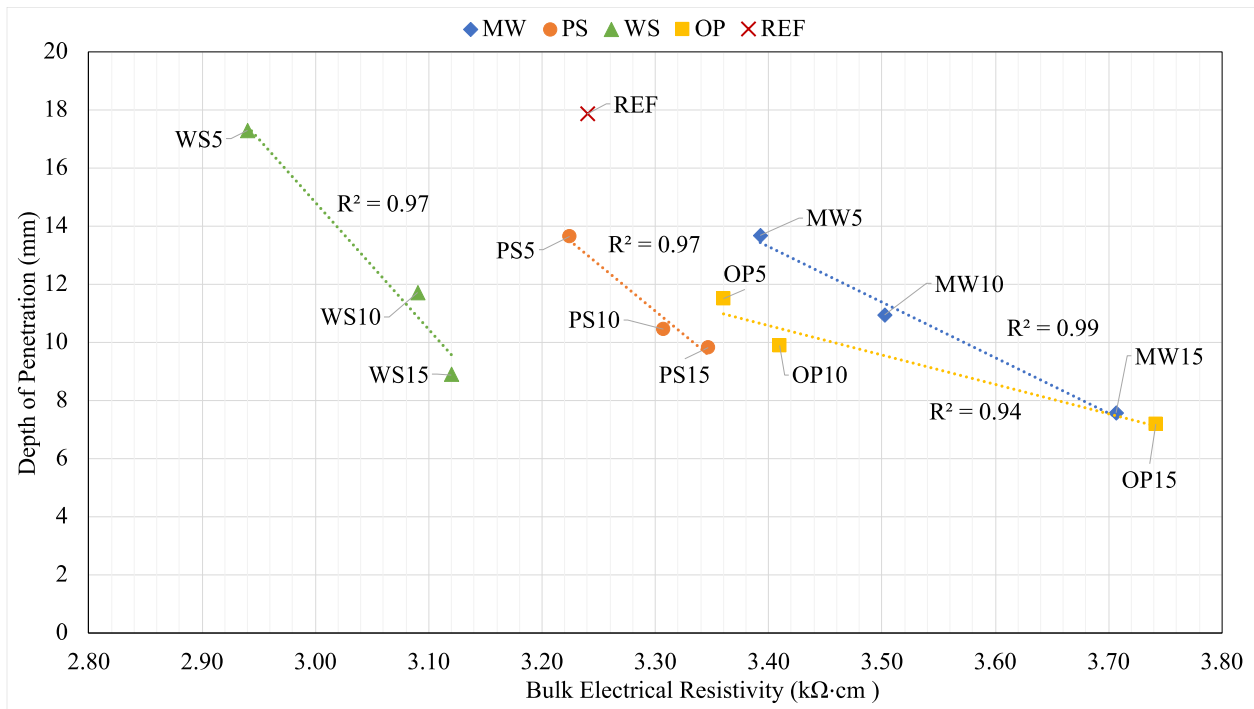


Figure 3.10 Relationship between depth of water penetration as a function of bulk electrical resistivity. Linear trend lines are included for each BC, showing a strong ( $R^2 > 0.94$ ) negative relationship

It is well established that electrical test methods can be affected by the conductivity of the pore solution [136]. During the early period of hydration, there are relatively high concentrations of  $\text{Ca}^{2+}$ ,  $\text{K}^+$ ,  $\text{Na}^+$ ,  $\text{SO}_4^{2-}$ , and  $\text{OH}^-$  in the pore solution. However, as the main calcium-containing hydration products are formed, the concentrations of  $\text{Ca}^{2+}$  and  $\text{SO}_4^{2-}$  decrease, and the pore solution is mainly composed of alkali hydroxides [157]. Yet, this is different in situations when cementitious composites contain supplementary materials, which can alter the chemical composition of the pore solution and consequently change its overall conductivity [158]. The direct method for determining the electrical conductivity of the pore solution requires pore solution expression [133] and subsequent analysis of the constituents via a conductivity meter. In this study, the pore solution was expressed from cement and BC pastes. The pore solution conductivity (PSC) and resistivity for each mix are documented in Table 3-9.

Table 3-9 Expressed pore solution conductivity ( $\sigma$ , in mS/m) and resistivity ( $\rho_o$ , in  $\text{k}\Omega\cdot\text{cm}$ )

BC	5 wt%		10 wt%		15 wt%		Percolation	
	$\sigma$	$\rho_o$	$\sigma$	$\rho_o$	$\sigma$	$\rho_o$	$\sigma$	$\rho_o$
MW	0.0132	0.0759	0.0141	0.0710	0.0144	0.0692	0.0162	0.0613
PS	0.0121	0.0827	0.0126	0.0791	0.0127	0.0787	0.0124	0.0808
WS	0.0132	0.0756	0.0131	0.0766	0.0128	0.0778	0.0127	0.0789
OP	0.0126	0.0792	0.0126	0.0791	0.0126	0.0791	0.0126	0.0794
REF	0.0129	0.0778						

As seen in Table 3-9, the PSC trend for both the MW and PS BC was an increase in conductivity as BC content was increased, the WS BC saw a decreasing PSC trend, whereas the OP BC had no effect on changes to the PSC. The pH was consistently at about 13.0, which is expected for a cement pore solution. To fully understand the effects of the BC on changes to PSC, we evaluated the evolution of soluble ions in the expressed pore solution before and after exposure to BC. The results of the ICP-AES analysis for this investigation are summarized in Figure 3.11, which shows the difference in ionic speciation between the cement pore solution and the solution filtrate after exposure to BC. The negative concentrations indicate that ions were removed from solution after exposure to BC, whereas the positive concentrations indicate an excess of ions compared to the pore solution. In other words, a positive value indicates that components of the BC are solubilized in the cement pore solution and contribute to its electrical conductivity.

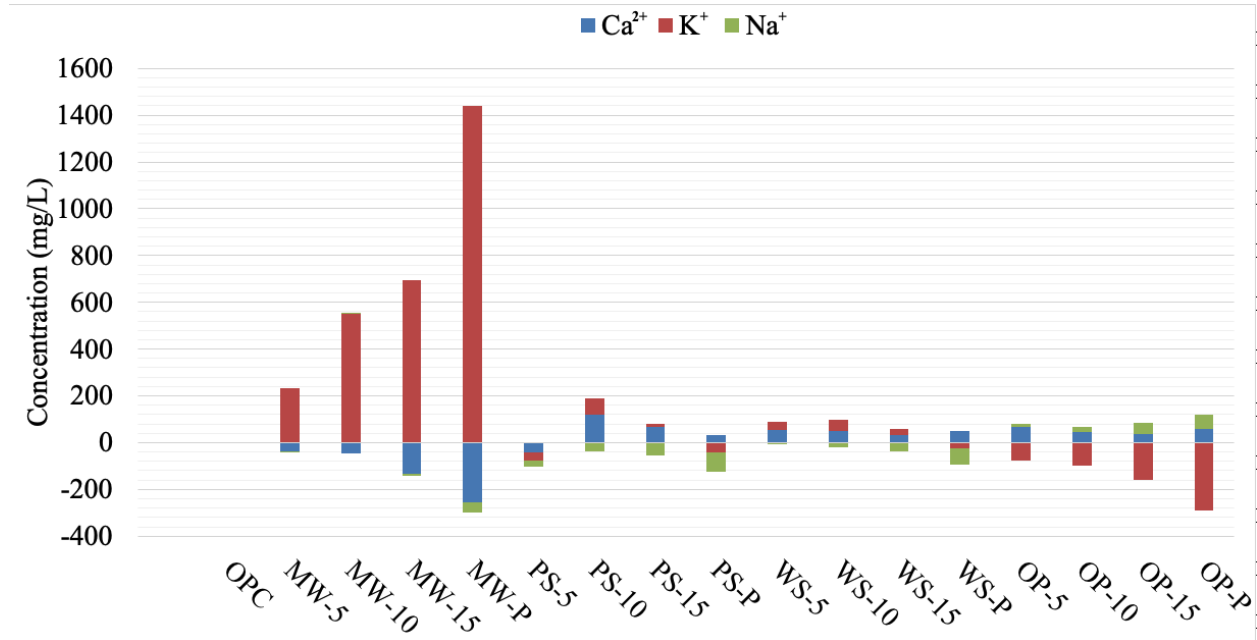


Figure 3.11 Difference in pore solution ionic speciation following BC exposure

From Figure 3.11, it can be seen that both the MW and PS contribute an excess of ions to solution, which would explain their increase in PSC. For the WS BC, there is an overall decrease in ions, which would explain its decrease in PSC, and for the OP BC a balance of ion concentration. Between the direct conductivity measurements and ICP results, there is strong evidence that the changes in resistivity of the BC mortars would be highly influenced by changes in ionic conductivity via changes in ionic strength and speciation of the cement pore solution.

The electrical resistivity of a saturated porous material relies largely on two microstructural properties, the connectivity,  $\beta$ , and the porosity,  $\phi$ , which together determine the Formation Factor,  $F$ , given in Equation 3.5:

$$\phi\beta = \frac{1}{F} \quad (3.5)$$

The Formation Factor is considered as a transport property because it can be used to describe the diffusion of ionic species in a porous material. The Nernst-Einstein equation correlates the Formation Factor to the diffusion coefficient through the relationship in Equation 3.6:

$$\frac{\rho_b}{\rho_o} = F = \frac{D_o}{D_b} \quad (3.6)$$

where,  $\rho_b$  is the bulk resistance,  $\rho_o$  is the pore solution resistivity,  $D_o$  is the self-diffusion coefficient associated with ion transport, and  $D_b$  is the diffusion coefficient of ions through the pore space [159], [160].

Generally speaking, an increase in the Formation Factor means that the concrete has become more resistant to the flow of electrical current, thus an increase in bulk electrical resistivity. The factors that influence the increase in Formation Factor are 1) microstructural changes via a decrease in porosity and/or connectivity as a result of lower w/c ratio or pore refinement due to the addition of supplementary cementitious materials; and 2) electrolytic changes influenced by an increase in pore solution conductivity due to the consumption of ions from the pore solution. Since connectivity,  $\beta$ , is difficult to measure directly,  $F$  was determined as the ratio of bulk resistivity to pore solution resistivity. If bulk resistivity is primarily controlled by microstructure, there should be a strong correlation between  $F$  and depth of penetration, which is also a function of microstructure. This relationship is explored in Figure 3.12 which depicts the depth of water penetration versus formation factor.

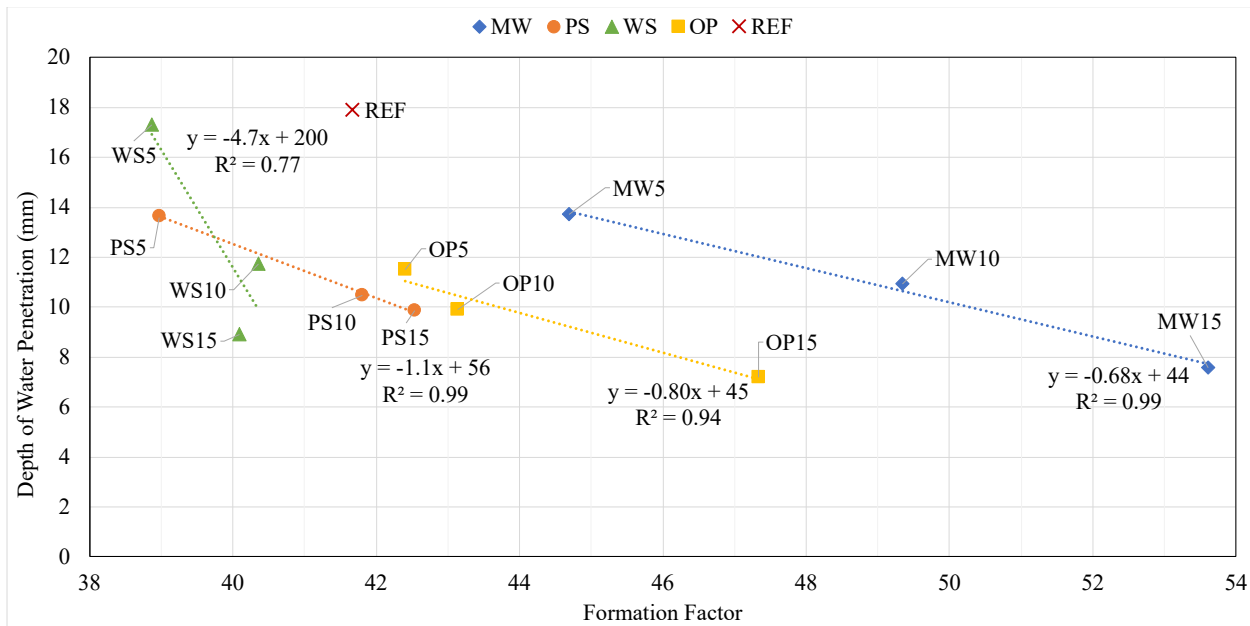


Figure 3.12 Depth of water penetration versus formation factor

For the MW, OP, and PS mortars,  $F$  increases with a decrease in depth of water penetration. The strong, negative linear relationship ( $R^2 > 0.94$ ), indicates that connectivity/porosity control the changes to Formation Factor in these mortars. Notably, the WS shows the same trend at both the 5 and 10 wt% replacement level, but then at 15 wt% replacement, the Formation Factor decreases while both depth of penetration and PSC still decrease. This results in only a moderate linear relationship ( $R^2 = 0.77$ ) between depth of water penetration and  $F$ , suggesting that the bulk resistivity of this mortar is influenced by more

than just  $F$ . Formation Factor determination via bulk resistivity measurements assumes that only electrolytic conductivity is occurring. However, if bulk resistivity is instead controlled by electric conduction via a percolating network of conductive inclusions, this will disrupt the linear relationship between microstructure and Formation Factor.

### 3.3.4 Percolation Threshold Prediction

As discussed in section 3.2.3.2, percolation threshold of BC was estimated to be 27.1 vol%; in other words, this is the predicted volume at which the BC can form a continuous network. Due to differences in BC density, this resulted in cement replacements of 25-43 wt%, which significantly increased water demand. To create a workable mix, instead of using a w/c of 0.45, a w/b of 0.45 was used and the BC was considered part of the binding phase. Since this resulted in a variable w/c, which could affect  $F$  and thus bulk electrical resistivity, all mixes were compared using depth of water penetration.

As shown in Table 3-10, the electrical resistivity for all percolation mixes decreased compared to the 5-15 wt% BC mixes (Table 3-8). If considering the mix design only, this reduction could be attributed to increased w/c ratios, which result in increased permeability and, in turn, increased electrolytic conductivity.

Table 3-10 Electrical resistivity of percolation mortars

Specimen	w/b	w/c	Mortar Resistivity (k $\Omega$ -cm)
P-MW	0.45	0.79	1.48
P-PS	0.45	0.61	1.85
P-WS	0.45	0.63	2.11
P-OP-0.45	0.45	0.61	1.47
P-OP-0.38	0.38	0.50	1.99

However, if the resistivity measurements are controlled by electrical conduction, as is the case for electrically conductive cementitious composites, the resistivity will decrease independent of permeability, since the electrons can flow through the solid phase. As seen in Figure 3.13, the relationship between depth of penetration and bulk resistivity for both the WS and PS BCs is as expected for electrically conductive cementitious composites. The decrease in resistivity of the P-PS and P-WS mixes cannot be attributed to the pore network alone because the permeability, as measured by depth of penetration, remains at the same level as the 5-15 wt% mixes and the PSC of the percolation mixes is either the same or lower than the 5-15 wt% mixes.

The driving force behind the reduced resistivity in the P-MW and P-OP mixes is less certain. The P-MW mix shows a notable drop in resistivity but also exhibits increased permeability and PSC, both of which could enhance ionic conductivity. Similarly, the P-OP-0.45 mix shows a sharp decrease in resistivity alongside increased permeability. To investigate whether this low resistivity is due to the high intrinsic conductivity of OP or simply a result of higher permeability, OP was tested at two different w/b ratios. At a w/b of 0.38, resistivity increased while penetration depth decreased. This indicates that bulk resistivity is at least partially influenced by the pore network. Furthermore, if electrical conduction were the dominant factor, resistivity would be significantly lower, given the OP BC's intrinsic resistivity of 0.00286 k $\Omega$ ·cm. These results suggest that a percolating conductive network did not form—despite theoretical expectations—likely due to insufficient dispersion of BC particles.

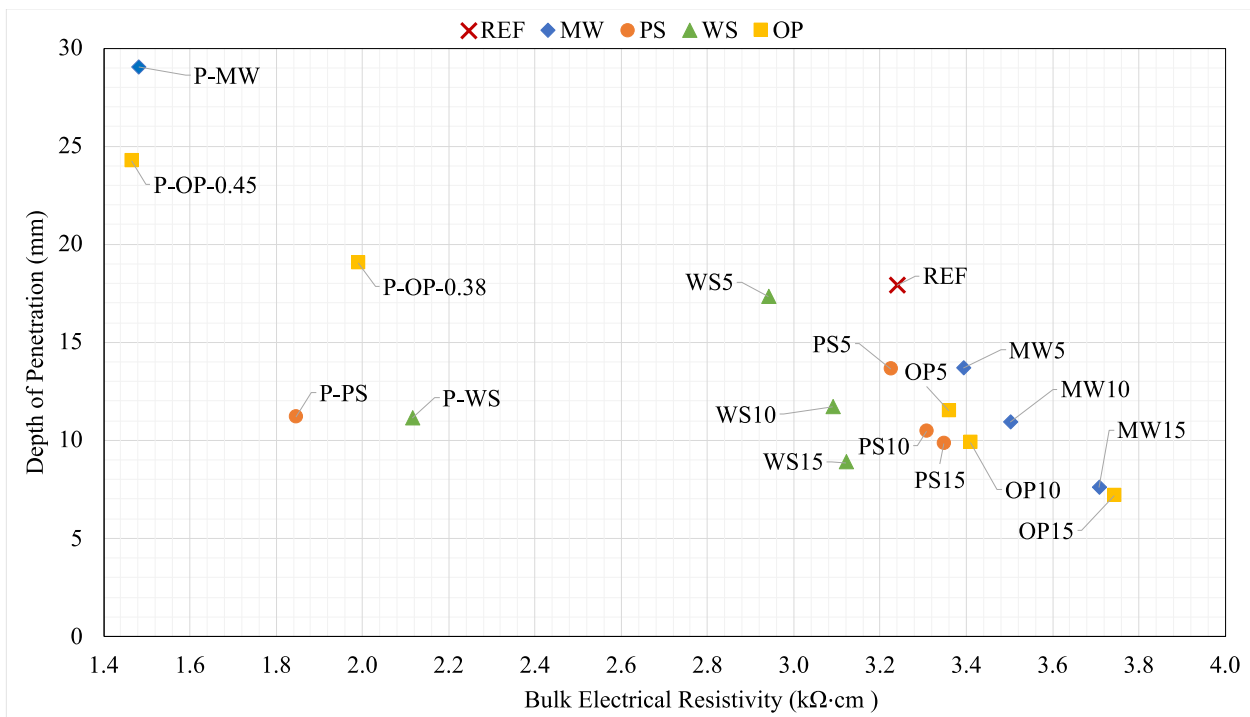


Figure 3.13 Electrical resistivity vs. depth of penetration of water of percolation mixes

### 3.4 Conclusion

This study investigated the bulk electrical resistivity of mortars containing increasing levels of cement replacement with BC, aiming to distinguish the influence of pore network modifications from that of matrix conductivity. Four distinct BCs were used in this study, with conductivities ranging from 80 to 3,500 mS/m. Results show that changes in bulk resistivity are not primarily governed by the formation of a percolative network of conductive inclusions. Instead, they are largely attributed to: 1) reduced

permeability, which tends to increase resistivity; and 2) ions solubilized from the BC, which tend to decrease resistivity.

Among the four BCs tested, only one reduced mortar resistivity relative to the control; the others increased it. Notably, the most conductive mortar was not produced using the most conductive BC. All four BCs reduced mortar permeability compared to the control, with the effect becoming more pronounced at higher BC content. Many studies have attributed an observed decrease in electrical resistivity with increasing BC to the addition of a conductive BC within the bulk matrix. However, given the results of the present work, it is possible that the previous studies are actually observing changes in conductivity via changes to the pore network. Percolation theory predicts that a BC volume fraction of  $\sim 0.27$  (corresponding to  $\sim 25\text{--}43$  wt% cement replacement in our mix designs) is necessary to form a continuous conductive network. This threshold is much higher than the  $5\text{--}15$  wt% replacements commonly used in the literature. Even at or above this threshold, conductive networks may not form due to inadequate BC dispersion—observed here for two of the four BCs tested.

Permeability is one of the most important characteristics for predicting concrete service life, as most degradation stems from water ingress into the matrix. While assessing concrete's permeability via non-destructive resistivity measurements is practical, this method may lead to erroneous conclusions in the case of BC cementitious composites. For example, if the WS BC were to be used as a cement replacement or filler, one might erroneously conclude that the concrete's decrease in resistivity compared to a control indicates increased permeability. However, depth of water penetration measurements show that BC cementitious composites are less permeable than conventional mixes.

As both electric conductivity and pore network changes can affect the measured resistivity in BC mortars, it is imperative that future works evaluating the electrical resistivity of BC cementitious composites validate their conclusions with secondary measurements. In addition to bulk resistivity measurements of the BC cementitious composites, it is recommended that the following values be routinely reported:

1. Direct conductivity of the BC
2. Depth of water penetration in the cementitious composite, or a similar indicator of water permeability
3. Changes in pore solution chemistry
  - a. Ideally, the electrolytic conductivity of a pore solution expressed from BC cementitious composites
  - b. Alternatively, changes in pore solution chemistry can be estimated using the method described in this paper

While BC offers promising benefits in cementitious systems, it can alter behavior compared to conventional concrete. As such, conventional test method may not apply, and careful validation is required to ensure desired performance outcomes.

## CHAPTER 4 AN EVALUATION OF BIOCHAR CONCRETE PERMEABILITY AND FROST DURABILITY WITHOUT AIR-ENTRAINMENT

### **Abstract**

This chapter explores the frost durability of non-air entrained biochar concrete. The frost durability of concrete has been extensively studied; however, its application to biochar concrete remains largely unexplored. Biochar is commonly used as a cement replacement due to cement's higher carbon footprint. Yet, the freeze-thaw performance of concrete lies largely in the paste. In this study, milled biochar was used as a partial replacement of sand to evaluate freeze-thaw durability at a constant paste volume. This was assessed through ASTM C666 [34] rapid-freeze testing, which was complimented with hardened air void analysis, compression testing, permeability measurements and electrical resistivity analysis. Despite improved permeability at some replacement levels, non-air-entrained biochar concrete failed in less than 15 freeze-thaw cycles, compared to conventional concrete which failed in 97 freeze-thaw cycles. This degraded freeze-thaw performance was attributed to biochar concrete's higher sorptivity, associated with pore refinement. When water freezes in small pores, higher tensile pressures are developed than when water freezes in large pores, leading to greater damage.

### **4.1 Introduction**

Concrete serves as a fundamental cornerstone of our modern infrastructure. Yet, there are significant environmental challenges associated with its use [161]. The manufacturing of cement, the key binding component in concrete, is responsible for ~8% of global anthropogenic CO<sub>2</sub> emissions [162], [163]. It is expected that the world's considerable need for cement will continue to grow due to increased demand from rapidly developing regions [164]. To help reduce the carbon footprint and improve the sustainability of cementitious composites, waste products like fly ash, granulated blast-furnace slag, and silica fume, have been routinely used as supplementary cementitious materials [165]. However, the availability of these traditional materials is diminishing as a result of the decarbonization of these high-emission sectors, motivating the investigation into alternative sources [166]. One such material that is gaining increasing attention as a sustainable additive in cementitious materials, is biochar. Biochar is a carbonaceous material obtained from the thermochemical conversion of biomass in an oxygen-deprived environment [3]. Instead of biomass naturally decomposing and gradually releasing CO<sub>2</sub> back into the atmosphere, the carbon remains as a stable solid. Even when accounting for the energy required to convert the biomass, the resulting biochar is highly carbon negative due to this avoidance [4]. Therefore, integrating biochar into concrete is an appealing approach for producing carbon-neutral construction materials.

The sustainability of concrete is mainly focused on its embodied carbon, determined as all the CO<sub>2</sub>-equivalent emissions from the entire life cycle of a concrete structure [167]. While many strategies to reduce embodied carbon focus on reducing cradle-to-gate emissions, enhancing the sustainability of concrete can also be achieved by designing for improved durability, which extends its service life and reduces the need for costly repair or replacement [168]. Some environmental conditions make concrete more susceptible to degradation; for example, cold temperate regions with repeated freezing and thawing cycles [169]. Freeze-thaw damage manifests in concrete as surface damage, called salt scaling, or through internal frost damage [80], which is the focus of the present work. Internal frost damage is caused by crystallization pressure [27] and hydraulic pressure [25], [26] due to the displacement of water and growth of ice crystals in the pores of the cement paste. It is well established that the best way to prevent internal cracking is to ensure that the hardened concrete has an adequate system of entrained air voids to act as pressure relief valves within the cement paste [80]. Frost resistance can also be improved by decreasing porosity and permeability through a lower water-to-cement (w/c) ratio and/or the addition of supplementary cementitious materials [23], [24]. This is why concrete exposed to freezing temperatures has requirements for permeability (w/c limits) and air-entrainment to ensure long term durability against frost damage [7]. The permeability of concrete at the same w/c ratio can also vary significantly with the incorporation of supplementary cementitious materials [8].

The fresh and hardened properties of biochar cementitious composites have been extensively investigated [29], [30], [126]; however, the long-term performance of concrete exposed to harsh environments is largely unknown [110]. Only three studies have investigated biochar's effect on the freeze-thaw durability of cementitious composites [31], [32], [33]. Each study incorporates biochar as a partial cement replacement and examines the freeze-thaw resistance of non-air-entrained biochar concrete. Two [31], [32], of the studies reported improved or similar freeze-thaw resistance at all replacement levels (up to 30 wt%), while the study by Chen et al. [33] reported improved freeze-thaw performance only at cement replacement levels below 5 wt%. In the two studies reporting improvement at high replacement levels, they evaluate freeze-thaw resistance through compressive strength testing after a certain number of freeze-thaw cycles, while the study by Chen et al. evaluates performance via relative dynamic modulus of elasticity (RDME), like what is prescribed in ASTM C666. The change in freeze-thaw performance is attributed to various mechanisms in these studies. When improvement is observed, it is attributed to the porous structure of biochar, which can act in the same way as air voids. When performance is degraded, it is attributed to the water retention capacity of the biochar, which can become sites of preferential fracture during a freezing event.

While these studies suggest that biochar does not inherently impair freeze-thaw performance, each study utilizes biochar as a cement substitute. Since freeze-thaw performance is primarily controlled by

paste content, it is possible these studies benefit from improved freeze-thaw performance due to a decreased cement paste content compared to their control. To evaluate this effect, the present work uses biochar as a sand replacement in non-air entrained concrete to evaluate its influence on freeze-thaw durability while maintaining the same paste content compared to the control. The replacement of sand with biochar isolates biochar's physical effect to pore structure, moisture transport, and freeze-thaw resistance, without influencing the variability of the binder content. Freeze-thaw durability was mainly assessed through Procedure A of ASTM C666 [34] rapid-freeze thaw testing. Although this is a much harsher test than the environmental conditions a serviceable concrete would experience [170], it permits the comparison to the performance of other non-air entrained concrete freeze-thaw studies found in the literature [97], [98], [171], [172].

#### **4.1.1 Research Objective**

The objective of this study was to 1) evaluate the frost resistance of biochar concrete mixtures formulated without air entrainment to establish a baseline of freeze-thaw performance compared to conventional concrete and 2) investigate the effects of permeability changes on biochar concrete freeze-thaw performance. understand how a wood-derived biochar (BC) affects the frost resistance of concrete as measured by ASTM C666 [34]. Rapid-freeze thaw testing was complimented by compressive strength testing, hardened air void analysis, permeability, and concrete sorptivity, to provide a more comprehensive understanding of how biochar influences freeze-thaw resistance through microstructural modification and moisture transport mechanisms.

## **4.2 Materials and Methods**

### **4.2.1 Biochar**

#### **4.2.1.1 Feedstock and preparation**

A Pine Wood feedstock heated to 800 °C was used to produce the biochar (BC) for this study, which was provided by a commercial biochar manufacturer. This type of BC was selected for this study because it was considered representative of a broad range of BCs our research group had previously evaluated based on its pyrolysis conditions, carbon content, and key physical and chemical characteristics.

#### **4.2.1.2 Biochar characterization**

The BC was first milled in a Retsch RS 300 vibratory disc mill for three minutes to minimize the presence of large pores. Following milling, a Microtrac S3500 laser particle size analyzer was used to

measure the effective particle size,  $d_{50}$ , of BC in isopropanol. The refractive index of the sample was set at 2.42. The particle size distribution of the BC, as compared to OPC and sand is shown in Figure 4.1.

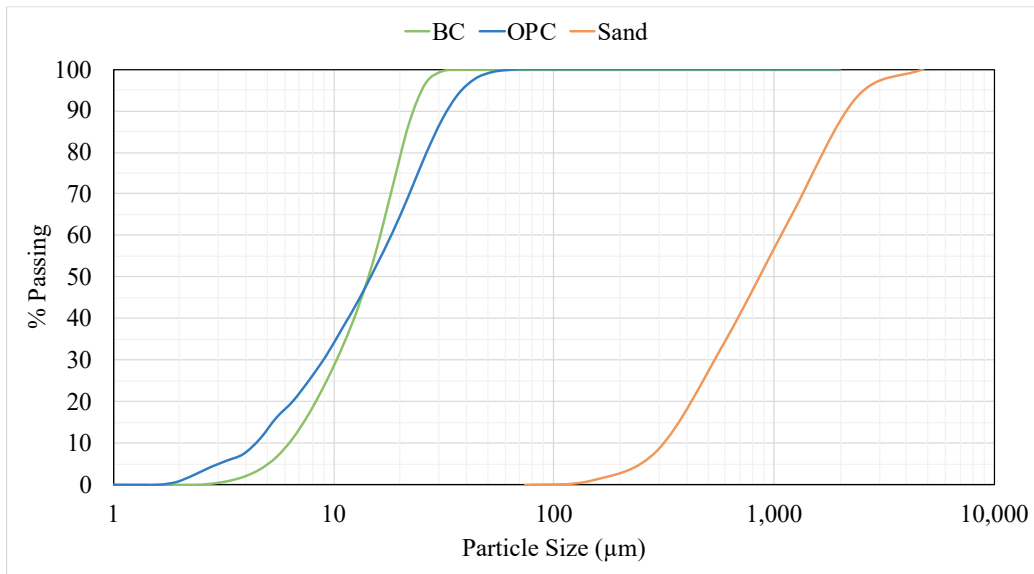


Figure 4.1 Particle size distribution of mix constituents

A Micromeritics AccuPyc II with helium as the displacement medium was used to measure the skeletal density of the milled BC without additional sample preparation steps. The density measurement was conducted by averaging five cycles of pressurized inlet gas into a known volume and sample mass. The BET surface area was measured with nitrogen adsorption-desorption using a Micromeritics ASAP 2020 Plus instrument. The BC was stored in closed buckets from the time of milling until use. Since these buckets still permit some exposure to the ambient atmosphere, the ambient moisture content of the BC was measured and accounted for in the concrete mix design as a component of the total mix water content. A PerkinElmer TGA 8000 was used to heat 5-20 mg of BC under a nitrogen flow to 105 °C at 10 °C/min. The BC was isothermally held until the weight stabilized, typically under 60 minutes. Per ASTM D7582 [123], proximate analysis of the BC was conducted using a LECO TGA and ceramic crucibles. The volatile matter, fixed carbon content, and ash content were reported as the wt% of the dry char (dry basis) to evaluate the influence of variable ambient moisture. The carbon, hydrogen, nitrogen, and sulfur mass percentages were determined from ultimate analysis. Oxygen content was reported as the difference between the carbon, hydrogen, nitrogen, sulfur, and ash content. The physical and chemical characteristics of the BC are reported in Table 4-1.

Table 4-1 BC Characteristics

BC	d50 ( $\mu\text{m}$ )	Skeletal Density ( $\text{g}/\text{cm}^3$ )	Surface Area ( $\text{m}^2/\text{g}$ )	Moisture Content %	SSD Moisture Content %	Ash Content %	Volatile Matter %	Fixed C%	C%	H%	N%	S%	O%
PW	14.47	1.36	243.2	1.92 - 4.95	12.3	22.8	22.8	49.7	50.4	1.9	0.47	0.10	24.4

#### 4.2.2 Concrete

The concrete in this study was prepared with a Quikrete<sup>®</sup> Type I/II cement conforming to ASTM C150 [124]. The aggregates used were a locally sourced mountain granite and quartzitic sand used in commercial concrete. The gravel had a maximum nominal aggregate size of 19 mm (3/4 in) and the sand a fineness modulus of 2.65. The aggregates were stored outdoors in plastic bin stockpiles, so the absorption and moisture content of the gravel and sand was determined via ASTM C566 [173] and ASTM C128 [174] and these percentages are provided in Table 4-2. To account for the high variability in moisture content of the sand caused by outdoor storage conditions, it was tested weekly for moisture content. The mix water was adjusted based on the difference between the aggregate’s measured moisture content and its absorption capacity to ensure that the water available for cement hydration reaction remained consistent.

Table 4-2 Aggregate characteristics

	Absorption (%)	Moisture Content (%)
Sand	0.82	1.16 – 8.95
Gravel	0.90	0.18

#### 4.2.3 Mix Design and Preparation

##### 4.2.3.1 Mix Design

A total of eight concrete mixes, including two control mixes (plain concrete with no additions), were prepared for study. BC concrete was prepared by incorporating BC dosages of 5%, 10%, and 15% by weight of cement into the mix. The sand was partially replaced with BC on a volumetric basis in order to maintain a consistent cement content and mix volume across all mixes. In addition, due to water demand differences of BC mixtures [38 - 44], two different approaches were used to ensure a consistent slump of 152 mm to 178 mm (6 to 7 inches). The slump for one mix at each replacement level and control was managed maintaining the same w/c of 0.45 and the addition of MasterEase 3000<sup>®</sup> superplasticizing admixture (BC0/5/10/15-SP). In addition, the slump for one mix at each replacement level and control

was also maintained by increasing the water content (BC0/5/10/15-w). These two approaches allowed us to understand the influence of water demand on the frost durability of BC concrete. Mix proportions for the mixes are provided in Table 4-3.

Table 4-3 Mix proportions (kg/m<sup>3</sup>)

Mix ID	w/c	Water	Cement	BC	Sand	C.Agg
BC0-SP	0.45	214	475	0	663	1011
BC5-SP	0.45	214	475	24	630	1011
BC10-SP	0.45	214	475	48	598	1011
BC15-SP	0.45	214	475	72	565	1011
BC0-w	0.48	229	475	0	663	1011
BC5-w	0.54	258	475	24	630	1011
BC10-w	0.58	274	475	48	598	1011
BC15-w	0.63	299	475	72	565	1011

The mixing procedure was as follows: the coarse aggregates, cement, BC (if used), and fine aggregates were dry mixed in a 3.5 cubic foot mixer for three minutes. Each material was added in the order given to prevent a large plume of BC and cement dust from exiting the mixer. If used, the superplasticizer (SP) was added to the mix water, and then both liquids were added to the mixer together. The concrete was then mixed for three minutes after all the ingredients were added into the mixer. Prior to casting, the workability of the concrete was monitored using the slump test prescribed in ASTM C143 [175]. The superplasticizer dosage and average slump for each mix is reported in Table 4-4.

Table 4-4 Superplasticizer dosage (mL/100kg) & slump (mm)

Mix ID	BC0-SP	BC5-SP	BC10-SP	BC15-SP	BC0-w	BC5-w	BC10-w	BC15-w
w/c	0.45	0.45	0.45	0.45	0.48	0.54	0.58	0.63
SP	157	400	450	630	0	0	0	0
Slump	163	170	166	169	170	171	170	163

### 4.2.3.2 Casting & Curing

After mixing, each concrete batch was cast in 10.2 cm (d) x 20.3 cm (h) disposable cylinder molds to test for variation in permeability, sorptivity, and compressive strength. To test hardened air void parameters, concrete was cast in 7.6 cm (d) x 15.2 cm (h) disposable cylinder molds; and for freeze-thaw testing, the concrete was cast in prismatic 76 x 102 x 406 cm steel molds. The fresh concrete was consolidated via rodding, following the procedure outlined in ASTM C192 [176]. Specimens were demolded after 24 hours and cured in a saturated calcium hydroxide (limewater) bath at room temperature for 14 days, which is the minimum curing period required to start freeze-thaw testing [34]. Each sample was evaluated at this minimum curing period.

### 4.2.4 Experimental Methods

To further understand how a wood-derived BC affects the frost resistance of concrete mixtures, the hardened air void system and resistance to rapid freezing and thawing cycles were measured in addition to testing by ASTM C666 [34]. Permeability and compressive strength were also analyzed to evaluate properties that are known to affect freeze-thaw performance. Permeability was assessed by measuring the depth of water penetration of concrete subjected to pressurized water. All experiments were conducted on 14-day cured concrete, following the minimum curing condition outlined in ASTM C666 [34]. Figure 4.2 provides an outline of the experimental plan to investigate these research tasks.

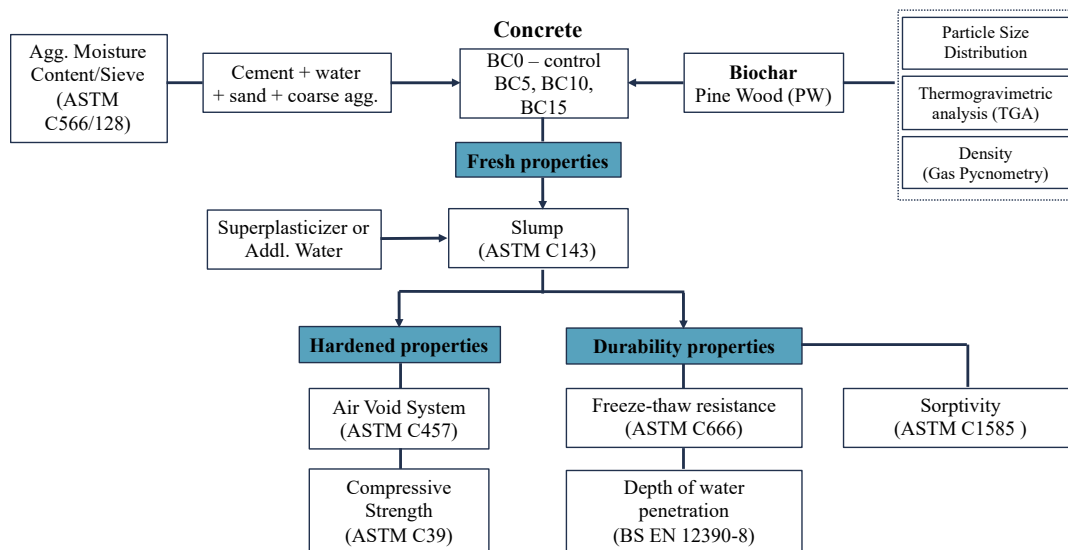


Figure 4.2 Experimental tasks to evaluate BC concrete frost resistance and permeability

#### 4.2.4.1 Compressive Strength

The 14-day compressive strength of the concrete cylinders was determined using a Forney load machine following ASTM C39 [177]. The loading rate was applied at 0.25 MPa per second (35 lbs. per second). The average compressive strength of six samples is reported as the final result.

#### 4.2.4.2 Freeze-Thaw Resistance

Freeze-thaw performance was evaluated following Procedure A of ASTM C666 [34]. The prismatic beam specimens were cured for 14 days prior to testing. The fundamental transverse frequency and weight of each specimen were measured prior to placing them in water. A Humboldt Elite Series Freeze Thaw Cabinet (HC-3186S.4F) was used to alternately lower the temperature of the specimens from 6 °C to -18 °C and then raise it from -18 °C to 6 °C to complete one freeze-thaw cycle. The cabinet maintains the temperature at the center of an air-entrained control specimen via an embedded temperature probe with the use of a 0.6-KW refrigeration unit and electric resistance heaters with fully automatic controls. Samples were removed from the freeze-thaw chamber in a thawed condition, at intervals not exceeding 36 cycles of exposure to test for fundamental transverse frequency and mass. Each specimen was then tested until its relative dynamic modulus of elasticity reached 60% of the initial modulus, a point at which concrete degradation accelerates, leading to substantial cracking and loss of engineering properties. The  $DF$  for each sample was calculated from the relative dynamic modulus of elasticity ( $P$ ) at the number of cycles ( $N$ ) at which the exposure was terminated, as described in Equation 4.1:

$$DF = \frac{P * N}{300} \quad (4.1)$$

#### 4.2.4.3 Depth of Water Penetration

As an evaluation of concrete permeability, British Standard EN 22390-8 [139] was implemented to determine the concrete's depth of water penetration under pressure. A three-test point TESTING Bluhm & Feuerherdt GmbH water impermeability tester with water measurement was used to test each mix. A total of three samples were tested for each BC at each replacement level and for the control concrete, totaling 24 samples. Concrete samples were withdrawn from limewater curing after 14 days, placed in the testing apparatus, and a water pressure of  $5 \pm 0.50$  bar was applied for a duration of 72 hours. Then the cylinders were split into two halves and the depth of penetration measured from the exposed face, using a digital caliper. The reported value is an average of the depth from each half for two samples.

#### 4.2.4.4 Determination of Parameters of the Air-Void System in Hardened Concrete

The automatic image analysis procedure by Fonseca and Scherer [178] was used to determine the air content and spacing factor ( $\bar{L}$ ) of the air-void system in the hardened concrete. This analysis procedure expands upon and provides more complex information about the air void properties than what is described in ASTM C457 [92], the standard test method for microscopical determination of parameters of the air-void system in hardened concrete. Cured cylinders were removed from the limewater bath at 14 days and wet-sawed every 5 cm (2 in) into three individual cross-sections for sample preparation. One surface on each cross-section was polished with Toolcity diamond hand polishing pads using successively finer abrasives for two minutes each, in a series of No. 50, 100, 200, 400, 800, 1500, and 3000 to remove any irregularities from the surface. Then, an even layer of permanent black ink from a Memento Luxe® pad was applied to the polished surface of the specimens. The ink was allowed to dry for 24 hours and then white barium sulfate powder was evenly distributed over the blackened surface and gently pressed into the voids with a rubber stopper. Excess powder was removed by scraping it off the surface with a single-sided razor blade to ensure only air voids were filled with powder. Prepared specimens were then placed on a flatbed scanner and scanned at 3,200 dpi. The MATLAB script provided by Fonseca and Scherer [178] was adapted to process the scanned images into binary images using Otsu's method of thresholding and then perform image analysis to quantify the air void system. Cylinders from three different mixes were evaluated for each BC and the control, totaling 9 samples (27 cross-sections).

#### 4.2.4.5 Concrete Sorptivity

The sorptivity of the concrete was assessed by measuring the increase in the mass of a specimen as a function time as outlined in ASTM C1585-20 [179]. However, in lieu of the standard concrete test specimen requirements and sample conditioning parameters defined by ASTM C1585, the casting, molding, curing, and conditioning procedures developed by Kabir et al. [180] were adopted for this study. These procedures are summarized as follows: 10 x 10 x 10 mm paste cubes were fabricated inside silicone molds at the same mix proportions of OPC, BC, water and SP detailed in Table 4-2 to model the eight different mix designs evaluated in this study. The mixing was conducted in a 50 mL polypropylene centrifuge tube using a vortex mixer at a constant speed for 2 minutes. The paste was then placed into the molds using a 1 mL syringe, which also simulated compaction through rodding, and then covered with a plastic Saran® sheet. The cubes were demolded after 24 hours and cured in a saturated calcium hydroxide (limewater) solution at room temperature (25 °C) for 7 days. To stop the cement hydration process, samples were then fully immersed in isopropyl alcohol for two days. Subsequently, samples were placed inside a vacuum desiccator at room temperature for 14 days for conditioning. To perform the water absorption test, the cubes were sealed on five sides with a Loctite® instant epoxy resin, leaving the sixth

side unsealed for exposure to water. Then following the procedure in ASTM C1585, the mass of the conditioned, sealed samples was recorded as the initial mass. The exposed surface of each sample was placed on 1.5-mm round stainless-steel rods in a container with tap water, where the level of the water was maintained at 2 mm above the support device for the duration of the test (Figure 4.3).



Figure 4.3 ASTM C1585 test set-up

The mass was then recorded at 1-hour intervals for 6 hours, and then once a day until the sample mass plateaued. The accumulative capillary water absorption height,  $I$  (mm), per unit area of the samples was then calculated using Equation 4.4:

$$I = \frac{m_t}{a*d} \quad (4.4)$$

where,  $m_t$  is the change in specimen mass (g), at the time  $t$  ( $s^{1/2}$ ),  $a$  is the area of the unexposed side ( $mm^2$ ), and  $d$  is the density of water ( $0.001 \text{ g}/mm^3$ ). The average absorption of six cubes was then plotted versus the square root of time in  $s^{1/2}$ . The initial rate of water absorption ( $mm/s^{1/2}$ ) was found using a least-square linear regression analysis of the plot of  $I$  versus  $t^{1/2}$  for the points from 1 hour to 6 hours. The secondary rate of water absorption ( $mm/s^{1/2}$ ) was found using a least-square linear regression analysis of the plot of  $I$  versus  $t^{1/2}$  for the points from 1 day to 3 days.

### 4.3 Results and Discussion

#### 4.3.1 Compressive Strength

Figures 4.4 presents the compressive strength of superplasticizer (SP) and water-controlled (w) mixtures. As seen in Figure 4.4, the 14-day compressive strength of both the BC5-SP mix (45.9 MPa) and

BC10-SP mix (41.6 MPa) were greater than the control BC0-SP mix (39.9 MPa). At 15 percent replacement, the BC15-SP mix (39.0 MPa) slightly reduced in strength (-2.2%) compared to the control. The compressive strength results for the SP mixes follow a similar trend as reported by Li et al. [181]. In this work, BC was also used as a partial sand replacement in concrete, but the study utilized a BC derived from *carya cathayensis* peel, which is the outer husk of a species of hickory tree native to China. Li et al. [181] reported that up to 15% replacement of sand with BC (nearly equivalent to the BC10-SP mix proportions of this study) resulted in concretes with better compressive strength. As replacement levels reached 25% sand replacement (similar to BC15-SP mix), compressive strength was slightly reduced compared to the control. They attribute the increased compressive strength to the internal curing effect of BC. As BC content increases, more mix water is absorbed by the BC, effectively lowering the water-to-cement ratio of the concrete and providing additional moisture for later cement hydration [103], [182], [183]. As reflected in Figure 4, all BC-w mixes (35.4, 31.5, and 27.9 MPa) had a reduced compressive strength compared to the control (38.4 MPa). This reduction is explained by the increase in w/c ratio for these mixes from 0.48 to 0.63 as seen in Figure 4.4. Since the strength of concrete is strongly correlated with its w/c, it is expected that the strength of the concrete would decrease with increasing w/c [21]. S. Praneeth et al. [184] also observed compressive strength decreases in their cement mortars as sand was replaced with BC up to 40% of weight basis. In lieu of superplasticizer to overcome loss of workability due to BC addition, they similarly added water in the range of w/c ratio of 0.50 for the control to upwards of 0.65 for BC mixes.

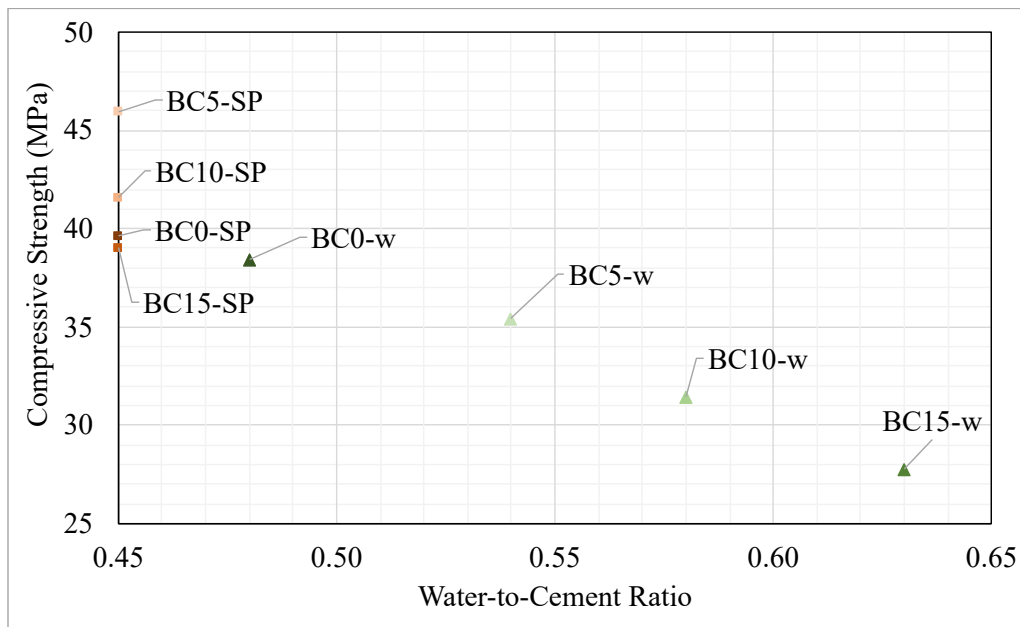


Figure 4.4 Correlation between w/c ratio and 14-day compressive strength

### 4.3.2 Permeability

As an evaluation of concrete permeability, the concrete's depth of water penetration under pressure was evaluated. A lower depth of water penetration typically indicates a finer pore network with less connectivity, qualities that correlate with low water permeability and enhanced frost protection [6]. As seen in Figure 4.5, the depth of water penetration for the BC5-SP, BC10-SP, and BC5-w mixes were less than their respective controls, which would suggest reduced permeability and enhanced freeze-thaw protection for these three mixes. The overall trend for water-controlled mixes is an increase in depth of water penetration as BC replacement increases, which from a durability assessment view suggests a corresponding increase in permeability and reduced freeze-thaw durability as BC content increases for these mixes.

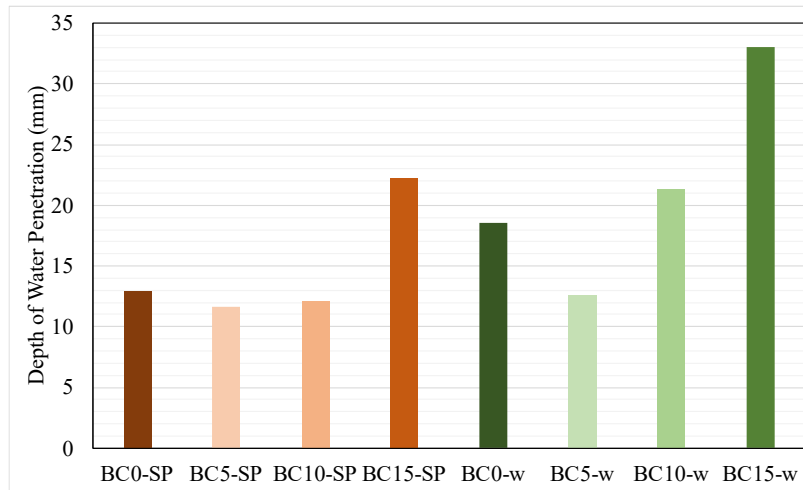


Figure 4.5 Depth of water penetration as an evaluation of concrete permeability

### 4.3.3 Hardened Air Void System

One of the main mechanisms contributing to enhanced freeze-thaw durability is an entrained air void system [24]. Although these samples were not intentionally air-entrained, hardened air void analysis was performed to evaluate the baseline air void system and assess its effect on freeze-thaw performance of the BC concrete. This was done to ensure that the higher dosage of SP used in the BC-SP mixes did not result in unintentional air-entrainment, which could skew interpretation of the results. The hardened air void analysis results provided in Figure 4.6 show a decrease in the air content of concrete with an increase in biochar content. The control-SP mix had the highest air content of 1.62%, followed by the control-w/c air content of 1.28%.

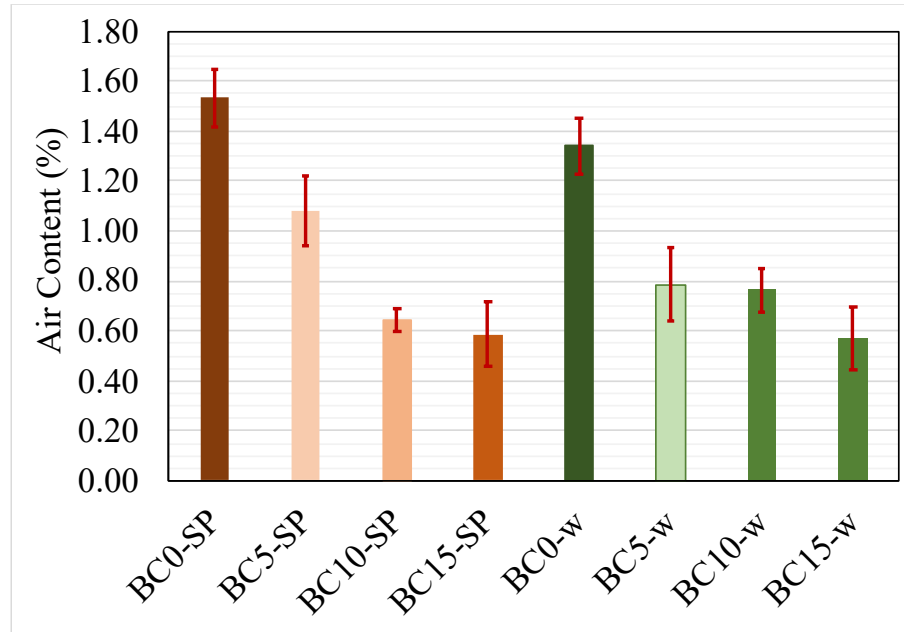


Figure 4.6 Hardened air content ASTM C457. Error bars indicate standard deviation of the triplicate samples tested.

In addition to air volume, the effectiveness of an air void system in providing freeze-thaw protection depends on the void spacing, commonly referred to as the spacing factor ( $\bar{L}$ ) [26], [91]. The spacing factors determined for the hardened concrete in this study are provided in Table 4-5. The Control-SP had the lowest spacing factor of all mixes at 0.33 mm, while the BC15-SP mix had the greatest at 1.07 mm. As reported in many other studies, [94], [96], [97], [98], [171], the spacing factor increases as either superplasticizer dosage or water content is increased. This is explained by the fact that one of the critical requirements of air bubble formation and stabilization is sufficient viscosity of the cementitious matrix to counteract bubble buoyancy [95]. In other words, as viscosity decreases bubbles tend to escape to the surface and rupture, reducing the total amount of air bubbles and increasing the distance between remaining bubbles. A spacing factor of 0.20 mm is generally recommended as the maximum value to ensure safe freeze-thaw durability [92]. This hardened air void analysis indicates that the air void system in these concretes is not expected to provide any benefit to the concrete’s freeze-thaw resistance.

Table 4-5 Air content & spacing factor

Mix ID	BC0-SP	BC5-SP	BC10-SP	BC15-SP	BC0-w	BC5-w	BC10-w	BC15-w
Air Content (%)	1.53	1.08	0.64	0.59	1.34	0.79	0.76	0.57
Spacing Factor (mm)	0.34	0.59	0.61	1.07	0.45	0.56	0.44	0.57

#### 4.3.4 Freeze-Thaw Resistance

The relative dynamic modulus of elasticity (RDME) is used to evaluate frost resistance because when concrete is exposed to freeze-thaw cycles, it gradually loses its elastic performance (stiffness), leading to the loss of dynamic modulus of elasticity and strength [87]. For all eight concrete samples, the change in RDME as a function of freeze-thaw cycle is presented in Figure 4.7. For the control concretes, Figure 4.7 shows that the SP and water-controlled mix dropped below 60% RDME at 97 freeze-thaw cycles (DF = 19) and 38 freeze-thaw cycles (DF = 7), respectively. Due to differences in w/c contents between the two control mixes, this variance in freeze-thaw performance is attributed to differences in permeability, as confirmed in section 4.3.2. These results align with a study by Malhotra [97] who also found that plain, non-air entrained concrete had very low durability factors (<31) and performance decreased as w/c increased. Figure 4.7 also shows that compared to the control concretes, biochar concrete, regardless of mix design, performs worse than the control in freeze-thaw testing, with reduction to 60% RDME after less than 15 cycles. Although the permeability of BC5-SP, BC5-w/c, and BC10-w/c was lower than their respective controls (see section 4.3.2), the DF was  $\leq 2$ .

The poor freeze-thaw performance of biochar concrete may be explained by the mass change of the samples. The mass change results presented in Figure 4.8 indicate that all biochar concretes exhibited a substantial increase in mass as they reached failure. The control-w mix gradually increased and then plateaued, while the control-SP concrete gradually decreased in mass until failure. These results are counter to Jia et al. [31], who initially observed a mass loss rate in their biochar concretes after 75 FT cycles and then an increase to 100 FT cycles for all samples. They attributed the mass gain from 75 to 100 FT cycles to BC's strong water sorption capacity; this is consistent with some of the sorption test data in the present work, which is further discussed in section 4.3.5. Depending on the sorption capacity of the BC concrete, the mass gain can exceed the mass loss from spalling, leading to a net increase in mass. The internal damage of concrete subject to freeze-thaw cycles evolves through three stages: water penetration, water freezing, and tensile cracking [24]. If the BC results in an increase in sorbed water, concrete containing BC could be more prone to freeze-thaw damage, particularly if the water remains trapped in the BC. This is consistent with the explanation proposed by Chen et al. [33]—ice crystal growth inside the BC itself causes deleterious expansive stresses leading to tensile cracking.

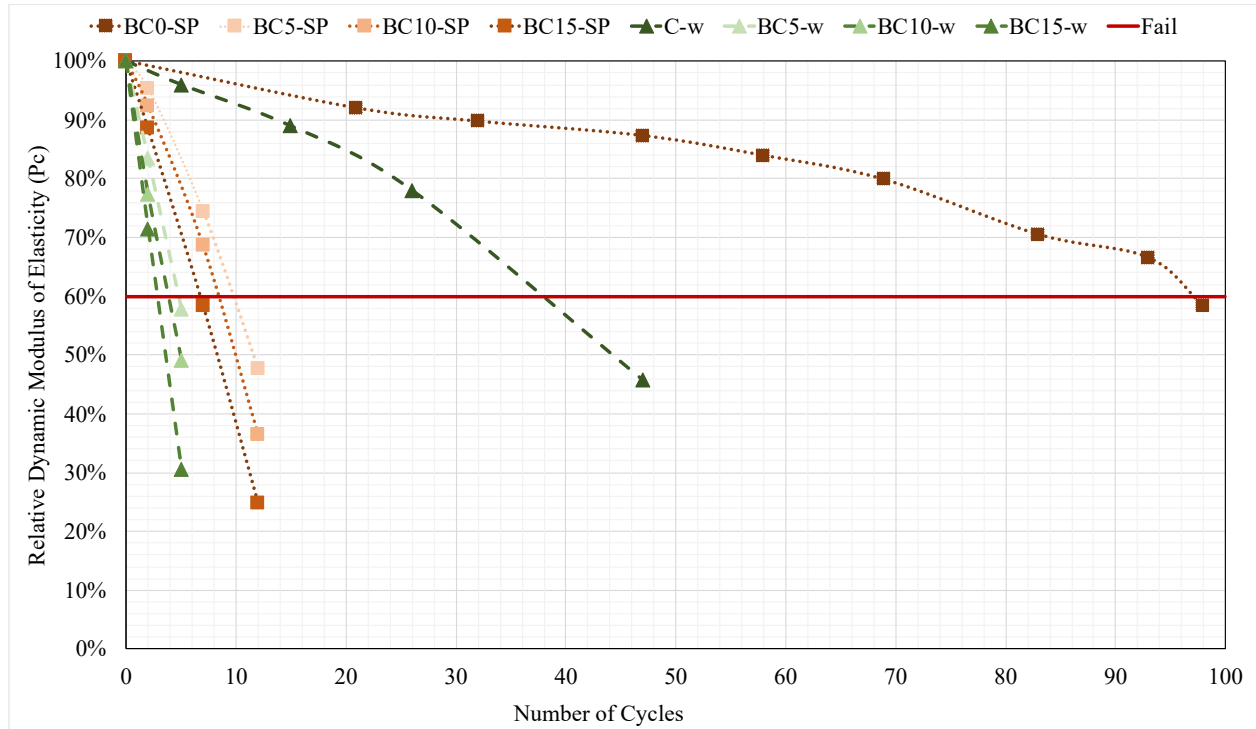


Figure 4.7 Test results of RMDE for non-air entrained concretes

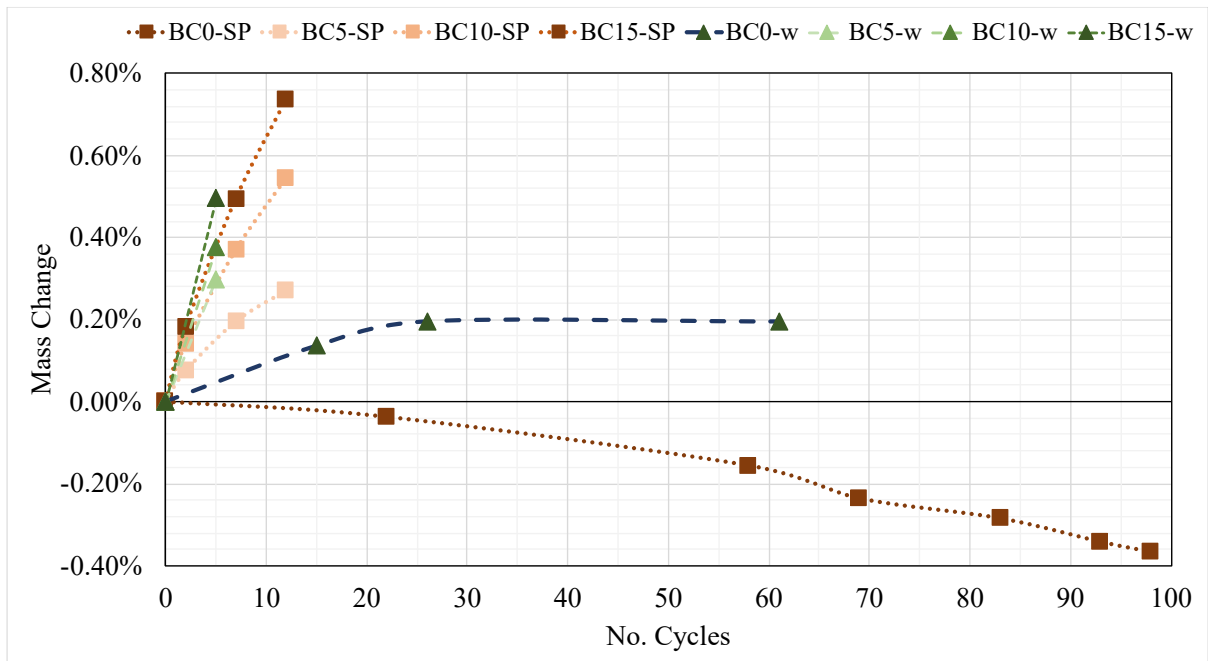


Figure 4.8 Mass change of concrete at associated freeze-thaw cycle

### 4.3.5 Water sorption

To evaluate the theory that the BC concretes are sorbing significant amounts of water, sorptivity of analogous pastes was measured following ASTM C1585-20 [179]. This test subjects pastes to water and evaluates mass gain over time. A plot of cumulative absorption versus the logarithmic function of time can be provided in Figure 4.9. As seen in Figure 4.9, the growth rate of capillary water absorption heights is significantly faster for the water-controlled mixes than the SP-controlled mixes, which is expected given the associated increase in porosity and permeability due to increased w/c for these mixes. This fast rate is also observed in the initial rate of sorptivity provided in Table 4-6, where  $I$  followed the trend of BC15-w > BC10-w > BC5-w > BC0-w. Notably, the BC15-w mix quickly reached a peak cumulative absorption at a time of 100 sec<sup>1/2</sup>, which equates to only 3 hours. Then this rate became nearly constant over the remainder of the 3 days of testing as reflected by a low secondary rate of sorption. The BC10-w and BC5-w mixes followed a very similar trend with a high rate of initial sorptivity and a transition to a lower secondary rate. These rates of sorptivity complement the substantial mass gains observed in Figure 4.8 for the water-controlled mixes. Similar results were observed by K Tan et al. [185] who noted that the initial sorptivity of BC-amended pervious concrete was significantly higher than the control and as sorptivity transitioned to the longer secondary rate, it slowed down for all concretes.

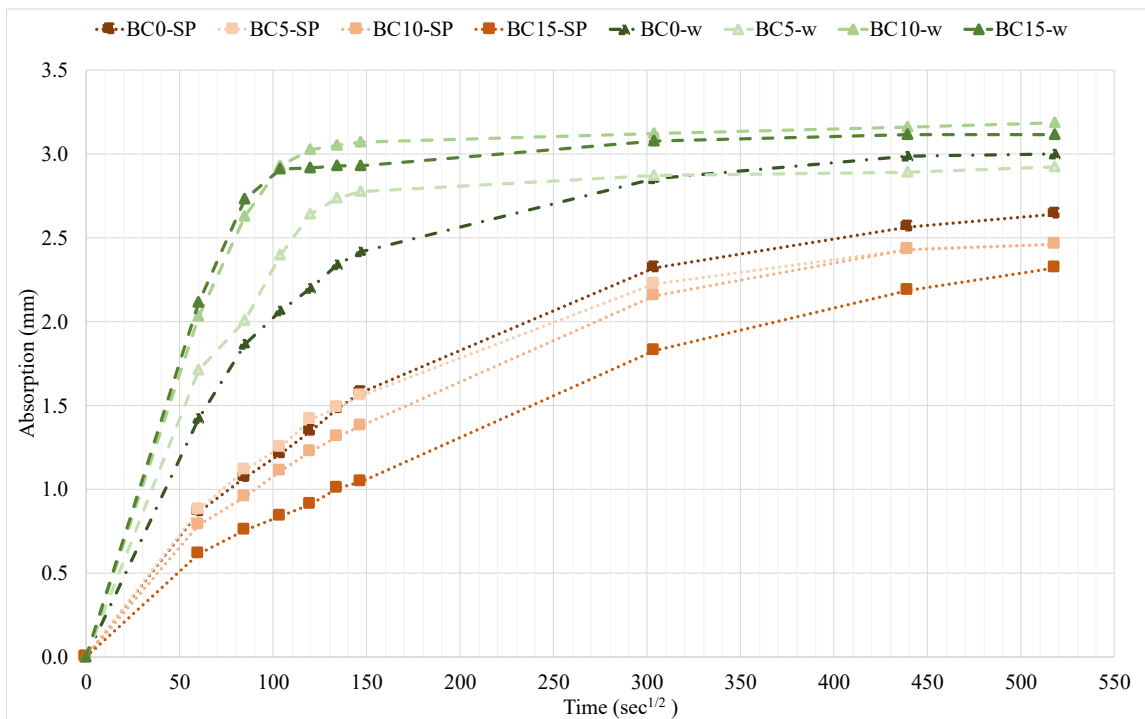


Figure 4.9 Water absorption vs. time

Table 4-6 Rates of sorptivity

Mix ID	Initial Rate of Sorptivity ( $\times 10^{-2}$ mm/s <sup>1/2</sup> )	Secondary Rate of Sorptivity ( $\times 10^{-2}$ mm/s <sup>1/2</sup> )
BC0-SP	1.1	0.29
BC5-SP	1.1	0.24
BC10-SP	0.92	0.29
BC15-SP	0.59	0.34
BC0-w	1.6	0.16
BC5-w	2.2	0.04
BC10-w	2.6	0.03
BC15-w	2.9	0.05

As seen in Table 4-6, the initial rates of sorptivity for the SP controlled mixes at BC0, BC5, and BC10, were nearly the same and lower for the BC15. This trend is counter to what was observed for the water-controlled mixes and complicates the significant mass gains observed in Figure 8. For the BC15-SP mix, the significant, early mass gained during freeze-thaw testing, despite lower initial sorptivity indicates that water ingress was controlled by the long-term absorption rather than rapid capillary uptake. A greater depth of water penetration (Figure 4.6) and higher secondary rate of sorptivity than the control suggests a more connected pore network, promoting more water retention over time. This increased saturation of the pores likely explains the poor-freeze thaw performance and high mass gain of these samples. Conversely, the BC5-SP and BC10-SP mixes had similar rates of initial sorptivity and slightly lower depth of water penetration (Figure 4.66) than the control, demonstrating that water ingress and retention were not governed by bulk permeability. It is possible that at these replacement levels, the BC is modifying the pore structure in a way that introduces additional, but disconnected porosity. This effect would reduce the rate of water movement but increase total water retention, leading to the observed mass gains and poorer freeze-thaw performance. Finally, the BC itself has a high internal porosity and likely retains water within its structure, which would contribute to greater mass gains for the BC concrete than the control, without necessarily affecting capillary-driven absorption rates. Overall, these results highlight the complex dynamics between water sorption mechanisms and pore structure and connectivity.

#### 4.4 Conclusion

In this chapter, the frost resistance of biochar concrete mixtures formulated without air entrainment was evaluated to establish a baseline for biochar concrete freeze-thaw performance compared to

conventional concrete. To evaluate the direct influence of biochar on frost durability, biochar was used as a partial replacement of sand. To explain the reason for observed changes in freeze thaw behavior, ASTM C666 [34] rapid-freeze thaw testing, hardened air void analysis, compression testing, and permeability measurement were performed. Overall, this work shows that non-air entrained biochar concrete performs significantly worse in freeze-thaw testing than conventional concrete. Although there was improved permeability at some replacement levels, the biochar concrete failed at less than 15 freeze-thaw cycles. Biochar concrete's poor freeze-thaw performance has been attributed to its tendency to sorb and retain water. If water inevitably penetrates the concrete during freeze-thaw cycles and remains held by the biochar, significant internal damage could result. It is also possible that the biochar used in the present work has a higher sorption capacity than the biochar used in these other studies. Further investigation is needed to confirm this mechanism and understand its implication to the frost durability of biochar concrete. Future research should explore these hypotheses by incorporating different types of biochar with varying sorption capacities.

Our results contradict the conclusions from other biochar concrete studies on freeze-thaw durability which show improved freeze-thaw durability compared to a control. However, there are a couple of notable differences in the present work compared to these other studies: 1) we follow ASTM C666 [34], which is a more aggressive testing protocol than what is used in these other studies; 2) we use finer particle-size biochar which may hold onto water more tightly; and 3) we replace the sand with biochar instead of the cement, which maintains the paste content to be the same as the control. Since freeze-thaw performance is primarily controlled by paste content, it is possible these other studies benefit from improved freeze-thaw performance due to a decreased cement paste content compared to their control. Future work should further explore integrating biochar as a cement replacement to further understand the effects of biochar and paste reduction on frost resistance.

The final chapter explores the frost resistance of air-entrained biochar concretes to evaluate biochar compatibility with air-entraining admixtures and its performance in comparison with conventional air-entrained concrete. Although improved permeability can enhance frost resistance in concrete, air entrainment is the primary method for protecting concrete against frost damage.

## CHAPTER 5 AN EVALUATION OF BIOCHAR CONCRETE FROST DURABILITY WITH AIR-ENTRAINMENT

### **Abstract**

This chapter investigates the frost durability of air-entrained biochar concrete. A review of the literature revealed that there have been no published studies evaluating the effect of air-entrainment on biochar concrete's freeze-thaw resistance. The goal of this work was to evaluate whether conventional prescriptive requirements for frost protectant concrete apply for biochar concrete, namely 6 vol% air and a spacing factor less than 0.2 mm. Two wood-derived biochars were used in this evaluation. Freeze-thaw durability was assessed through ASTM C666 rapid-freeze thaw testing, hardened air void analysis, compression testing, and foam index testing. This work found that biochar concretes required a 970% to 2,800% increase in air-entraining dosage compared to conventional concrete to entrain an equivalent target 6 vol% air content. Despite meeting requirements for a proper air void system, biochar concrete failed between 165 and 185 freeze-thaw cycles. This degraded freeze-thaw performance is attributed to the higher sorptivity of biochar concrete, attributed to pore refinement. When water in the small pores of biochar concrete freezes, significant internal damage results.

### **5.1 Introduction**

In concrete, the resistance to internal cracking due to freezing and thawing cycles can be achieved if the mixture contains an adequate system of entrained air voids [23], [24]. Due to the movement of water and the growth of ice crystals in the pores of cement paste, hydraulic pressure [25], [26] and crystallization pressure [27] develop, causing damaging internal forces. Concrete's air void system provides escape boundaries to shorten the length that displaced water must travel, decreasing damaging hydraulic pressures in the paste [25]. These purposeful air voids also host ice crystals that attract water from the capillary pores, inducing shrinkage to offset crystallization pressure [27]. *Air entrainment* is the process by which numerous, small air bubbles are intentionally integrated and dispersed throughout the concrete paste matrix. This effect is achieved through the use of an air-entraining admixture (AEA), a surfactant-based solution, added to the fresh concrete mixture that promotes air bubble formation and stabilization [28], [95]. The compatibility of biochar with AEAs is unknown and air-entrained biochar concrete's resistance to rapid freezing and thawing cycles has not yet been evaluated. Given the well-known challenges of entraining air in concrete containing carbon-contaminated fly ash, higher dosages of AEA are anticipated to obtain a target air content [89], [111], [112], [113], [186], [187], [188]. The foam index test as prescribed in ASTM C1827 [189] can be used to predict the dosage of AEA required to

achieve a given air content in fresh concrete. This is typically used to anticipate increased dosage requirements for systems containing fly ash but can be extended for other material combinations.

### 5.1.1 Research Objective

The objectives of this evaluation are twofold: 1) to evaluate the compatibility of AEAs with two wood-derived biochars via foam index testing and verification of air content in freshly mixed concrete; and 2) to evaluate the frost resistance of air-entrained biochar concrete compared to conventional air-entrained concrete. To further investigate the reason for changes in freeze-thaw performance, hardened air void analysis and sorptivity testing were also performed.

## 5.2 Materials and Methods

### 5.2.1 Biochar

Two wood-based feedstocks were used to produce the BC for this investigation and provided by separate commercial biochar manufacturers: 1) a pine wood (PW) BC produced by slow pyrolysis, heated to 800 °C and 2) a mixed wood (MW) forest residue BC produced through fast pyrolysis, heated to 700 °C.

#### 5.2.1.1 Biochar Characterization

The BCs were first milled in a Retsch RS 300 vibratory disc mill for three minutes to minimize the presence of large pores. Following milling, a Microtrac S3500 laser particle size analyzer was used to measure the effective particle size,  $d_{50}$ , of BC in isopropanol. The refractive index of the sample was set at 2.42. The particle size distribution of the two BCs, as compared to OPC is shown in Figure 5.1.

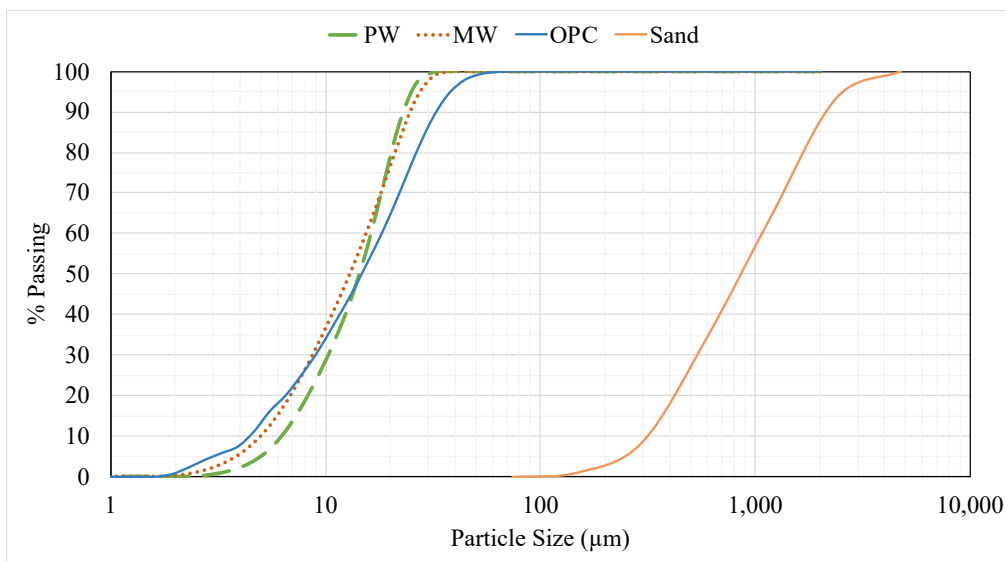


Figure 5.1 Particle Size Distribution of BC & OPC

A Micromeritics AccuPyc II with helium as the displacement medium was used to measure the skeletal density of the milled BC without additional sample preparation steps. The density measurement was conducted by averaging five cycles of pressurized inlet gas into a known volume and sample mass. The BET surface area was measured with nitrogen adsorption-desorption using an NAD device. The BC was stored in closed buckets from the time of milling until use. Since these buckets still permit some exposure to the ambient atmosphere, the ambient moisture content of the BC was routinely measured and accounted for in the concrete mix design as a component of the total mix water content. A PerkinElmer TGA 8000 was used to heat 5-20 mg of BC under a nitrogen flow to 105 °C at 10 °C/min. The BC was isothermally held until the weight stabilized, typically under 60 minutes. Per ASTM D7582 [123], proximate analysis of the BC was conducted using a LECO TGA and ceramic crucibles. The volatile matter, fixed carbon content, and ash content were reported as the wt% of the dry char (dry basis) to evaluate the influence of variable ambient moisture. The carbon, hydrogen, nitrogen, and sulfur mass percentages were determined from ultimate analysis. Oxygen content is reported as the difference between the other elements. The physical and chemical characteristics of the BC are reported in Table 5-1.

Table 5-1 BC characteristics

BC	d50 ( $\mu\text{m}$ )	Skeletal Density ( $\text{g}/\text{cm}^3$ )	Surface Area ( $\text{m}^2/\text{g}$ )	Moisture Content %	SSD Moisture Content %	Ash Content %	Volatile Matter %	Fixed C%	C%	H%	N%	S%	O%
PW	14.47	1.36	243.2	1.92 - 4.95	12.3	22.8	22.81	49.7	50.4	1.9	0.47	0.10	47.3
MW	12.96	1.57	271.4	1.21 - 6.25	15.9	4.5	27.6	88.6	89	1.9	0.70	0.01	3.9

### 5.2.2 Concrete

The concrete in this study was prepared with a Quikrete<sup>®</sup> Type I/II cement conforming to ASTM C150 [124]. The aggregates used were a locally sourced mountain granite and quartzitic sand used in commercial concrete. The gravel had a maximum nominal aggregate size of 19 mm (3/4 in) and the sand a fineness modulus of 2.65. The absorption and moisture content of the gravel and sand was determined via ASTM C566 [173] and ASTM C128 [174]. These percentages are provided in Table 5-2 and accounted for in the concrete mix designs as a component of the total mix water content. To account for the high variability in moisture content caused by outdoor storage conditions, the sand was tested weekly for moisture and adjusted accordingly during mixing.

Table 5-2 Aggregate characteristics

	Absorption (%)	Moisture Content (%)
Sand	0.82	1.16 – 8.95
Gravel	0.90	0.18

### 5.2.3 Air-Entraining Admixture

CHRYSO® Air G100, a sulfonate-based air-entraining admixture (AEA) meeting the requirements of ASTM C260 [190] was used to establish a stable air system in the concrete. As later detailed in the results section, BC mixes required substantially higher AEA dosages than the control. In an effort to avoid inadvertently affecting the slump, the water content of the AEA was also accounted for in the concrete mix designs as a component of the total mix water. Table 5-3 provides the AEA characteristics related to mix proportioning.

Table 5-3 AEA characteristics

Specific Gravity (g/mL)	Water Content (%)	Manufacturer Recommended Dosage (mL/100 kg CM)
1.008	93.5	13 - 488

### 5.2.4 Mix Design and Preparation

#### 5.2.4.1 Mix Design

A total of 3 concrete mixes, including a control, were prepared for this investigation. A water-to-cement ratio of 0.54 was used for all mixes to maintain a consistent slump of 152 mm to 178 mm (6 to 7 inches). No superplasticizers were used in these mixes to manage workability due to the possibility of antagonistic interactions between superplasticizers and air-entraining admixtures (AEAs) [94], [96], [97], [98]. However, AEAs can lubricate the mix due to the “ball bearing” effect of air bubbles, which improves workability [191]. A BC content of 10% by weight of cement was integrated into the BC concrete mixes. To maintain a consistent cement content across all mixes, the sand was partially replaced with biochar on a volumetric basis, which ensured the water-to-cement ratio remained constant. The water-to-cement ratio and BC replacement level were selected based on the results from the study detailed in Chapter 4. These parameters were found to support sufficient workability without significantly compromising mechanical properties. A target air content of  $6 \pm 1\%$  was selected according to the F2

class freezing and thawing requirements of ACI 318-19(22) [7]. Mix proportions for each sample are provided in Table 5-4.

Table 5-4 Mix proportions (kg/m<sup>3</sup>)

Mix ID	Water	Cement	BC	Sand	C.Agg
Control	209	386	0	666	1,011
PW	209	386	39	592	1,011
MW	209	386	41	602	1,011

The mixing procedure was as follows: the coarse aggregates, cement, BC (if used), and fine aggregates were dry mixed in a 3.5 cubic foot mixer for three minutes. Per manufacturer guidance, the AEA was first added to the mix water, and then both liquids were added to the mixer together. The concrete was then mixed for two minutes after all the ingredients were added into the mixer. Prior to casting, the workability of the concrete was monitored using the slump test prescribed in ASTM C143 [175]. The average slump for three mixes is reported in Table 5-5.

Table 5-5 Slump (mm)

Control	PW	MW
208	163	174

#### 5.2.4.2 Casting and Curing

After mixing, each concrete batch was cast in 7.6 cm (d) x 15.2 cm (h) disposable cylinder molds to test for variation in hardened air void parameters and compressive strength; in 10.2 cm (d) x 20.3 cm (h) disposable cylinder molds to test for sorptivity; and for freeze-thaw testing, the concrete was cast in prismatic 76 x 102 x 406 cm steel molds. The fresh concrete was consolidated via rodding, following the procedure outlined in ASTM C192 [176]. Specimens were demolded after 24 hours and cured in a saturated calcium hydroxide (limewater) bath at room temperature for 14 days, after which the samples were evaluated in freeze-thaw testing [34].

#### 5.2.5 Experimental Methods

As the main objective of this investigation was to evaluate how BC impacts the frost resistance of air-entrained concrete, the resistance to rapid freezing and thawing cycles and the hardened air void system were evaluated. Additionally, the foam index test was conducted on cement-BC slurries to assess the

compatibility of a synthetic AEA with BC and to estimate a baseline dosage of AEA. The AEA efficacy was further evaluated by establishing the dosage required to stabilize 6% air in freshly mixed concrete. Finally, the compressive strength was examined to evaluate properties that are known to influence freeze-thaw performance. Figure 5.2 provides an outline of the experimental plan to examine these research tasks.

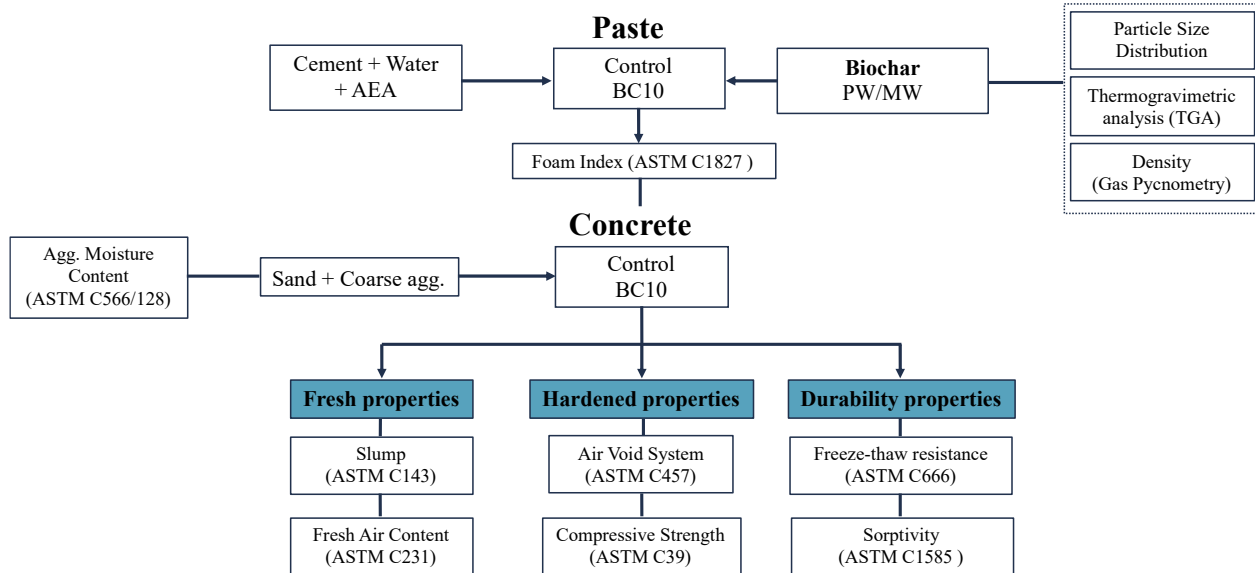


Figure 5.2 Experimental tasks to evaluate biochar concrete frost resistance and biochar compatibility with AEA

### 5.2.5.1 Foam Index Test

The foam index test as described by ASTM C1827 [189] was employed to evaluate the compatibility of BC with a synthetic AEA. In this method, a combination of 10 grams of cement and 1 gram of biochar was added to tap water in a 250 mL wide-mouth plastic container and vigorously agitated for 30 seconds. Then, a dilute solution of AEA was added one drop at a time from a standardized pipette and agitated for 10 seconds to produce foam. The stability of the foam was observed, and this process was repeated until a stable foam was achieved. The total number of drops,  $N_D$ , required to attain this stable foam was then annotated. The specific foam index ( $SFI$ ) was calculated using Equations 5.1 and 5.2, based on the work of Harris et al. [192], [193], [194], to normalize the volume of AEA by mass of cementitious material:

$$FI (\mu\text{L}) = N_D V_D C_s \quad (5.1)$$

where,  $V_D$  = standardized single drop volume ( $\mu\text{L}/\text{drop}$ ) and  $C_s$  = AEA Solution Concentration (%)

$$SFI = \frac{FI}{10 \text{ g CM}} * 100 \quad (5.2)$$

where,  $SFI$  = Specific Foam Index (mL/100 kg CM)

The foam index test was executed five times and the range of SFI required to produce a stable foam was reported.

### 5.2.5.2 Evaluation of Air Content of Freshly Mixed Concrete

The air content of the freshly mixed concrete was verified by the Pressure Method, ASTM C231 [107]. The first step in the method was to fill, consolidate, and level fresh concrete in the bottom chamber of the pressure meter. The pressure meter lid is then secured to the bottom chamber with clamps, the main air valve is closed, and both petcocks are opened. Water is added through one petcock until water emerges from the other petcock. Then, the top chamber is pressurized to 100 kPa (14.5 psi) and permitted to stabilize. Finally, the petcocks are closed and the lever is held for at least 10 seconds to bring the chambers to equilibrium as the bottom chamber is struck with a rubber mallet on all sides. The value from the digital gauge is recorded as the air content in the concrete.

### 5.2.5.3 Determination of Parameters of the Air-Void System in Hardened Concrete

The automatic image analysis procedure by Fonseca and Scherer [178] was used to determine the air content and spacing factor ( $\bar{L}$ ) of the air-void system in the hardened concrete. This analysis procedure expands upon and provides more complex information about the air void properties than what is described in ASTM C457 [92], the standard test method for microscopical determination of parameters of the air-void system in hardened concrete. Cured cylinders were removed from the limewater bath at 14 days and wet-sawed every 5 cm (2 in) into three individual cross-sections for sample preparation. One surface on each cross-section was polished with Toolcity diamond hand polishing pads at successively finer abrasives for two minutes each, in a series of No. 50, 100, 200, 400, 800, 1500, and 3000 to remove any irregularities from the surface. Then, an even layer of permanent black ink from a Memento Luxe® pad was applied to the polished surface of the specimens. The ink was allowed to ambiently dry for 24 hours and then white barium sulfate powder was evenly distributed over the blackened surface and gently pressed into the voids with a rubber stopper. Excess powder was removed by scraping it off the surface with a single-sided razor blade to ensure only air voids were filled with powder. Prepared specimens were then placed on a flatbed scanner and scanned at 9,600 dpi. The MATLAB script provided by Fonseca and Scherer [178] was adapted to process the scanned images into binary images using Otsu's method of thresholding; then image analysis was performed to quantify the air void system. Cylinders from three different batches were evaluated for each BC and the control, totaling 5 samples (15 cross-sections).

#### 5.2.5.4 Freeze-thaw resistance

Freeze-thaw resistance was evaluated following Procedure A of ASTM C666 [34]. The prismatic beam specimens were cured for 14 days prior to testing. The fundamental transverse frequency and weight of each specimen were measured prior to placing them in water. A Humboldt Elite Series Freeze Thaw Cabinet (HC-3186S.4F) was used to alternately lower the temperature of the specimens from 6 °C to -18 °C and then raise it from -18 °C to 6 °C to complete one freeze-thaw cycle. The cabinet maintains the temperature at the center of an air-entrained control specimen via an embedded temperature probe with the use of a 0.6-KW refrigeration unit and electric resistance heaters with fully automatic controls. Samples were removed from the freeze-thaw chamber in a thawed condition, at intervals not exceeding 36 cycles of exposure to test for fundamental transverse frequency and mass. Each specimen was then tested until it was subjected to 300 cycles or until its relative dynamic modulus of elasticity reached 60% of the initial modulus. The durability factor ( $DF$ ) for each sample was calculated from the relative dynamic modulus of elasticity ( $P$ ) at the number of cycles ( $N$ ) at which the exposure was terminated, as described in Equation 5.3:

$$DF = \frac{P * N}{300} \quad (5.3)$$

#### 5.2.5.5 Concrete Sorptivity

The sorptivity of the concrete was assessed in accordance with ASTM C1585-20 [179]. Following 14 days of curing, 10.2 cm (d) x 20.3 cm (h) cylinders were sawed into four cylinders of length equal to 5 cm. The samples were conditioned inside a humidity chamber at 30 °C and 80% RH for three days. After 3 days, each sample was placed in a sealable container and stored for 18 days. Then the samples were sealed on the sides with 5-cm adhesive aluminum tape; water exposure of the ends of the sample was avoided by securing a plastic sheet with an elastic band. The mass of the conditioned, sealed samples was recorded as the initial mass. The exposed surface of each sample was placed on 1.5 mm round stainless-steel rods in a pan with tap water, where the level of the water was maintained at 2 mm above the support device for the duration of the 8-day test (Figure 5.3). The mass was then recorded at predefined intervals outlined in C1585-20 [179]. Initial and secondary rates of water absorption were determined from using a least-square linear regression analysis for data between 1 min to 6 hours and 1 d to 7 d respectively.

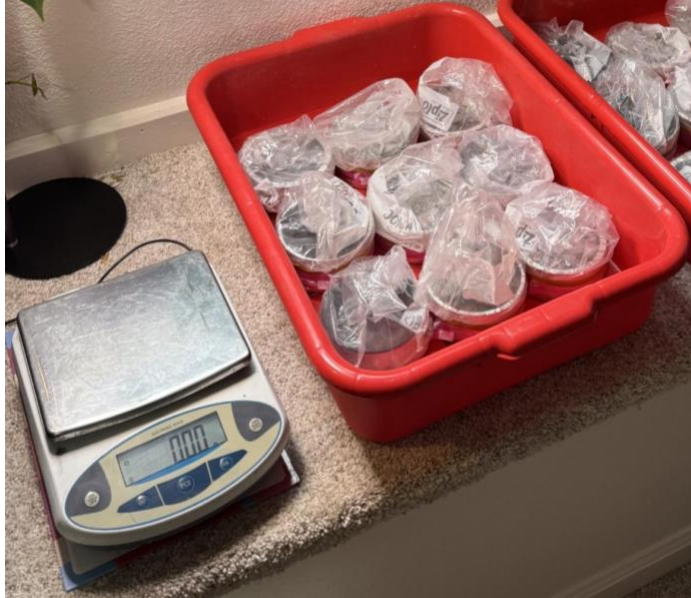


Figure 5.3 ASTM C1585 test set-up

#### 5.2.5.6 Compressive Strength

The 14-day compressive strength of the concrete cylinders was determined using a Forney load machine following ASTM C39 [177]. The loading rate was applied at 0.25 MPa per second (35 lbs per second). The average compressive strength of nine samples is reported as the final result.

### 5.3 Results and Discussion

#### 5.3.1 AEA Efficacy

The foam index method as prescribed in ASTM C1827 [189] was employed to evaluate the compatibility of BC with the synthetic AEA used in this study. The calculated specific foam indexes (SFIs) are provided in Table 5-5. The SFI for a cement-only slurry was within the manufacturer's recommended range of 13 – 488 mL per 100 kg of cementitious materials; however, both BCs required substantially more AEA to produce a stable foam. It is also important to note that it was necessary to increase the AEA solution concentration ( $C_g$ ) from 2.5% for the OPC-only test to 10% for the BC tests to fall within an acceptable range of drops (10 to 20) in order to provide a consistent measure of the AEA adsorption potential of system [189]. The test end point, which is defined as the point where the liquid-air interface is completely covered with foam [192], is depicted in Figure 5.4.

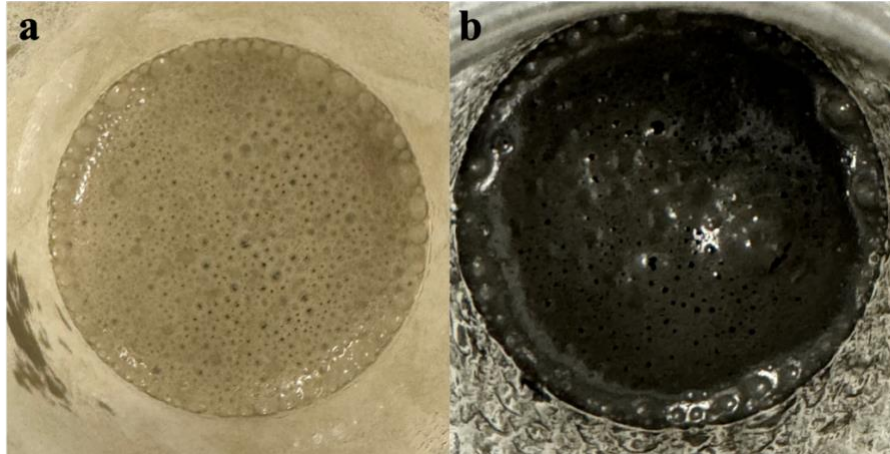


Figure 5.4 FI Test End Point; (a) OPC-only and (b) PW BC

The results of the FI test distinctly indicate that like carbon-containing fly ash, biochar interferes with air-entrainment. The SFI for each material was used as a predicted dosage to determine the actual AEA dosage required to stabilize 6 +/- 1% air in freshly mixed concrete. Several trial batch mixes were conducted for each material and the air content of the freshly mixed concrete was verified by the ASTM C231 [107] Pressure Method. The results of these trial batches and actual AEA dosages are provided in Table 5-6.

Table 5-6 Predicted vs. actual AEA dosages (mL/100kg CM)

	OPC	PW	MW
SFI	52 - 78	1,040 - 1,352	864 - 1,011
Actual	75	2,000	750

As seen in Table 5-6, the control mix actual dosage of 75 mL per 100 kg CM was well predicted by the foam index test; however, both BC mixes required adjustments from their predicted values. The PW BC required a 2,800% increase in AEA dosage and the MW BC required a 970% increase. A comparison of the differing amounts of AEA required for a 22-L mix are displayed in Figure 5.5. Note 9 in ASTM C1827 [189] highlights that the precision of the foam index test is based on a supplementary cementitious replacement level of 20%, which can account for the difference in SFI versus actual dosage of AEA for the BC mixes. Nevertheless, the foam index test is still a useful tool for researchers and industry because it can 1) provide a baseline AEA dosage for use in trial batching mixes and 2) conclusively indicate that BC interferes with bubble formation/stability.

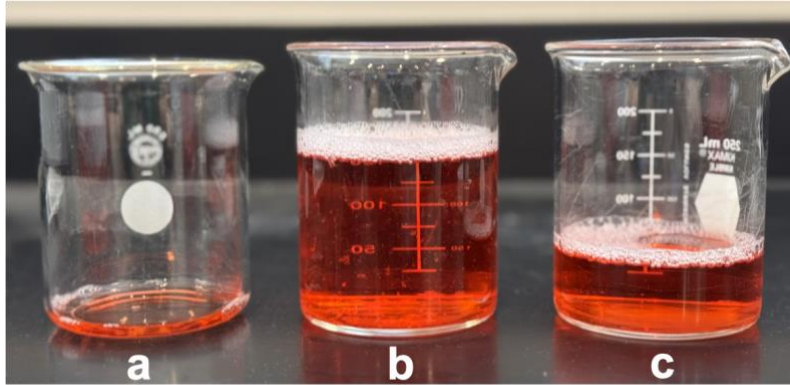


Figure 5.5 Comparison of AEA dose; (a) Control, (b) PW, (c) MW

### 5.3.2 Air Void System

The primary mechanism to enhance freeze-thaw resistance in concrete is to ensure that the hardened concrete has an adequate system of entrained air voids [80], which is defined by both total air content and proximity of air voids in the concrete. ACI 318-22 [7] recommends that fresh air be in the range of 3% to 7% depending on the size and type of aggregates and the severity of the exposure conditions. Also, based on the work of Powers [26], [91], the effectiveness of an entrained air system depends on the void spacing. The maximum value of the spacing factor ( $\bar{L}$ ) is usually taken as 0.20 mm [92], but recent work suggests that a better estimate is 0.30 mm [95]. The air void system parameters for the concretes evaluated in this study are documented in Table 5-7. By prescriptive standards, both air content and spacing factor indicate that all three concretes have developed an adequate system of entrained air voids according to conventional practices.

Table 5-7 AVS parameters

	Control	PW	MW
Fresh Air Content (%)	6.6	6.6	6.9
Hardened Air Content (%)	6.1	5.6	5.7
Spacing Factor (mm)	0.26	0.26	0.34

### 5.3.3 Freeze-Thaw Resistance

The relative dynamic modulus of elasticity (RDME) is used to evaluate frost resistance because when concrete is exposed to freeze-thaw cycles, it gradually loses its elastic performance (stiffness), leading to the loss of RDME and strength [87]. For the three concrete mixes, the change in RDME as a function of

freeze-thaw cycle is provided in Figure 5.6. As expected, the RDME of the air-entrained control remains greater than 90% for 300 freeze-thaw cycles (DF = 91) [97]. A DF greater than 80 is generally considered as providing good freeze-thaw durability [195]. On the other hand, the RDME of air-entrained BC concrete attained less than 60% RDME by 185 cycles. The PW mixture failed at 165 freeze-thaw cycles (DF = 33), while the MW BC failed at 185 freeze-thaw cycles (DF = 37).

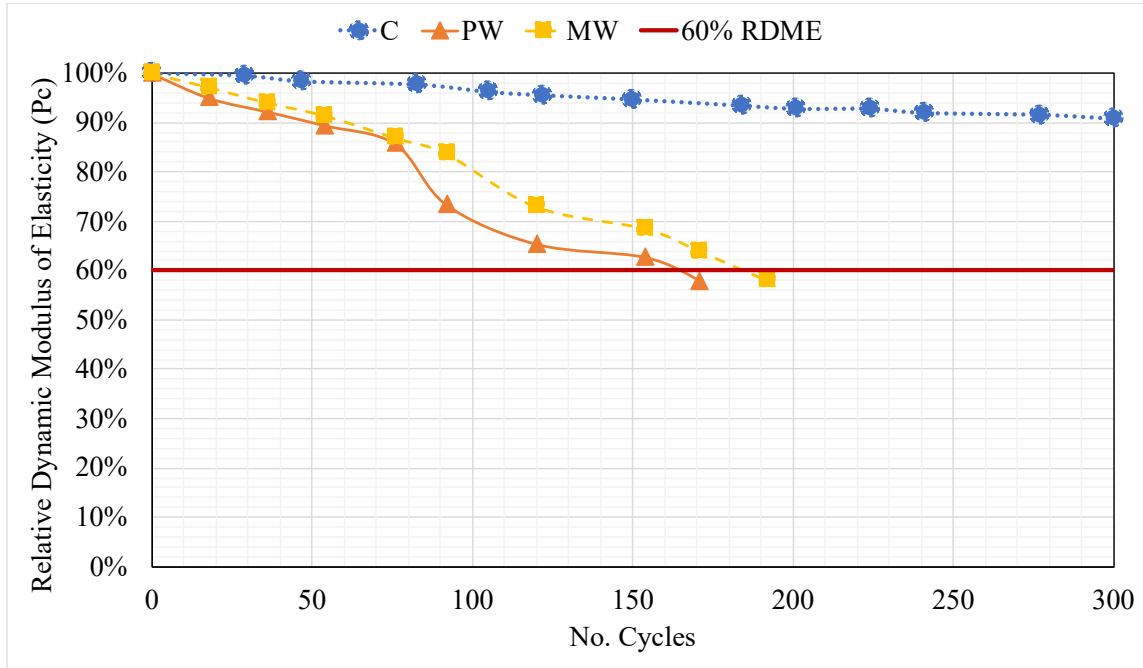


Figure 5.6 Test Results of RDME

According to best practices for conventional concrete, the BC concretes should have had similar frost resistance to the control since their air void systems were similar. Yet, both samples failed well before 300 freeze-thaw cycles. Compared to the performance of the non-air-entrained concretes reported in section 4.3.4, it is evident that the air-entrained BC concretes have much higher freeze-thaw resistance than non-air-entrained BC concretes. However, the poor freeze-thaw performance of both air-entrained and non-air-entrained BC concrete could also be due to BC refining the pore network, resulting in larger pressures developed during a freezing event. This is discussed further in section 5.3.4.

In Chapter 4, the BC concretes exhibited a substantial increase in mass as they reached failure. This effect was not as significant in the air-entrained BC samples. As seen in Figure 5.7, the control concrete maintained a constant mass profile (+0.10%) for the entirety of the 300-cycle test duration, with very little observable physical deterioration. Although there was an initial mass gain for the PW BC, beginning at around 30 cycles, these concrete samples began to lose mass rapidly until reaching below 60% RDME. The MW BC maintained a positive mass profile for nearly 90 cycles, before it too began to lose mass. As

shown in Figure 5.8, the physical mass loss experienced by PW BC concrete was much greater than the mass gain induced by BC water sorption.

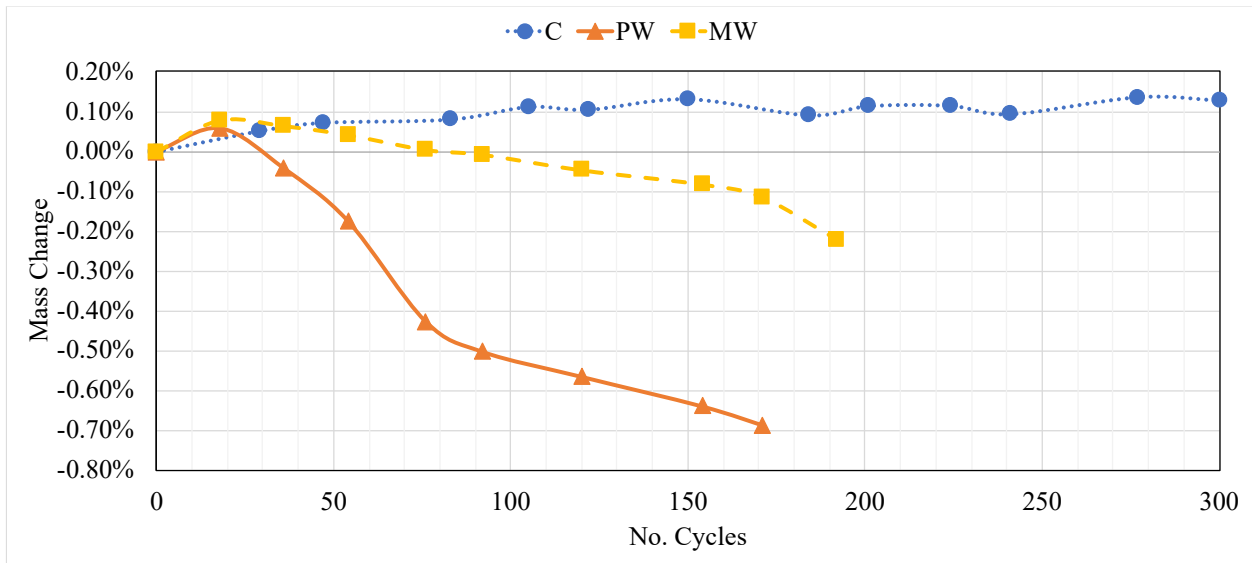


Figure 5.7 Mass Change of Concrete exposed to Freeze-Thaw Cycles



Figure 5.8 PW BC Concrete Mass Loss at 170 FT cycles

### 5.3.4 Water sorption

To evaluate the theory that sorption of biochar concrete is controlling the freeze-thaw performance, sorptivity of these mixes were evaluated and reported in Table 5-8. ASTM C1585-20 [179] divides the sorptivity profile into two regions: 1) the initial rate of sorptivity is the rapid capillary water penetration,

which accelerates the approach to critical saturation and susceptibility to freeze-thaw damage and 2) the secondary rate of sorptivity, which is a diffusion-driven absorption over a longer period of time and is more related to overall pore connectivity and structure [196].

Table 5-8 Concrete Rates of Sorptivity

	Initial Rate of Sorptivity ( $\times 10^{-3}$ mm/s <sup>1/2</sup> )	Secondary Rate of Sorptivity ( $\times 10^{-3}$ mm/s <sup>1/2</sup> )
Control	2.0	0.7
PW	2.4	0.9
MW	4.1	1.2

The sorptivity results indicate that both the initial and secondary rates of sorptivity are higher for the BC concrete than the control. As sorptivity transitioned to the longer secondary rate, it slowed down for all concretes. Similar results were observed by K Tan et al. [185] who observed that the initial sorptivity of biochar-amended pervious concrete was significantly higher than the control. These results also complement the initial weight gain profiles shown in Figure 5.7, where the mass gain of the MW and PW BC concretes was rapid, compared to a much gradual increase for the control. Despite having higher rates of sorptivity and lower compressive strength (5.3.5), and a greater spacing factor (5.3.2) the MW BC slightly outperformed the PW BC in freeze-thaw performance, suggesting that sorptivity and microstructure may not be the only factor controlling freeze-thaw performance of BC-amended concretes.

As proposed in section 4.3.5, it is possible that the BC is modifying the pore structure in a way that affects both pore size distribution and connectivity, which would affect both water ingress and retention behavior, and ultimately freeze-thaw performance. However, although both mixes displayed poor freeze-thaw durability, the PW BC experienced more significant mass loss (Figure 5.7) and physical deterioration (Figure 5.8) than the MW BC sample. This is consistent with the explanation proposed by Chen et al. [33]—higher water retention in the PW BC itself and subsequent ice crystal growth inside the BC pores may cause deleterious expansive stresses leading to tensile cracking and worse freeze-thaw performance. However, petrographic examination of sample thin sections does not reveal any obvious defects originating from biochar particles. Thermoporometry via differential scanning calorimetry (DSC) is one technique that could be used to analyze the amount of freezable and non-freezable water, providing insights into how BC modifies the pore structure, affects water retention, and influences ice nucleation and growth [197], [198].

### 5.3.5 Compressive Strength

The 14-day compressive strengths of the three concrete mixes are presented in Figure 5.9. The compressive strength of the PW BC mix (31.7 MPa) was 15% greater than the control mix (27.5 MPa). The MW BC mix (28.0 MPa) was also slightly stronger (2%) compared to the control. A decrease in compressive strength is generally expected with an increase in porosity; however, the hardened properties are sensitive to the mix design parameters [21].

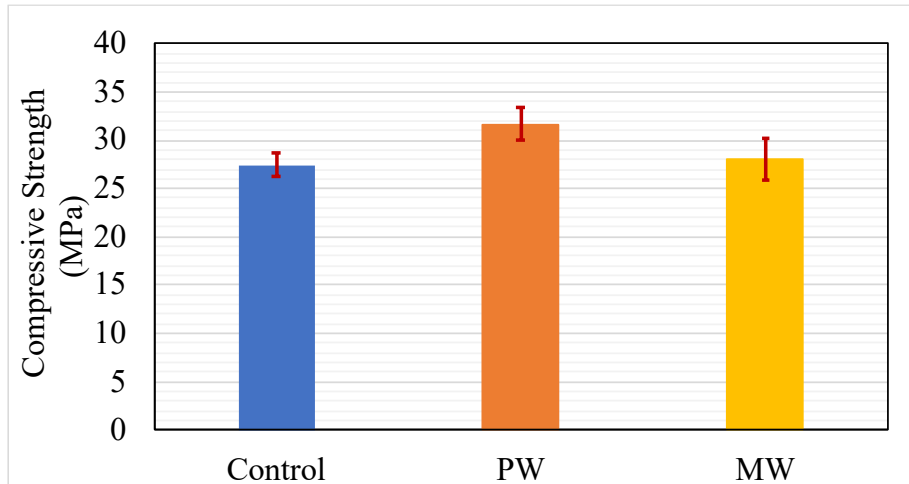


Figure 5.9 14-day compressive strength of air-entrained concrete. Error bars indicate the standard deviation of the nine samples tested.

Similarly, Li et al. reported that up to 15% replacement of sand with BC (nearly equivalent to the mix proportions of this study) resulted in concretes with better compressive strength, which they attributed to the internal curing effect of BC. As BC content increases, more mix water is absorbed by the BC, effectively lowering the water-to-cement ratio of the concrete and providing additional moisture for later cement hydration [103], [182], [183]. Since all three of these mixes are at the same water-to-cement ratio of 0.54, these strength increases may be attributed to the internal curing effect of BC, but this requires additional exploration that is outside of the scope of the current project. Increased compressive strength would also usually be an indicator of a denser microstructure and enhanced FT protection. However, the PW BC was a stronger concrete but performed worse in freeze-thaw testing, suggesting factors other than enhanced microstructure play a factor in freeze-thaw performance.

## 5.4 Conclusion

In this final chapter, the frost durability of air-entrained biochar concretes was evaluated. Two wood-derived biochars were used as a partial replacement of sand and analyzed through ASTM C666 [34] rapid-freeze thaw testing, hardened air void analysis, compression testing, and foam index testing. As

postulated, this experimental work found that like fly ash, biochar concretes similarly interfered with air entrainment. To entrain 6 vol% air, biochar concrete requires a 970-2,800% increase in air-entraining dosage compared to conventional concrete.

Surprisingly, despite acquiring an adequate air void system, biochar concrete failed the freeze-thaw test between 165 and 185 freeze-thaw cycles (DF = 33-37). These results are counter to precedence, where proper air-entrainment in concrete has proven to provide adequate frost resistance. As also observed in Chapter 4, the overall poor freeze-thaw performance of both air-entrained and non-air-entrained BC concrete could also be due to BC refining the pore network, resulting in larger pressures developed during a freezing event.

This study focused on the efficacy of a single, industry used synthetic air entraining admixture. Moreover, only wood-derived biochar was investigated as a sand replacement in the concrete. Future work should consider a multitude of air entraining admixtures to further understand biochar/AEA compatibility. Additional biochar biomasses should also be considered to further elucidate the findings from this study. Finally, a target 6% air content was selected based on industry standards for the size of aggregate used in the concrete and exposure category. However, future research should evaluate if higher entrained air contents, like required for very impermeable ultra-high-performance concretes, is a simple, viable solution.

## CHAPTER 6 CONCLUSIONS

### 6.1 Major Contributions

This thesis advances the understanding of biochar-amended concrete durability performance, specifically by improving the understanding of frost durability and durability assessment. This work lays the foundation for emerging advancements into a more sustainable and versatile concrete material. The integration of a carbon-negative, renewable material like biochar into cementitious materials shows considerable promise for a more sustainable construction industry. The major scientific conclusions related to each research objective are detailed in section 6.2 and recommendations for future research are suggested in section 6.3.

### 6.2 Major Conclusions

This section presents the major scientific conclusions related to each research objective.

#### 6.2.1 Objective 1: Separate the effects of changes in pore structure from changes in matrix conductivity.

- Biochar has a significant influence on the electrical properties of cementitious composites through changes to both electrical and electrolytic conductivity. Assessing the permeability of conventional concrete via non-destructive electrical resistivity measurements is practical, but may lead to erroneous conclusions in the case of biochar cementitious composites.
- Direct conductivity measurements of the biochar were conducted; however, the most conductive mortar was not produced using the most conductive biochar.
- A geometrical model was used to predict that a biochar volume fraction of  $\sim 0.27$  (corresponding to  $\sim 25\text{--}43$  wt% cement replacement in the mix designs) was necessary to form a continuous conductive network. This threshold is much higher than the  $5\text{--}15$  wt% replacements commonly used in the literature. Even at or above this threshold, conductive networks only formed for two of the four biochars tested. Biochar does have potential to act as conductive filler material as other researchers have suggested, but only at high concentrations.
- Among the four biochars tested, only one reduced mortar resistivity relative to the control; the others increased it. These results can be attributed to: 1) reduced permeability as verified through depth of water penetration testing, which tends to increase resistivity; and 2) ions solubilized from the biochar into the cement pore solution, which tend to decrease resistivity.

### **6.2.2 Objective 2: Evaluate the frost resistance of biochar concrete without air entrainment.**

- Depth of water penetration measurements indicate that at some sand replacement levels, biochar concrete was less permeable than conventional mixes. As a cement replacement, the findings demonstrate that like other supplementary cementitious materials, biochar is more effective at reducing permeability by directly influencing overall paste content, which plays a critical role in overall concrete durability.
- Non-air entrained biochar concrete performs significantly worse in freeze-thaw testing than conventional concrete.
- Although there was improved permeability at some replacement levels, the biochar concrete failed at less than 15 freeze-thaw cycles.

### **6.2.3 Objective 3a: Assess the efficacy of a sulfonate-based air-entraining admixture with biochar.**

- Biochar concretes required a 970% to 2,800% increase in air-entraining dosage compared to conventional concrete in order to entrain an equivalent target 6 vol% air content

### **6.2.4 Objective 3b: Evaluate the first resistance of biochar concrete with air entrainment.**

- Despite meeting requirements for a proper air void system, biochar concrete failed between 165 and 185 freeze-thaw cycles (DF = 33-37).
- Compared to the performance of the non-air entrained concretes reported in Chapter 4, it is evident that air entrainment has a positive effect on freeze-thaw resistance of air-entrained biochar concretes compared non-air-entrained biochar concretes.
- According to the prescriptive requirements for conventional concrete, the RDME of the air-entrained control remained greater than 90% for 300 freeze-thaw cycles (DF = 91).
- While air-entrainment improves biochar concrete's frost durability, it does not obtain the same frost resistance as conventional concrete.
- The degraded freeze-thaw performance is suspected to be due the higher sorptivity of biochar concrete, attributed to pore refinement. When water in the small pores of biochar concrete freezes, significant internal damage results.

## **6.3 Recommendations for Future Work**

Based on the outcomes of this thesis, the following are recommendations for areas of future work to improve the durability performance of biochar-amended cementitious composites and to promote industry acceptance of this carbon-negative construction material.

- A method for estimating changes in pore solution conductivity was explored in Chapter 3. The chemical composition and electrical conductivity of the pore solution varied greatly when different biochars were introduced into the mix. A future area of research should be to further elucidate biochar impact on cement pore solution. The understanding of this is not only critical to its influence on the electrical properties of the composite, but to the deleterious chemical effects from durability issues like sulfate attack, alkali-silica reaction, and rebar corrosion.
- The poor freeze-thaw performance of biochar concrete has been attributed to biochar sorbing water and not releasing it, resulting in defect sites during a freezing event. However, permeability and sorptivity results from this work highlight the complex dynamics between water sorption mechanisms and pore structure and connectivity. Thus, the poor freeze-thaw durability could be due to biochar refining the pore network, resulting in larger pressures developed during a freezing event. Future research should explore these hypotheses by incorporating different types of biochar with varying sorption capacities and by integrating biochar as a cement replacement to further understand the effects of biochar and paste reduction on frost resistance. Future work should also consider thermoporometry via differential scanning calorimetry (DSC) to analyze the amount of freezable and non-freezable water, providing insights into how biochar modifies the pore structure, affects water retention, and influences ice nucleation and growth.
- This study focused on the efficacy of a single, industry used sulfonate-based air entraining admixture. Future work should consider a multitude of air entraining admixtures to further understand biochar/AEA compatibility. Two-wood based biochars were used in this investigation. Additional biochar biomasses should also be considered to further expound the findings from this study. Finally, a target 6% air content was selected based on industry standards for the size of aggregate used in the concrete and exposure category. However, future research should evaluate if higher entrained air contents is a simple, viable solution.

## REFERENCES

- [1] “The Paris Agreement.” [Online]. Available: <https://unfccc.int/process-and-meetings/the-paris-agreement>
- [2] E. Rutkowski, H. Pitt, and K. Larsen, “The Global Cement Challenge,” Mar. 2024. [Online]. Available: <https://rhg.com/research/the-global-cement-challenge/>
- [3] International Biochar Initiative, “Standardized Product Definition and Product Testing Guidelines for Biochar That Is Used in Soil,” Nov. 23, 2015. [Online]. Available: <http://www.biochar-international.org/characterizationstandard>.
- [4] Y. Zhang *et al.*, “Biochar as construction materials for achieving carbon neutrality,” Dec. 01, 2022, *Springer*. doi: 10.1007/s42773-022-00182-x.
- [5] ACI Committee 201, “PRC-201.2-23: Guide to Durable Concrete,” 2023.
- [6] P. Azarsa and R. Gupta, “Electrical Resistivity of Concrete for Durability Evaluation: A Review,” 2017, *Hindawi Limited*. doi: 10.1155/2017/8453095.
- [7] ACI Committee 318, “ACI 318-19(22): Building Code Requirements for Structural Concrete and Commentary,” Farmington Hills, 2019.
- [8] K. H. Obla and C. L. Lobo, “Acceptance Criteria for Durability Tests,” *Concrete International*, vol. 29, no. 5, 2007, [Online]. Available: [https://www.nrmca.org/wp-content/uploads/2020/09/AcceptanceCriteria\\_CIF\\_Winter\\_07.pdf](https://www.nrmca.org/wp-content/uploads/2020/09/AcceptanceCriteria_CIF_Winter_07.pdf)
- [9] T. Honorio, F. Benboudjema, T. Bore, M. Ferhat, and E. Vourc’H, “The pore solution of cement-based materials: Structure and dynamics of water and ions from molecular simulations,” *Physical Chemistry Chemical Physics*, vol. 21, no. 21, pp. 11111–11121, 2019, doi: 10.1039/c9cp01577a.
- [10] A. Vollpracht, B. Lothenbach, R. Snellings, and J. Haufe, “The pore solution of blended cements: a review,” *Materials and Structures/Materiaux et Constructions*, vol. 49, no. 8, pp. 3341–3367, Aug. 2016, doi: 10.1617/s11527-015-0724-1.
- [11] O. Sengul and O. E. Gjrrv, “Effect of Embedded Steel on Electrical Resistivity Measurements on Concrete Structures,” *ACI Mater J*, vol. 106, no. 1, pp. 11–18, 2009.
- [12] G. B. Wally, F. C. Magalhes, and L. C. Pinto da Silva Filho, “From prescriptive to performance-based: An overview of international trends in specifying durable concretes,” Jul. 15, 2022, *Elsevier Ltd*. doi: 10.1016/j.job.2022.104359.
- [13] K. Khan, M. A. Aziz, M. Zubair, and M. N. Amin, “Biochar Produced from Saudi Agriculture Waste as a Cement Additive for Improved Mechanical and Durability Properties—SWOT Analysis and Techno-Economic Assessment,” *Materials*, vol. 15, no. 15, Aug. 2022, doi: 10.3390/ma1515345.
- [14] A. Mobili, C. Giosu, T. Bellezze, G. M. Revel, and F. Tittarelli, “Gasification char and used foundry sand as alternative fillers to graphene nanoplatelets for electrically conductive mortars with and without virgin/recycled carbon fibres,” *Applied Sciences (Switzerland)*, vol. 11, no. 1, pp. 1–16, Jan. 2021, doi: 10.3390/app11010050.

- [15] A. Mobili, G. Cosoli, T. Bellezze, G. M. Revel, and F. Tittarelli, "Use of gasification char and recycled carbon fibres for sustainable and durable low-resistivity cement-based composites," *Journal of Building Engineering*, vol. 50, Jun. 2022, doi: 10.1016/j.jobbe.2022.104237.
- [16] M. I. Haque, R. I. Khan, W. Ashraf, and H. Pendse, "Production of sustainable, low-permeable and self-sensing cementitious composites using biochar," *Sustainable Materials and Technologies*, vol. 28, Jul. 2021, doi: 10.1016/j.susmat.2021.e00279.
- [17] J. Jeong, G. Jeon, S. Ryu, and J. H. Lee, "Ecofriendly and Electrically Conductive Cementitious Composites Using Melamine-Functionalized Biochar from Waste Coffee Beans," *Crystals (Basel)*, vol. 12, no. 6, Jun. 2022, doi: 10.3390/cryst12060820.
- [18] S. Kamaluddin, D. Kurniawan, M. S. A. Bakar, and Z. A. Samah, "Biochar as a conducting filler to enhance electrical conduction monitoring for concrete structures," in *Key Engineering Materials*, Trans Tech Publications Ltd, 2020, pp. 149–154. doi: 10.4028/www.scientific.net/KEM.847.149.
- [19] X. Yang and X. Y. Wang, "Hydration-strength-durability-workability of biochar-cement binary blends," *Journal of Building Engineering*, vol. 42, Oct. 2021, doi: 10.1016/j.jobbe.2021.103064.
- [20] B. Vafaei and A. Ghahremaninezhad, "Effects of Biochar as a Green Additive on the Self-Healing and Properties of Sustainable Cementitious Materials," *ACS Sustain Chem Eng*, May 2024, doi: 10.1021/acssuschemeng.4c02045.
- [21] P. K. Mehta and P. J. M. Monteiro, *Concrete: Microstructure, Properties, and Materials*, Fourth. Mc-Graw-Hill Education, 2014.
- [22] K. P. Mehta and B. C. Gerwick, "Cracking-Corrosion Interaction in Concrete Exposed to Marine Environment," *Concrete International*, vol. 4, no. 10, pp. 45–51, Oct. 1982.
- [23] H. A. Shah, Q. Yuan, and S. Zuo, "Air entrainment in fresh concrete and its effects on hardened concrete-a review," Mar. 08, 2021, *Elsevier Ltd*. doi: 10.1016/j.conbuildmat.2020.121835.
- [24] R. Wang, Z. Hu, Y. Li, K. Wang, and H. Zhang, "Review on the deterioration and approaches to enhance the durability of concrete in the freeze–thaw environment," Feb. 28, 2022, *Elsevier Ltd*. doi: 10.1016/j.conbuildmat.2022.126371.
- [25] T. C. Powers, "A Working Hypothesis for Further Studies of Frost Resistance of Concrete," *Proceedings of the American Concrete Institute*, vol. 41, no. 1, pp. 245–272, 1945, doi: <https://doi.org/10.14359/8684>.
- [26] T. C. Powers, C. Treval, and T. F. Willis, "The air requirement of frost-resistance concrete," *Highway research board proceedings*, vol. 32, pp. 184–211, 1949, [Online]. Available: <https://trid.trb.org/view.aspx?id=101611>.
- [27] T. C. Powers and R. A. Helmuth, "Theory of Volume Changes in Hardened Portland Cement Paste During Freezing," *Highway research board proceedings*, vol. 32, 1953.
- [28] W. L. Dolch, "Air-Entraining Admixtures," in *Concrete admixtures handbook*, William Andrew Publishing, 1996, ch. 8, pp. 518–557. doi: <https://doi.org/10.1016/B978-081551373-5.50012-X>.
- [29] B. A. Akinyemi and A. Adesina, "Recent advancements in the use of biochar for cementitious applications: A review," Nov. 01, 2020, *Elsevier Ltd*. doi: 10.1016/j.jobbe.2020.101705.

- [30] A. Danish, M. Ali Mosaberpanah, M. Usama Salim, N. Ahmad, F. Ahmad, and A. Ahmad, "Reusing biochar as a filler or cement replacement material in cementitious composites: A review," Sep. 20, 2021, *Elsevier Ltd.* doi: 10.1016/j.conbuildmat.2021.124295.
- [31] Y. Jia, H. Li, X. He, P. Li, and Z. Wang, "Effect of biochar from municipal solid waste on mechanical and freeze–thaw properties of concrete," *Constr Build Mater*, vol. 368, Mar. 2023, doi: 10.1016/j.conbuildmat.2023.130374.
- [32] P. Sikora *et al.*, "A systematic experimental study on biochar-cementitious composites: Towards carbon sequestration," *Ind Crops Prod*, vol. 184, Sep. 2022, doi: 10.1016/j.indcrop.2022.115103.
- [33] T. Chen, Z. Yang, H. Liu, L. Li, L. Qin, and X. Gao, "Effect of biochar characteristics on freeze–thaw durability of biochar-cement composites," *Journal of Building Engineering*, vol. 102, May 2025, doi: 10.1016/j.jobe.2025.111959.
- [34] ASTM, "ASTM C666: Standard Test Method for Resistance of Concrete to Rapid Freezing and Thawing," 2015, *ASTM International, West Conshohocken, Pennsylvania, United States.* doi: 10.1520/C0666\_C0666M-15.
- [35] "AASHTO T-358, Standard Method of Test for Surface Resistivity Indication of Concrete's Ability to Resist Chloride Ion Penetration," Washington D.C., 2022.
- [36] R. Nazari *et al.*, "Biochar: An Overview on its Production, Properties and Potential Benefits," *Biology, biotechnology and sustainable development*, vol. 1, pp. 13–40, 2015, [Online]. Available: <https://www.researchgate.net/publication/281060403>
- [37] M. B. Ahmed, J. L. Zhou, H. H. Ngo, and W. Guo, "Insight into biochar properties and its cost analysis," Jan. 01, 2016, *Elsevier Ltd.* doi: 10.1016/j.biombioe.2015.11.002.
- [38] P. R. Yaashikaa, P. S. Kumar, S. Varjani, and A. Saravanan, "A critical review on the biochar production techniques, characterization, stability and applications for circular bioeconomy," Dec. 01, 2020, *Elsevier B.V.* doi: 10.1016/j.btre.2020.e00570.
- [39] H. S. Kambo and A. Dutta, "A comparative review of biochar and hydrochar in terms of production, physico-chemical properties and applications," 2015, *Elsevier Ltd.* doi: 10.1016/j.rser.2015.01.050.
- [40] A. Demirbas, "Biomass resource facilities and biomass conversion processing for fuels and chemicals," *Energy Convers Manag*, no. 42, pp. 1357–1378, Oct. 2000, doi: [https://doi.org/10.1016/S0196-8904\(00\)00137-0](https://doi.org/10.1016/S0196-8904(00)00137-0).
- [41] D. C. Li and H. Jiang, "The thermochemical conversion of non-lignocellulosic biomass to form biochar: A review on characterizations and mechanism elucidation," Dec. 01, 2017, *Elsevier Ltd.* doi: 10.1016/j.biortech.2017.07.029.
- [42] M. Tripathi, J. N. Sahu, and P. Ganesan, "Effect of process parameters on production of biochar from biomass waste through pyrolysis: A review," Mar. 01, 2016, *Elsevier Ltd.* doi: 10.1016/j.rser.2015.10.122.
- [43] J. S. McDonald-Wharry, M. Manley-Harris, and K. L. Pickering, "Reviewing, Combining, and Updating the Models for the Nanostructure of Non-Graphitizing Carbons Produced from Oxygen-Containing Precursors," Oct. 20, 2016, *American Chemical Society.* doi: 10.1021/acs.energyfuels.6b00917.

- [44] A. Funke and F. Ziegler, "Hydrothermal carbonization of biomass: A summary and discussion of chemical mechanisms for process engineering," *Biofuels, Bioproducts and Biorefining*, vol. 4, pp. 160–177, 2010.
- [45] S. Kane, R. Ulrich, A. Harrington, N. P. Stadie, and C. Ryan, "Physical and chemical mechanisms that influence the electrical conductivity of lignin-derived biochar," *Carbon Trends*, vol. 5, p. 88, 2021, doi: 10.1016/j.cartre.2021.10.
- [46] A. Ngan, C. Q. Jia, and S.-T. Tong, "Production, Characterization and Alternative Applications of Biochar," *Biofuels and Biorefineries*, vol. 9, pp. 117–152, 2019, [Online]. Available: <http://www.springer.com/series/11687>
- [47] K. Nishimiya, T. Hata, and S. Ishihara, "Mechanism and Clarification of Electrical Conduction through Wood Charcoal," May 31, 1995, *Wood Research Institute Kyoto University*. Accessed: Sep. 27, 2023. [Online]. Available: <http://hdl.handle.net/2433/53229>
- [48] Z. Tang, Z. Li, J. Qian, and K. Wang, "Experimental study on deicing performance of carbon fiber reinforced conductive concrete," *J Mater Sci Technol*, pp. 113–117, 2005.
- [49] M. Solazzo, F. J. O'Brien, V. Nicolosi, and M. G. Monaghan, "The rationale and emergence of electroconductive biomaterial scaffolds in cardiac tissue engineering," Dec. 01, 2019, *American Institute of Physics Inc.* doi: 10.1063/1.5116579.
- [50] M. Cheytani and S. L. I. Chan, "The applicability of the Wenner method for resistivity measurement of concrete in atmospheric conditions," *Case Studies in Construction Materials*, vol. 15, Dec. 2021, doi: 10.1016/j.cscm.2021.e00663.
- [51] "ASTM C1876–19: Standard Test Method for Bulk Electrical Resistivity or Bulk Conductivity of Concrete 1", doi: 10.1520/C1876-19.
- [52] H. Layssi, P. Ghods, A. R. Alizadeh, and M. Salehi, "Electrical Resistivity of Concrete Concepts, applications, and measurement techniques," May 2015. [Online]. Available: [www.concreteinternational.com|Ci|MAY201541](http://www.concreteinternational.com/Ci|MAY201541)
- [53] K. Seng Chia and M.-H. Zhang, "Water permeability and chloride penetrability of high-strength lightweight aggregate concrete," *Cem Concr Res*, no. 32, pp. 639–645, Nov. 2001.
- [54] G. Cosoli, A. Mobili, F. Tittarelli, G. M. Revel, and P. Chiariotti, "Electrical resistivity and electrical impedance measurement in mortar and concrete elements: A systematic review," *Applied Sciences (Switzerland)*, vol. 10, no. 24, pp. 1–43, Dec. 2020, doi: 10.3390/app10249152.
- [55] ASTM C1876, "ASTM C1876, Standard Test Method for Bulk Electrical Resistivity or Bulk Conductivity of Concrete," 2019, *ASTM International, West Conshohocken, Pennsylvania, United States*,. doi: 10.1520/C1876-19.
- [56] H. Layssi, P. Ghods, A. R. Alizadeh, and M. Salehi, "Electrical Resistivity of Concrete Concepts, applications, and measurement techniques." [Online]. Available: [www.concreteinternational.com|Ci|MAY201541](http://www.concreteinternational.com/Ci|MAY201541)
- [57] L. Wang and F. Aslani, "A review on material design, performance, and practical application of electrically conductive cementitious composites," Dec. 30, 2019, *Elsevier Ltd.* doi: 10.1016/j.conbuildmat.2019.116892.

- [58] S. Q. Ding, L. Q. Zhang, S. W. Sun, J. Ou-Yang, and B. G. Han, “Nano-engineered strong, durable and multifunctional/smart concretes,” in *Key Engineering Materials*, Trans Tech Publications Ltd, 2017, pp. 1084–1088. doi: 10.4028/www.scientific.net/KEM.727.1084.
- [59] S. Wen and D. D. L. Chung, “Electromagnetic interference shielding reaching 70 dB in steel fiber cement,” *Cem Concr Res*, vol. 34, no. 2, pp. 329–332, Feb. 2004, doi: 10.1016/j.cemconres.2003.08.014.
- [60] A. S. El-Dieb, M. A. El-Ghareeb, M. A. H. Abdel-Rahman, and E. S. A. Nasr, “Multifunctional electrically conductive concrete using different fillers,” *Journal of Building Engineering*, vol. 15, pp. 61–69, Jan. 2018, doi: 10.1016/j.jobbe.2017.10.012.
- [61] P. Xie, P. Gu, and J. J. Beaudoin, “Electrical percolation phenomena in cement composites containing conductive fibres,” 1996.
- [62] H. Maljaee, R. Madadi, H. Paiva, L. Tarelho, and V. M. Ferreira, “Incorporation of biochar in cementitious materials: A roadmap of biochar selection,” May 10, 2021, *Elsevier Ltd*. doi: 10.1016/j.conbuildmat.2021.122757.
- [63] Y. Zheng, X. Huang, J. Chen, K. Wu, J. Wang, and X. Zhang, “A review of conductive carbon materials for 3d printing: Materials, technologies, properties, and applications,” *Materials*, vol. 14, no. 14, Jul. 2021, doi: 10.3390/ma14143911.
- [64] S. Li, X. Li, Q. Deng, and D. Li, “Three kinds of charcoal powder reinforced ultra-high molecular weight polyethylene composites with excellent mechanical and electrical properties,” *Mater Des*, vol. 85, pp. 54–59, Nov. 2015, doi: 10.1016/j.matdes.2015.06.163.
- [65] Y. Shao, C. Guizani, P. Grosseau, D. Chaussy, and D. Beneventi, “Biocarbons from microfibrillated cellulose/lignosulfonate precursors: A study of electrical conductivity development during slow pyrolysis,” *Carbon N Y*, vol. 129, pp. 357–366, Apr. 2018, doi: 10.1016/j.carbon.2017.12.037.
- [66] P. Savi, M. Yasir, M. Bartoli, M. Giorelli, and M. Longo, “Electrical and microwave characterization of thermal annealed sewage sludge derived biochar composites,” *Applied Sciences (Switzerland)*, vol. 10, no. 4, Feb. 2020, doi: 10.3390/app10041334.
- [67] S. Y. Wang and C. P. Hung, “Electromagnetic shielding efficiency of the electric field of charcoal from six wood species,” *Journal of Wood Science*, vol. 49, no. 5, pp. 450–454, 2003, doi: 10.1007/s10086-002-0506-6.
- [68] Y. R. Rhim *et al.*, “Changes in electrical and microstructural properties of microcrystalline cellulose as function of carbonization temperature,” *Carbon N Y*, vol. 48, no. 4, pp. 1012–1024, Apr. 2010, doi: 10.1016/j.carbon.2009.11.020.
- [69] M. Bartoli *et al.*, “Effect of heating rate and feedstock nature on electrical conductivity of biochar and biochar-based composites,” *Applications in Energy and Combustion Science*, vol. 12, Dec. 2022, doi: 10.1016/j.jaecs.2022.100089.
- [70] H. Zhang, C. Chen, E. M. Gray, and S. E. Boyd, “Effect of feedstock and pyrolysis temperature on properties of biochar governing end use efficacy,” *Biomass Bioenergy*, vol. 105, pp. 136–146, 2017, doi: 10.1016/j.biombioe.2017.06.024.
- [71] K. Qian, A. Kumar, H. Zhang, D. Bellmer, and R. Huhnke, “Recent advances in utilization of biochar,” 2015, *Elsevier Ltd*. doi: 10.1016/j.rser.2014.10.074.

- [72] R. S. Gabhi, D. W. Kirk, and C. Q. Jia, "Preliminary investigation of electrical conductivity of monolithic biochar," *Carbon N Y*, vol. 116, pp. 435–442, May 2017, doi: 10.1016/j.carbon.2017.01.069.
- [73] W. Suliman, J. B. Harsh, N. I. Abu-Lail, A. M. Fortuna, I. Dallmeyer, and M. Garcia-Perez, "Influence of feedstock source and pyrolysis temperature on biochar bulk and surface properties," *Biomass Bioenergy*, vol. 84, pp. 37–48, Jan. 2016, doi: 10.1016/j.biombioe.2015.11.010.
- [74] R. Azargohar, S. Nanda, J. A. Kozinski, A. K. Dalai, and R. Sutarto, "Effects of temperature on the physicochemical characteristics of fast pyrolysis bio-chars derived from Canadian waste biomass," *Fuel*, vol. 125, pp. 90–100, Jun. 2014, doi: 10.1016/j.fuel.2014.01.083.
- [75] A. M. Poulouse *et al.*, "Date palm biochar-polymer composites: An investigation of electrical, mechanical, thermal and rheological characteristics," *Science of the Total Environment*, vol. 619–620, pp. 311–318, Apr. 2018, doi: 10.1016/j.scitotenv.2017.11.076.
- [76] B. C. C. Fernandes *et al.*, "Impact of pyrolysis temperature on the properties of eucalyptus wood-derived biochar," *Materials*, vol. 13, no. 24, pp. 1–13, Dec. 2020, doi: 10.3390/ma13245841.
- [77] S. Adhikari *et al.*, "Influence of pyrolysis parameters on phosphorus fractions of biosolids derived biochar," *Science of the Total Environment*, vol. 695, Dec. 2019, doi: 10.1016/j.scitotenv.2019.133846.
- [78] M. Giorcelli and M. Bartoli, "Development of coffee biochar filler for the production of electrical conductive reinforced plastic," *Polymers (Basel)*, vol. 11, no. 12, 2019, doi: 10.3390/polym11121916.
- [79] A. Sassani *et al.*, "Carbon fiber-based electrically conductive concrete for salt-free deicing of pavements," *J Clean Prod*, vol. 203, pp. 799–809, Dec. 2018, doi: 10.1016/j.jclepro.2018.08.315.
- [80] M. Pigeon, J. Marchand, and R. Pleau, "Frost resistant concrete," 1996.
- [81] R. F. Feldman and P. J. Sereda, "A New Model for Hydrated Portland Cement and Its Practical Implications," *Engineering Journal*, vol. 53, no. 8/9, pp. 53–59, 1970.
- [82] K. C. Hover, "The influence of water on the performance of concrete," *Constr Build Mater*, vol. 25, no. 7, pp. 3003–3013, Jul. 2011, doi: 10.1016/j.conbuildmat.2011.01.010.
- [83] T. C. Powers, "Structure and Physical Properties of Hardened Portland Cement Paste Structure and physical properties of Hardened Portland Cement Paste," *Journal of the American Ceramic Society*, vol. 41, no. 1, 1958.
- [84] S. Chatterji, "Freezing of air-entrained cement-based materials and specific actions of air-entraining agents," *Cem Concr Compos*, vol. 25, no. 7, pp. 759–765, Oct. 2003, doi: 10.1016/S0958-9465(02)00099-9.
- [85] J. J. Valenza and G. W. Scherer, "A review of salt scaling: II. Mechanisms," 2007, *Elsevier Ltd.* doi: 10.1016/j.cemconres.2007.03.003.
- [86] Q. Zeng, K. Li, T. Fen-chong, and P. Dangla, "A study of the behaviors of cement-based materials subject to freezing," in *2010 International Conference on Mechanic Automation and Control Engineering*, IEEE, Jun. 2010, pp. 1611–1616. doi: 10.1109/MACE.2010.5535987.
- [87] C. S. Shon, A. Abdigaliyev, S. Bagitova, C. W. Chung, and D. Kim, "Determination of air-void system and modified frost resistance number for freeze-thaw resistance evaluation of ternary

- blended concrete made of ordinary Portland cement/silica fume/class F fly ash,” *Cold Reg Sci Technol*, vol. 155, pp. 127–136, Nov. 2018, doi: 10.1016/j.coldregions.2018.08.003.
- [88] G. Gelardi, S. Mantellato, D. Marchon, M. Palacios, A. B. Eberhardt, and R. J. Flatt, “Chemistry of chemical admixtures,” in *Science and Technology of Concrete Admixtures*, Elsevier Inc., 2016, pp. 149–218. doi: 10.1016/B978-0-08-100693-1.00009-6.
- [89] V. H. Dodson, *Concrete Admixtures*. Springer US, 1990. doi: 10.1007/978-1-4757-4843-7.
- [90] M. J. Rosen and J. T. Kunjappu, *Surfactants and interfacial phenomena*, 4th ed. Hoboken, New Jersey: John Wiley & Sons, Inc., 2012.
- [91] T. C. Powers, “Void Space as a Basis for Producing Air-Entrained Concrete,” *ACI Journal Proceedings*, vol. 50, no. 5, pp. 741–760, May 1954, doi: 10.14359/11792.
- [92] ASTM, “ASTM C457: Standard Test Method for Microscopical Determination of Parameters of the Air-Void System in Hardened Concrete,” 2023, *ASTM International, West Conshohocken, Pennsylvania, United States*. doi: 10.1520/C0457\_C0457M-23A.
- [93] D. Whiting and D. Stark, “Control of air content in concrete,” May 1983, *Transportation Research Board, Washington, D.C.* [Online]. Available: [http://onlinepubs.trb.org/Onlinepubs/nchrp/nchrp\\_rpt\\_258.pdf](http://onlinepubs.trb.org/Onlinepubs/nchrp/nchrp_rpt_258.pdf)
- [94] P.-C. Aitcin, C. Jolicoeur, and J. G. Macgregor, “Superplasticizers: How they Work and Why They Occasionally Don’t,” *Concrete International*, vol. 16, no. 5, pp. 45–52, 1994.
- [95] L. E. Tunstall, M. T. Ley, and G. W. Scherer, “Air entraining admixtures: Mechanisms, evaluations, and interactions,” *Cem Concr Res*, vol. 150, Dec. 2021, doi: 10.1016/j.cemconres.2021.106557.
- [96] P. Plante, M. Pigeon, and C. Foy, “The Influence of Water-Reducers on the Production and Stability of the Air Void System in Concrete,” *Cem Concr Res*, vol. 19, no. 4, pp. 621–633, 1989, doi: [https://doi.org/10.1016/0008-8846\(89\)90014-8](https://doi.org/10.1016/0008-8846(89)90014-8).
- [97] V. M. Malhotra, “Mechanical Properties and Freezing and Thawing Resistance of Non-Air-Entrained, Air-Entrained, and Air-Entrained Superplasticized Concrete Using ASTM Test C 666, Procedures A and B,” *Cement, Concrete, and Aggregates*, vol. 4, no. 1, pp. 3–23, Jul. 1982, doi: 10.1520/CCA10219J.
- [98] R. Felice, J. M. Freeman, and M. T. Ley, “Durable Concrete with Modern Air-Entraining Admixtures,” *Concrete International*, vol. 36, no. 8, pp. 37–45, 2014.
- [99] A. Sirico *et al.*, “Biochar from wood waste as additive for structural concrete,” *Constr Build Mater*, vol. 303, Oct. 2021, doi: 10.1016/j.conbuildmat.2021.124500.
- [100] S. Gupta and H. W. Kua, “Effect of water entrainment by pre-soaked biochar particles on strength and permeability of cement mortar,” *Constr Build Mater*, vol. 159, pp. 107–125, Jan. 2018, doi: 10.1016/j.conbuildmat.2017.10.095.
- [101] D. Cuthbertson, U. Berardi, C. Briens, and F. Berruti, “Biochar from residual biomass as a concrete filler for improved thermal and acoustic properties,” *Biomass Bioenergy*, vol. 120, pp. 77–83, Jan. 2019, doi: 10.1016/j.biombioe.2018.11.007.

- [102] S. Muthukrishnan, S. Gupta, and H. W. Kua, “Application of rice husk biochar and thermally treated low silica rice husk ash to improve physical properties of cement mortar,” *Theoretical and Applied Fracture Mechanics*, vol. 104, Dec. 2019, doi: 10.1016/j.tafmec.2019.102376.
- [103] A. Dixit, S. Gupta, S. D. Pang, and H. W. Kua, “Waste Valorisation using biochar for cement replacement and internal curing in ultra-high performance concrete,” *J Clean Prod*, vol. 238, Nov. 2019, doi: 10.1016/j.jclepro.2019.117876.
- [104] A. Sirico *et al.*, “Effects of biochar addition on long-term behavior of concrete,” *Theoretical and Applied Fracture Mechanics*, vol. 122, Dec. 2022, doi: 10.1016/j.tafmec.2022.103626.
- [105] P. Klieger, “Effect of Entrained Air on Strength and Durability of Concrete made with Various Maximum Sizes of Aggregate,” 1952, *Portland Cement Association*.
- [106] P. Klieger, “Further Studies on the Effect of Entrained Air on Strength and Durability of Concrete With Various Sizes of Aggregates,” 1956, *Portland Cement Association*.
- [107] “ASTM C231: Standard Test Method for Air Content of Freshly Mixed Concrete by the Pressure Method,” 2024, *ASTM International, West Conshohocken, Pennsylvania, United States*. doi: 10.1520/C0231\_C0231M-24.
- [108] “ASTM C173: Standard Test Method for Air Content of Freshly Mixed Concrete by the Volumetric Method,” 2024, *ASTM International, West Conshohocken, Pennsylvania, United States*. doi: 10.1520/C0173\_C0173M-24.
- [109] “ASTM C138: Standard Test Method for Density (Unit Weight), Yield, and Air Content (Gravimetric) of Concrete,” 2023, *ASTM International, West Conshohocken, Pennsylvania, United States*. doi: 10.1520/C0138\_C0138M-23.
- [110] K.-H. Tan, T.-Y. Wang, Z.-H. Zhou, and Y.-H. Qin, “Biochar as a Partial Cement Replacement Material for Developing Sustainable Concrete: An Overview,” *Journal of Materials in Civil Engineering*, vol. 33, no. 12, Dec. 2021, doi: 10.1061/(asce)mt.1943-5533.0003987.
- [111] S. Gebler and P. Klieger, “Effect of Fly Ash on the Air-Void Stability of Concrete,” vol. 79, no. Special Publication, pp. 103–142, May 1983, doi: 10.14359/6688.
- [112] D. S. Lane, “Testing Fly Ash in Mortars for Air-Entrainment Characteristics,” *Cement, Concrete, and Aggregates*, vol. 13, no. 1, pp. 25–31, Jul. 1991, doi: <https://doi.org/10.1520/CCA10546J>.
- [113] D. S. Zhang, “Air Entrainment in Fresh Concrete with PFA,” *Cem Concr Compos*, vol. 18, no. 6, pp. 409–416, 1996, doi: [https://doi.org/10.1016/S0958-9465\(96\)00033-9](https://doi.org/10.1016/S0958-9465(96)00033-9).
- [114] A. U. Rajapaksha *et al.*, “Engineered/designer biochar for contaminant removal/immobilization from soil and water: Potential and implication of biochar modification,” Apr. 01, 2016, *Elsevier Ltd*. doi: 10.1016/j.chemosphere.2016.01.043.
- [115] G. G. Ying, “Fate, behavior and effects of surfactants and their degradation products in the environment,” 2006, *Elsevier Ltd*. doi: 10.1016/j.envint.2005.07.004.
- [116] Q. Chai *et al.*, “Effects and mechanisms of anionic and nonionic surfactants on biochar removal of chromium,” *Environmental Science and Pollution Research*, vol. 25, no. 19, pp. 18443–18450, Jul. 2018, doi: 10.1007/s11356-018-1933-2.

- [117] F. Wang, Q. Zeng, W. Su, M. Zhang, L. Hou, and Z. L. Wang, “Adsorption of Bisphenol A on Peanut Shell Biochars: The Effects of Surfactants,” *J Chem*, vol. 2019, 2019, doi: 10.1155/2019/2428505.
- [118] C. Li *et al.*, “Synergistic effects of anionic surfactants on adsorption of norfloxacin by magnetic biochar derived from furfural residue,” *Environmental Pollution*, vol. 254, Nov. 2019, doi: 10.1016/j.envpol.2019.113005.
- [119] A. L. N. Krause, L. Nguyen, C. Tuan, J. Bonsell, and B. Chen, *Conductive Concrete as an Electromagnetic Shield*. 2012.
- [120] D. Wanasinghe, F. Aslani, G. Ma, and D. Habibi, “Advancements in electromagnetic interference shielding cementitious composites,” Jan. 20, 2020, *Elsevier Ltd*. doi: 10.1016/j.conbuildmat.2019.117116.
- [121] B. Han, S. Ding, and X. Yu, “Intrinsic self-sensing concrete and structures: A review,” 2015, *Elsevier B.V.* doi: 10.1016/j.measurement.2014.09.048.
- [122] R. Wang, Q. Shi, Y. Li, Z. Cao, and Z. Si, “A critical review on the use of copper slag (CS) as a substitute constituent in concrete,” Jul. 19, 2021, *Elsevier Ltd*. doi: 10.1016/j.conbuildmat.2021.123371.
- [123] ASTM D7582, “ASTM D7582: Test Methods for Proximate Analysis of Coal and Coke by Macro Thermogravimetric Analysis,” Apr. 01, 2024, *ASTM International, West Conshohocken, Pennsylvania, United States*. doi: 10.1520/D7582-24.
- [124] ASTM C150, “ASTM C150: Standard Specification for Portland Cement,” 2022, *ASTM International, West Conshohocken, Pennsylvania, United States*.
- [125] ASTM C778, “ASTM C778: Standard Specification for Standard Sand,” 2021, *ASTM International, West Conshohocken, Pennsylvania, United States*.
- [126] J. Hylton, A. Hugen, S. M. Rowland, M. Griffin, and L. E. Tunstall, “Relevant biochar characteristics influencing compressive strength of biochar-cement mortars,” *Biochar*, vol. 6, no. 1, Dec. 2024, doi: 10.1007/s42773-024-00375-6.
- [127] ASTM C1437, “ASTM C1437: Standard Test Method for Flow of Hydraulic Cement Mortar,” 2020, *ASTM International, West Conshohocken, Pennsylvania, United States*. doi: 10.1520/C1437.
- [128] E. J. Garboczi, K. A. Snyder, J. F. Douglas, and M. F. Thorpe, “Geometrical percolation threshold of overlapping ellipsoids,” *Phys Rev E*, vol. 52, no. 1, p. 819, Jul. 1995, doi: <https://doi.org/10.1103/PhysRevE.52.819>.
- [129] A. Sirico *et al.*, “Mechanical characterization of cement-based materials containing biochar from gasification,” *Constr Build Mater*, vol. 246, Jun. 2020, doi: 10.1016/j.conbuildmat.2020.118490.
- [130] S. Gupta, H. W. Kua, and S. D. Pang, “Effect of biochar on mechanical and permeability properties of concrete exposed to elevated temperature,” *Constr Build Mater*, vol. 234, Feb. 2020, doi: 10.1016/j.conbuildmat.2019.117338.
- [131] S. Muthukrishnan, S. Gupta, and H. W. Kua, “Application of rice husk biochar and thermally treated low silica rice husk ash to improve physical properties of cement mortar,” *Theoretical and Applied Fracture Mechanics*, vol. 104, Dec. 2019, doi: 10.1016/j.tafmec.2019.102376.

- [132] M. Giorcelli, P. Savi, A. Khan, and A. Tagliaferro, “Analysis of biochar with different pyrolysis temperatures used as filler in epoxy resin composites,” *Biomass Bioenergy*, vol. 122, pp. 466–471, Mar. 2019, doi: 10.1016/j.biombioe.2019.01.007.
- [133] R. S. Barneyback and S. Diamond, “Expression and Analysis of Pore Fluids from Hardened Cement Pastes and Mortars,” *Cem Concr Res*, vol. 2, no. 11, pp. 279–285, Mar. 1981.
- [134] K. A. Snyder, X. Feng, B. D. Keen, and T. O. Mason, “Estimating the electrical conductivity of cement paste pore solutions from OH<sup>-</sup>, K<sup>+</sup> and Na<sup>+</sup> concentrations,” *Cem Concr Res*, vol. 33, no. 6, pp. 793–798, Jun. 2003, doi: 10.1016/S0008-8846(02)01068-2.
- [135] P. Gao, J. Wei, T. Zhang, J. Hu, and Q. Yu, “Modification of chloride diffusion coefficient of concrete based on the electrical conductivity of pore solution,” *Constr Build Mater*, vol. 145, pp. 361–366, Aug. 2017, doi: 10.1016/j.conbuildmat.2017.03.220.
- [136] R. Spragg *et al.*, “Leaching of conductive species: Implications to measurements of electrical resistivity,” *Cem Concr Compos*, vol. 79, pp. 94–105, May 2017, doi: 10.1016/j.cemconcomp.2017.02.003.
- [137] M. D. Newlands, M. R. Jones, S. Kandasami, and T. A. Harrison, “Sensitivity of electrode contact solutions and contact pressure in assessing electrical resistivity of concrete,” *Materials and Structures/Materiaux et Constructions*, vol. 41, no. 4, pp. 621–632, May 2008, doi: 10.1617/s11527-007-9257-6.
- [138] AASHTO T-402, “AASHTO T-402, Standard Method of Test for Electrical Resistivity of a Concrete Cylinder Tested in a Uniaxial Resistance Test,” 2023, *American Association of State and Highway Transportation Officials, Washington, DC*.
- [139] British Standards EN 22390-8, “Testing hardened concrete. Part 8, Depth of penetration of water under pressure.,” 2020, *BSI*.
- [140] ASTM, “ASTM C642: Standard Test Method for Density, Absorption, and Voids in Hardened Concrete,” 2021, *ASTM International, West Conshohocken, Pennsylvania, United States*,. doi: 10.1520/C0642-21.
- [141] A. Akhtar and A. K. Sarmah, “Novel biochar-concrete composites: Manufacturing, characterization and evaluation of the mechanical properties,” *Science of the Total Environment*, vol. 616–617, pp. 408–416, Mar. 2018, doi: 10.1016/j.scitotenv.2017.10.319.
- [142] M. Haris Javed, M. Ali Sikandar, W. Ahmad, M. Tariq Bashir, R. Alrowais, and M. Bilal Wadud, “Effect of various biochars on physical, mechanical, and microstructural characteristics of cement pastes and mortars,” *Journal of Building Engineering*, vol. 57, Oct. 2022, doi: 10.1016/j.jobbe.2022.104850.
- [143] A. C. Ferrari and J. Robertson, “Interpretation of Raman spectra of disordered and amorphous carbon,” *Phys Rev B*, vol. 61, no. 20, May 2000, doi: <https://doi.org/10.1103/PhysRevB.61.14095>.
- [144] C. Guizani, K. Haddad, L. Limousy, and M. Jeguirim, “New insights on the structural evolution of biomass char upon pyrolysis as revealed by the Raman spectroscopy and elemental analysis,” Aug. 01, 2017, *Elsevier Ltd*. doi: 10.1016/j.carbon.2017.04.078.
- [145] D. Torsello, G. Ghigo, M. Giorcelli, M. Bartoli, M. Rovere, and A. Tagliaferro, “Tuning the microwave electromagnetic properties of biochar-based composites by annealing,” *Carbon Trends*, vol. 4, p. 62, 2021, doi: 10.1016/j.cartre.2021.10.

- [146] K. Zhang, P. Sun, M. C. A. S. Faye, and Y. Zhang, “Characterization of biochar derived from rice husks and its potential in chlorobenzene degradation,” *Carbon N Y*, vol. 130, pp. 730–740, Apr. 2018, doi: 10.1016/j.carbon.2018.01.036.
- [147] J. McDonald-Wharry, “2013–2014 Survey of Chars Using Raman Spectroscopy,” *C (Basel)*, vol. 7, no. 3, p. 63, Aug. 2021, doi: 10.3390/c7030063.
- [148] A. Tagliaferro, M. Rovere, E. Padovano, M. Bartoli, and M. Giorcelli, “Introducing the novel mixed gaussian-lorentzian lineshape in the analysis of the raman signal of biochar,” *Nanomaterials*, vol. 10, no. 9, pp. 1–19, Sep. 2020, doi: 10.3390/nano10091748.
- [149] A. Cuesta, P. Dhamelincourt, J. Laureyns, A. Martínez-Alonso, and J. M. D. Tascóna, “Materials Comparative performance of X-ray diffraction and Raman microprobe techniques for the study of carbon materials,” *J Mater Chem*, vol. 8, no. 12, pp. 2875–2879, 1998, doi: <https://doi.org/10.1039/A805841E>.
- [150] P. Kim *et al.*, “Surface functionality and carbon structures in lignocellulosic-derived biochars produced by fast pyrolysis,” *Energy and Fuels*, vol. 25, no. 10, pp. 4693–4703, Oct. 2011, doi: 10.1021/ef200915s.
- [151] B. Singh and M. D. Raven, “X-ray diffraction analysis of biochar,” in *Biochar: A guide to Analytical Methods*, 2017, pp. 245–252.
- [152] H. Hamdan, M. Nazlan, M. Muhid, S. Endud, E. Listiorini, and Z. Ramli, “Si MAS NMR, XRD and FESEM studies of rice husk silica for the synthesis of zeolites,” *J Non Cryst Solids*, vol. 211, pp. 126–131, 1997, doi: [https://doi.org/10.1016/S0022-3093\(96\)00611-4](https://doi.org/10.1016/S0022-3093(96)00611-4).
- [153] M. Almarshoud *et al.*, “Use of electrical resistivity-based tests for concrete penetrability measurement,” *ACI Mater J*, vol. 118, no. 1, pp. 21–30, 2021, doi: 10.14359/51729334.
- [154] Y. Bu, R. Spragg, and W. J. Weiss, “Comparison of the Pore Volume in Concrete as Determined Using ASTM C642 and Vacuum Saturation,” *Adv Civ Eng Mater*, vol. 3, no. 1, pp. 308–315, Jun. 2014, doi: 10.1520/ACEM20130090.
- [155] M. Safiuddin and N. Hearn, “Comparison of ASTM saturation techniques for measuring the permeable porosity of concrete,” *Cem Concr Res*, vol. 35, no. 5, pp. 1008–1013, May 2005, doi: 10.1016/j.cemconres.2004.09.017.
- [156] C. M. Tibbetts, J. M. Paris, C. C. Ferraro, K. A. Riding, and T. G. Townsend, “Relating water permeability to electrical resistivity and chloride penetrability of concrete containing different supplementary cementitious materials,” *Cem Concr Compos*, vol. 107, Mar. 2020, doi: 10.1016/j.cemconcomp.2019.103491.
- [157] H. F. W. Taylor, *Cement Chemistry*, 2nd ed. London: Thomas Telford, 1997.
- [158] J. Milla, T. L. Cavalline, T. D. Rupnow, B. Melugiri-Shankaramurthy, G. Lomboy, and K. Wang, “Methods of test for concrete permeability: A critical review,” Jan. 01, 2021, *ASTM International*. doi: 10.1520/ACEM20200067.
- [159] R. Spragg, Y. Bu, K. Snyder, D. Bentz, and J. Weiss, “Electrical Testing of Cement-Based Materials: Role of Testing Techniques, Sample Conditioning,” Dec. 31, 2013, *Joint Transportation Research Program, Indiana Department of Transportation and Purdue University, West Lafayette, Indiana*. doi: <https://doi.org/10.5703/1288284315230>.

- [160] K. A. Snyder, “The relationship between the formation factor and the diffusion coefficient of porous materials saturated with concentrated electrolytes: theoretical and experimental considerations,” *Concrete Science and Engineering*, vol. 3, no. 12, pp. 216–224, 2001, [Online]. Available: [https://tsapps.nist.gov/publication/get\\_pdf.cfm?pub\\_id=860304](https://tsapps.nist.gov/publication/get_pdf.cfm?pub_id=860304)
- [161] F. Belaïd, “How does concrete and cement industry transformation contribute to mitigating climate change challenges?,” Nov. 01, 2022, *Elsevier Inc.* doi: 10.1016/j.rcradv.2022.200084.
- [162] D. Cheng *et al.*, “Projecting future carbon emissions from cement production in developing countries,” *Nat Commun*, vol. 14, no. 1, Dec. 2023, doi: 10.1038/s41467-023-43660-x.
- [163] M. Purton, “Cement is a big problem for the environment. Here’s how to make it more sustainable,” World Economic Forum. Accessed: Apr. 15, 2025. [Online]. Available: <https://www.weforum.org/stories/2024/09/cement-production-sustainable-concrete-co2-emissions/#:~:text=Global%20cement%20manufacturing%20produced%201.6,to%20achieving%20global%20climate%20targets.>
- [164] M. Perez Villa *et al.*, “Decarbonizing Concrete Deep decarbonization pathways for the cement and concrete cycle in the United,” Mar. 2021. Accessed: Apr. 15, 2025. [Online]. Available: [https://www.climateworks.org/wp-content/uploads/2021/03/Decarbonizing\\_Concrete.pdf](https://www.climateworks.org/wp-content/uploads/2021/03/Decarbonizing_Concrete.pdf)
- [165] J. Yang and X. He, “Durability and Sustainability of Cement and Concrete Composites,” Aug. 01, 2023, *Multidisciplinary Digital Publishing Institute (MDPI)*. doi: 10.3390/ma16165693.
- [166] “CEMBUREAU Activity Report 2023,” 2023. Accessed: Apr. 15, 2025. [Online]. Available: <https://www.cembureau.eu/media/dnbf4xzc/activity-report-2023-for-web.pdf>
- [167] G. P. Hammond and C. I. Jones, “Embodied energy and carbon in construction materials,” *Proceedings of Institution of Civil Engineers: Energy*, vol. 161, no. 2, pp. 87–98, 2008, doi: 10.1680/ener.2008.161.2.87.
- [168] A. Adesina and J. Zhang, “Impact of concrete structures durability on its sustainability and climate resiliency,” *Next Sustainability*, vol. 3, p. 100025, 2024, doi: 10.1016/j.nxsust.2024.100025.
- [169] J. Bai, “Durability of sustainable concrete materials,” in *Sustainability of Construction Materials*, Woodhead Publishing, 2009, ch. 10, pp. 239–253. doi: 10.1533/9781845695842.239.
- [170] S. Chatterji, “An explanation for the unsaturated state of water stored concrete,” *Cem Concr Compos*, vol. 26, no. 1, pp. 75–79, Jan. 2004, doi: 10.1016/S0958-9465(02)00124-5.
- [171] G. Lomboy and K. Wang, “Effects of Strength, Permeability, and Air Void Parameters on Freezing-Thawing Resistance of Concrete with and Without Air Entrainment,” 2009. [Online]. Available: [www.astm.org](http://www.astm.org)
- [172] M. Pigeon, R. Gagne, P.-C. Aitcin, and N. Banthia, “Freezing and Thawing Tests of High Strength Concrete,” *Cem Concr Res*, vol. 21, pp. 44–852, 1991.
- [173] “ASTM C566: Standard Test Method for Total Evaporable Moisture Content of Aggregate by Drying,” 2019, *ASTM International, West Conshohocken, Pennsylvania, United States*. doi: 10.1520/C0566-19.
- [174] “ASTM C128: Standard Test Method for Relative Density (Specific Gravity) and Absorption of Fine Aggregate,” 2022, *ASTM International, West Conshohocken, Pennsylvania, United States*. doi: 10.1520/C0128-22.

- [175] “ASTM C143: Standard Test Method for Slump of Hydraulic-Cement Concrete,” 2015, *ASTM International, West Conshohocken, Pennsylvania, United States*.
- [176] “ASTM C192: Standard Practice for Making and Curing Concrete Test Specimens in the Laboratory,” 2019, *ASTM International, West Conshohocken, Pennsylvania, United States*. doi: 10.1520/C0192\_C0192M-19.
- [177] “ASTM C39: Standard Test Method for Compressive Strength of Cylindrical Concrete Specimens,” 2023, *ASTM International, West Conshohocken, Pennsylvania, United States*. doi: 10.1520/C0039\_C0039M-23.
- [178] P. C. Fonseca and G. W. Scherer, “An image analysis procedure to quantify the air void system of mortar and concrete,” *Materials and Structures/Materiaux et Constructions*, vol. 48, no. 10, pp. 3087–3098, Oct. 2015, doi: 10.1617/s11527-014-0381-9.
- [179] ASTM, “ASTM C1585: Test Method for Measurement of Rate of Absorption of Water by Hydraulic-Cement Concretes,” Sep. 01, 2020, *ASTM International, West Conshohocken, Pennsylvania, United States*. doi: 10.1520/C1585-20.
- [180] H. Kabir, J. Wu, S. Dahal, T. Joo, and N. Garg, “Automated estimation of cementitious sorptivity via computer vision,” *Nature Communications*, vol. 15, no. 1, Dec. 2024, doi: 10.1038/s41467-024-53993-w.
- [181] Z. Li, W. Xue, and W. Zhou, “Mechanical Properties of Concrete with Different Carya Cathayensis Peel Biochar Additions,” *Sustainability (Switzerland)*, vol. 15, no. 6, Mar. 2023, doi: 10.3390/su15064874.
- [182] S. Gupta, H. W. Kua, and C. Y. Low, “Use of biochar as carbon sequestering additive in cement mortar,” *Cem Concr Compos*, vol. 87, pp. 110–129, Mar. 2018, doi: 10.1016/j.cemconcomp.2017.12.009.
- [183] W. C. Choi, H. Do Yun, and J. Y. Lee, “Mechanical Properties of Mortar Containing Bio-Char From Pyrolysis,” *Journal of the Korea Institute for Structural Maintenance and Inspection*, vol. 5, pp. 67–74, 2012.
- [184] S. Praneeth, L. Saavedra, M. Zeng, B. K. Dubey, and A. K. Sarmah, “Biochar admixed lightweight, porous and tougher cement mortars: Mechanical, durability and micro computed tomography analysis,” *Science of the Total Environment*, vol. 750, Jan. 2021, doi: 10.1016/j.scitotenv.2020.142327.
- [185] K. Tan, Y. Qin, and J. Wang, “Evaluation of the properties and carbon sequestration potential of biochar-modified pervious concrete,” *Constr Build Mater*, vol. 314, Jan. 2022, doi: 10.1016/j.conbuildmat.2021.125648.
- [186] L. Hachmann, A. Burnett, Y.-M. Gao, R. H. Hurt, and E. M. Suuberg, “Surfactant Adsorptivity of Solid Products from Pulverized-Coal Combustion Under Controlled Conditions,” 1998.
- [187] K. H. Pedersen, A. D. Jensen, M. S. Skjøth-Rasmussen, and K. Dam-Johansen, “A review of the interference of carbon containing fly ash with air entrainment in concrete,” Apr. 2008. doi: 10.1016/j.pecs.2007.03.002.
- [188] L. E. Tunstall, G. W. Scherer, and R. K. Prud’homme, “A new hypothesis for air loss in cement systems containing fly ash,” *Cem Concr Res*, vol. 142, Apr. 2021, doi: 10.1016/j.cemconres.2021.106352.

- [189] “ASTM C1827: Standard Test Method for Determination of the Air-Entraining Admixture Demand of a Cementitious Mixture,” 2020, *ASTM International, West Conshohocken, Pennsylvania, United States*. doi: 10.1520/C1827-20.
- [190] ASTM, “ASTM C260: Specification for Air-Entraining Admixtures for Concrete,” Dec. 15, 2024, *ASTM International, West Conshohocken, Pennsylvania, United States*. doi: 10.1520/C0260\_C0260M-24.
- [191] P. C. Aïtcin, “Entrained air in concrete: Rheology and freezing resistance,” in *Science and Technology of Concrete Admixtures*, Elsevier Inc., 2016, pp. 87–95. doi: 10.1016/B978-0-08-100693-1.00006-0.
- [192] N. J. Harris, K. C. Hover, K. J. Folliard, and M. T. Ley, “The Use of the Foam Index Test to Predict Air-Entraining Admixture Dosage in Concrete Containing Fly Ash: Part I-Evaluation of the State of Practice,” *J ASTM Int*, vol. 5, no. 7, pp. 1–15, 2008.
- [193] N. J. Harris, K. C. Hover, K. J. Folliard, and M. T. Ley, “The Use of the Foam Index Test to Predict Air-Entraining Admixture Dosage in Concrete Containing Fly Ash: Part II—Development of a Standard Test Method: Apparatus and Procedure,” *J ASTM Int*, vol. 5, no. 7, pp. 1–15, Jul. 2008, doi: 10.1520/JAI101602.
- [194] N. J. Harris, K. C. Hover, K. J. Folliard, and M. T. Ley, “The Use of the Foam Index Test to Predict Air-Entraining Admixture Dosage in Concrete Containing Fly Ash: Part III -- Development of a Standard Test Method: Proportions of Materials,” *J ASTM Int*, vol. 5, no. 7, pp. 1–15, 2008, [Online]. Available: [www.astm.org](http://www.astm.org)
- [195] V. Penttala, “Causes and mechanisms of deterioration in reinforced concrete,” in *Failure, Distress and Repair of Concrete Structures*, Norbert Delatte, Ed., Woodhead Publishing, 2009, ch. 1, pp. 3–31. doi: <https://doi.org/10.1533/9781845697037.1.3>.
- [196] C. Hall, “Water sorptivity of mortars and concretes: a review,” *Magazine of Concrete Research*, vol. 41, no. 147, pp. 51–61, Jun. 1989, doi: 10.1680/mac.1989.41.147.51.
- [197] Z. Sun and G. W. Scherer, “Pore size and shape in mortar by thermoporometry,” *Cem Concr Res*, vol. 40, no. 5, pp. 740–751, May 2010, doi: <https://doi.org/10.1016/j.cemconres.2009.11.011>.
- [198] Z. Sun and G. W. Scherer, “Effect of air voids on salt scaling and internal freezing,” *Cem Concr Res*, vol. 40, no. 2, pp. 260–270, Feb. 2010, doi: 10.1016/j.cemconres.2009.09.027.

## APPENDIX A      PERMISSIONS

<b>License Number</b>	6017710223928	<a href="#">Printable Details</a>
<b>License date</b>	Apr 28, 2025	
<b>📄 Licensed Content</b>		<b>📄 Order Details</b>
<b>Licensed Content Publisher</b>	Elsevier	<b>Type of Use</b>
<b>Licensed Content Publication</b>	Cement and Concrete Research	reuse in a thesis/dissertation
<b>Licensed Content Title</b>	Water permeability and chloride penetrability of high-strength lightweight aggregate concrete	<b>Portion</b>
<b>Licensed Content Author</b>	Kok Seng Chia, Min-Hong Zhang	figures/tables/illustrations
<b>Licensed Content Date</b>	Apr 1, 2002	<b>Number of figures/tables/illustrations</b>
<b>Licensed Content Volume</b>	32	1
<b>Licensed Content Issue</b>	4	<b>Format</b>
<b>Licensed Content Pages</b>	7	both print and electronic
		<b>Are you the author of this Elsevier article?</b>
		No
		<b>Will you be translating?</b>
		No
<b>📄 About Your Work</b>		<b>📄 Additional Data</b>
<b>Title of new work</b>	INVESTIGATING THE EFFECT OF BIOCHAR ON THE FROST DURABILITY AND DURABILITY ASSESSMENT OF CONCRETE	<b>Portions</b>
<b>Institution name</b>	CO School of Mines	Figure 1
<b>Expected presentation date</b>	Apr 2025	<b>The Requesting Person / Organization to Appear on the License</b>
		Adam Dunne
<b>📍 Requestor Location</b>		<b>📄 Tax Details</b>
<b>Requestor Location</b>	Mr. Adam Dunne 1500 Illinois St. CEEN Department  Golden, CO 80401 United States	<b>Publisher Tax ID</b>
		98-0397604

Figure A. 1      Permission to include Figure 1 from Cement and Concrete Research in Chapter 2.

License Number	6017710569394	<a href="#">Printable Details</a>	
License date	Apr 28, 2025		
<b>📄 Licensed Content</b>		<b>📄 Order Details</b>	
Licensed Content Publisher	Elsevier	Type of Use	reuse in a thesis/dissertation
Licensed Content Publication	Biomass and Bioenergy	Portion	figures/tables/illustrations
Licensed Content Title	Insight into biochar properties and its cost analysis	Number of figures/tables/illustrations	1
Licensed Content Author	Mohammad Boshir Ahmed, John L. Zhou, Huu Hao Ngo, Wenshan Guo	Format	both print and electronic
Licensed Content Date	Jan 1, 2016	Are you the author of this Elsevier article?	No
Licensed Content Volume	84	Will you be translating?	No
Licensed Content Issue	n/a		
Licensed Content Pages	11		
<b>📄 About Your Work</b>		<b>📄 Additional Data</b>	
Title of new work	INVESTIGATING THE EFFECT OF BIOCHAR ON THE FROST DURABILITY AND DURABILITY ASSESSMENT OF CONCRETE	Portions	Table 1
Institution name	CO School of Mines	The Requesting Person / Organization to Appear on the License	Adam Dunne
Expected presentation date	Apr 2025		
<b>📍 Requestor Location</b>		<b>📄 Tax Details</b>	
Requestor Location	Mr. Adam Dunne 1500 Illinois St. CEEN Department  Golden, CO 80401 United States	Publisher Tax ID	98-0397604

Figure A. 2 Permission to include Table 1 from Journal Biomass and Bioenergy in Chapter 2.